Mass Transfer in Structured Packing

By

André Brink Erasmus

Thesis submitted in partial fulfilment of the requirements for the degree of Master of Science in Engineering (Chemical Engineering) in the Department of Chemical Engineering at the University of Stellenbosch

Supervisor : Prof. Izak Nieuwoudt

Stellenbosch

October 1999

Declaration

I, the undersigned, hereby declare that the work contained in this thesis is my own original work and that I have not previously in its entirety or in part submitted it at any university for a degree.

André Brink Erasmus 8 October 1999

Abstract

Distillation forms the core of all liquid mixture separation processes. It is the benchmark to which all new separation processes are compared. In the design of these columns, especially those containing structured packing, design engineers still rely on rules of thumb or data interpolation, which lead to the addition of huge safety margins. This study is a contribution towards establishing a dependable mass transfer model for structured packing. It is based on the analogy between a short wetted wall column and the flow passages found inside structured packing.

The two-film theory was used to separate the total resistance to mass transfer in a gas side- and a liquid side resistance. A gas phase mass transfer correlation was developed by evaporating several pure liquids in a short wetted wall column. The effect that the complex surface of the structured packing, Mellapak 350Y, has on the gas phase mass transfer rate was investigated. It was found that the liquid surface profile created by this surface causes higher mass transfer rates than measured for the smooth surface. The liquid side resistance to mass transfer was investigated by evaporating binary mixtures in the wetted wall column. No substantial liquid side resistance was found. Significant enhancement of the gas phase mass transfer was observed for mixtures where there were a difference between the surface tension of the solvent and solute. The gas phase mass transfer correlations based on the wetted wall experimental work for both the smooth and complex surfaces was used to predict the separation efficiency of the structured packing, Mellapak 350Y, in binary total-reflux distillation. The complex surface correlation proved to be more accurate. It was found that the predicted packed height is sensitive towards the estimation of the binary gas phase diffusion coefficient.

Opsomming

Distillasie is die proses wat die meeste gebruik word vir die skeiding van vloeistofmengsels. Alle nuwe skeidings prosesse word direk hiermee vergelyk ten einde die effektiwitiet daarvan te bepaal. In die ontwerp van distillasie kolomme, veral die wat gestruktureerde pakking bevat, gebruik ontwerpingenieurs meestal duimreëls of data interpolasie. Dit lei tot baie konserwatiewe ontwerpe met groot veiligheidsfaktore. Hierdie werk is 'n bydrae tot die skepping van 'n betroubare massa-oordragsmodel vir gestruktureerde pakking. Dit is gebaseer op die analogie tussen 'n kort benatte wand kolom en die kanale wat in gestruktureerde pakking gevind word.

Die twee-film teorie was gebruik om die totale weerstand teen massa-oordrag te skei in 'n gasfase- en 'n vloeistoffase weerstand. 'n Gasfase massa-oordragskorrelasie is ontwikkel gebaseer op die verdamping van 'n paar suiwer vloeistowwe in 'n kort benatte wand kolom. Die effek wat die komplekse oppervlak van die gestruktureerde pakking, Mellapak 350Y, op die gasfase massa-oordrag het, is ondersoek. Daar is gevind dat die vloeistofoppervlakprofiel wat deur die komplekse oppervlak gegenereer word 'n hoër massa-oordrag tempo veroorsaak in vergelyking met die gladde oppervlak. Die vloeistoffase weerstand is ondersoek deur binêre mengsels in die benatte wand kolom te verdamp. Geen betekenisvolle weerstand is gevind nie. 'n Beduidende verhoging in die gasfase massa-oordrag is waargeneem vir die binêre sisteme waar daar 'n verskil in die oppervlakspanning van die komponente is. Die gasfase massa-oordragskorrelasies, gebaseer op die benatte wand eksperimentele werk vir beide die gladde- en die komplekse oppervlak, is gebruik om die skeidingsdoeltreffendheid van die gestruktureerde pakking, Mellapak 350Y, te voorspel in totale terugvloei binêre distillasie. Die korrelasie vir die komplekse oppervlak was meer akkuraat. Daar is gevind dat die voorspelde pakkingshoogte baie sensitief is vir die beraming van die binêre gasfase diffusiekoeffisiënt.

Acknowledgements

I would like to express my gratitude towards all the people who supported me throughout this project.

A special word of thanks to my supervisor, Prof. Izak Nieuwoudt, for his support and guidance over the past two years.

I would also like to thank Me. Marli du Rand for her help with some of the wetted-wall experimental work and Me. Nelke van de Ven for the distillation experimental work.

Lastly I would like to thank Sasol Ltd for their financial support throughout my studies and Sulzer for providing the structured packing used in this work

Table of Contents

List of figures

List of Tables

CHAPTER 1 Introduction

1.1 Distillation in chemical engineering

The separation of liquid mixtures into their different components is one of the major operations in the chemical industry. Distillation forms the core of these operations. It has been used for hundreds of years and today still forms the benchmark to which all new separation processes are compared. In 1992 it was estimated [Porter, 1995] that the total throughput of distillation columns equalled a staggering 5.23 billion ton per year. In the United States alone it is estimated that there is approximately 40 000 distillation columns in operation which perform 90-95% of all the separations in the chemical industry. It consumes the energy equivalent to 1.2 million barrels of crude oil per day [Humphrey, 1991]. These figures show that it is a significant business area and it is estimated that by simply improving the estimates of height equivalent to a theoretical plate, energy savings of up to 5% and capital savings of up to 20% can be made.

1.2 Process description

In distillation liquid mixtures are separated in their different components by making use of the difference in their boiling points. It is a column type process where liquid and vapour phases flow countercurrently within the mass transfer zone. Trays or packing are used to maximise the interfacial contact between phases. In columns equipped with trays the liquid flowing down the column is held up in series of trays which are stacked on top of each other. The trays are equipped with weirs and downcomers which enable a level of liquid to be held back on each tray. The trays are perforated (sieve type) or equipped with special valves (bubble cap, valve). The perforations and valves allow the vapour to bubble through the liquid on each tray as it flows up in the column and intimate contact between the two phases is ensured in this way. An alternative way of creating interfacial contact between vapour and liquid phases is by supplying a large wetting area for the liquid in the form of packing material. This packing material can either be random or structured. The random type is usually in the form of small rings or related geometries. The structured type is made up out of corrugated sheets positioned in a parallel arrangement.

1.3 Structured packing in distillation applications

Structured packing were developed in the 1970s for low-pressure distillation applications. It is especially suited to this type of distillation where pressure drop is a concern. Compared to conventional trays and random packing, structured packing produce the lowest pressure drop per theoretical stage. Today it is also popular in the retrofitting of existing near-atmospheric columns to increase their load. The advantages and disadvantages of this type of packing can be summed up as follows [Bravo, 1997]:

Advantages :

- High capacity at low flow parameters
- High volumetric efficiency at low pressures
- Very low pressure drop
- Low entrainment
- Good performance in foaming systems

Disadvantages:

- Low capacity at high flow parameters
- Sensitive to fouling
- High volumetric cost
- Lower efficiency at high pressure

There exist conflicting views regarding the performance of structured packing at high pressure. According to Kurtz [1991] it can increase the capacity of high-pressure columns, but should be used with caution.

1.4 State of existing models for mass transfer in structured packing

When predicting the mass transfer efficiency of structured packing, there are three common approaches used to predict HETP (height equivalent to a theoretical plate): mass transfer models, rules of thumb and data interpolation. The state of existing mass transfer models is such that Kister [1992] recommends using rules of thumb or data interpolation to obtain design HETP.

In recent years some progress has been made in understanding the theory describing the process. Most notably by Bravo et al. [1985] and Rocha et al. [1995]. Their proposed models are based on the two-film theory and assume resistance to mass transfer in both phases. This is a step in the right direction, but there is some concern as to whether the correlations used in obtaining these resistances are valid in a column containing structured packing. For example, the resistance to mass transfer in the vapour phase is calculated by using the empirical correlation developed by Sherwood and Gilliland [1934]. This correlation was developed in a long wetted wall column where the flow is completely developed, which is not necessarily true in structured packing. More recently Crause [1998] used a much shorter wetted wall column in obtaining a correlation for the mass transfer resistance in the vapour phase. Preliminary results showed his correlation and model to be superior to that of Rocha et al. [1995].

1.5 Aim of this study

The present study was undertaken to promote a better understanding of the underlying theory and is a contribution towards equipping design engineers with the necessary tools to design a column containing structured packing without relying on rules of thumb or data interpolation. It is a continuation of the work done by Crause [1998] and relies strongly on wetted wall work to obtain a correlation based on physical properties and flow parameters to model the mass transfer process in structured packing.

More specifically the objectives of this study were:

- To extend the database for the correlation of the vapour phase mass transfer resistance in a short wetted wall column.
- To investigate the influence that the surface profile of the structured packing has on the vapour phase mass transfer resistance.
- To evaluate the resistance to mass transfer in the liquid phase and the effect that the packing surface profile will have on this resistance.
- To develop a model to predict the performance of structured packing in conventional distillation applications.

CHAPTER 2 Gas phase mass transfer

2.1 Introduction

The two film theory for mass transfer enables one to separate the overall resistance to mass transfer into a gas- and a liquid phase resistance. The effect that the micro structure of the mass transfer interface has on the gas phase mass transfer resistance is investigated in this chapter by first quantifying the gas phase mass transfer resistance from a smooth surface and then comparing it to that of a complex surface. This chapter is therefore divided into two parts. The first part deals with smooth surfaces and the second part with complex surfaces. The liquid phase resistance will be investigated in chapter 3.

2.2 Smooth surface

2.2.1 Literature review

One of the earliest publications dealing with vaporization of a volatile liquid into a countercurrent air stream in a wetted wall column is by Sherwood and Gilliland [1934]. They used a column with an inner diameter of 26.7 mm, 1.17 m long and vaporized nine fluids countercurrently and cocurrently into an air stream. This was done at various liquid and gas flow rates, with Re_g relative to the wall varying between 2000 and 20000. They found that their results could be correlated by:

$$Sh_g = 0.023\,\mathrm{Re}_g^{\,0.83}\,Sc_g^{\,0.44} \tag{2.1}$$

Chilton and Colburn [1934] proposed that the mass transfer process is analogous to heat transfer. They used an extensive data bank, including the data of Sherwood et al. and their proposed correlation can be written in the following form [Crause, 1998]:

$$Sh_g = 0.0296\,\mathrm{Re}_g^{\,0.8}\,Sc_g^{\,0.33} \tag{2.2}$$

Barnet and Kobe [1941] measured evaporation rates for water into air in a wetted wall column similar to that used by Sherwood and Gilliland [1934], although slightly longer (1.22 m). Their results can be correlated by:

$$Sh_g = 0.02\,\mathrm{Re}_g^{\,0.83}\,Sc_g^{\,0.44} \tag{2.3}$$

Jackson and Ceaglske [1950] measured the mass transfer rate of water and two organic compounds into air in a wetted wall column. They found that their evaporation data agreed well with that of Barnet and Kobe [1941] and Chilton and Colburn [1934]. When compared to that obtained by Sherwood and Gilliland [1934], they found that their results were substantially lower. Their results are given in the form of graphs where the mass transfer factor j_D is plotted against gas phase Reynolds number. The velocity used in this Reynolds number is the velocity of the gas relative to the liquid interface.

Cairns and Roper [1954] conducted evaporation experiments under different humidities of the gas phase. They only used water in these experiments. They found that their results could be correlated by:

$$Sh_g\left(\frac{p_{Bm}}{P}\right)^{0.83} = 0.021\,\mathrm{Re}_g^{\,0.83}\,Sc_g^{\,0.44} \tag{2.4}$$

They found that the liquid rate influenced the mass transfer coefficient, but did not include a Reynolds number for the liquid phase in their correlation.

McCarter and Stutzman [1959] used several organic liquids and water in their wetted wall studies. They found that their data could be correlated best by using the velocity of the gas phase relative to the liquid interface:

$$Sh_g = 0.024\,\mathrm{Re}_{g,r}^{\,0.8}\,Sc_g^{\,0.4} \tag{2.5}$$

Kafesjian et al. [1961] studied the effect of rippling- and nonrippling films on the gas phase mass transfer. They took this phenomenon into account by including a liquid Reynolds number in their correlation for rippling films. In their correlation for nonrippling films they use the velocity of the gas phase relative to the liquid interface to calculate the gas phase Reynolds number. They only used water to obtain the following correlations:

Rippling films $$Sh_g\left(\frac{p_{Bm}}{P}\right) = 0.0065\,\mathrm{Re}_g^{\,0.83}\,\mathrm{Re}_l^{\,0.15} \tag{2.6}$$

Nonrippling films $$Sh_g\left(\frac{p_{Bm}}{P}\right) = 0.013\,\mathrm{Re}_{g,r}^{\,0.83} \tag{2.7}$$

For systems other than water Mills [1995] recommends that their correlation for rippling films be changed to:

$$Sh_g = 0.00814\,\mathrm{Re}_g^{\,0.83}\,\mathrm{Re}_l^{\,0.15}\,Sc_g^{\,0.44} \tag{2.8}$$

Strummillo and Porter [1965] used carbon tetrachloride to investigate the effect of rippling on the gas phase mass transfer in a wetted wall column. They found that the liquid rate had a larger influence on the gas film controlled mass transfer of carbon tetrachloride than for water. Their results are correlated as follows:

$$Sh_g\left(\frac{p_{Bm}}{P}\right) = 0.0093\,\mathrm{Re}_g^{\,0.68}\,\mathrm{Re}_l^{\,0.34} \tag{2.9}$$

Reker et al. [1966] accounted for the liquid rate by empirically modeling the surface area increase caused by rippling. The increase in surface area is used in their correlation instead of the liquid Reynolds number. They used methanol and carbon tetrachloride in their countercurrent vaporization experiments and their results are correlated in the following manner :

$$Sh_g\left(\frac{p_{Bm}}{P}\right) = 0.163\,\mathrm{Re}^{\,0.83}\,Sc_g^{\,0.5}\,\Delta S^{\varepsilon} \tag{2.10}$$

ε takes on different values for each system. The fractional increase in surface area is given by :

$$\Delta S = 0.721\,\mathrm{Re}_l^{\,5/3}\left(g\upsilon_l\right)^{1/3}\frac{\mu_l}{\sigma} \tag{2.11}$$

Spedding and Jones [1988] measured vaporization rates of water in a wetted wall column where the height varied between 0.723 and3.538 m. They incorporated end effects and found that the liquid flow rate had a definite effect on the mass transfer rate. They correlated their data with:

$$Sh_g = 0.020\,\mathrm{Re}_{g,r}^{\,0.83}\,Sc^{0.44} \tag{2.12}$$

Dudukovic et al. [1996] used the data obtained by Sherwood and Gilliland [1934] and Barnet and Kobe [1941] and correlated it as follows:

$$Sh_g = 0.0318\,\mathrm{Re}_g^{\,0.790}\,Sc_g^{\,0.5} \tag{2.13}$$

Nielsen et al. [1998] measured the mass transfer coefficients for both the gas- and liquid phases in a long wetted wall column (5 m) at high Reynolds numbers. They absorbed a lean SO_2 in air mixture into a strong NaOH solution to determine the gas phase mass transfer coefficient. To determine the liquid phase mass transfer coefficient they absorbed O_2 from air into deoxygenated distilled water. They used a cocurrent setup and their results are correlated with:

$$Sh_g = 0.00031\,\mathrm{Re}_g^{\,1.05}\,\mathrm{Re}_l^{\,0.207}\,Sc_g^{\,0.5} \tag{2.14}$$

$$Sh_l = 0.01613\,\mathrm{Re}_g^{\,0.664}\,\mathrm{Re}_l^{\,0.426}\,Sc_l^{\,0.5} \tag{2.15}$$

and is valid for $7500<\mathrm{Re}_g<13500$ and $4700<\mathrm{Re}_l<12000$

(It is unlikely that such high flow rates will be encountered in distillation columns.)

Crause [1998] investigated the mass transfer rate for several organic liquids in the same wetted wall column used in the present study. His results were correlated by:

$$Sh_g = 0.00283\,\mathrm{Re}_g\,\mathrm{Re}_l^{\,0.08}\,Sc_g^{\,0.5} \qquad (2.16)$$

Re_g varied between 2000 and 8000 and Re_l between 50 and 480.

Most of the wetted wall columns used in the various experiments varied in length between 0.5 and 1.8 m. Crause [1998] argued that for structured packing it would be more appropriate to study the mass transfer in a shorter wetted wall column. The rationale for this is that entrance effects could influence the mass transfer in structured packing and that the mass transfer correlation must account for this. This view is shared by the author.

It is also clear from the literature that the influence of the liquid flow rate on the mass transfer is not fully understood yet. Some of the investigators mention an increase in the mass transfer rate with an increase in the liquid flow rate, but do not include a term for the liquid phase in their correlation [Cairns & Roper, 1954]. A large number of investigators only used water in their work. Other discrepancies include:

- The exponent of the Schmidt number varies between 0.33-0.5
- The exponent of the gas Reynolds number varies between 0.68-1.05

2.2.2 Theory

The two film theory of Whitman [Coulson & Richardson, 1991] for mass transfer across a phase boundary, which is described in Chapter 4, is applied to describe the process taking place when a liquid is vaporized into an air stream. In the case of a pure liquid, there exists no concentration gradient in the liquid film. The molar flux per unit area of

species A diffusing through a stagnant gas B is calculated in the following manner [Coulson & Richardson, 1991]:

$$N_A = \frac{D_{AB}}{\Delta z}\frac{P}{P_{Bm}RT}(P_{Ai} - P_{Ab}) \tag{2.17}$$

P_{Bm} is the logarithmic mean of P_{Bi} and P_{Bb} and is given by:

$$P_{Bm} = \frac{P_{Bb} - P_{Bi}}{\ln\left(\frac{P_{Bb}}{P_{Bi}}\right)} \tag{2.18}$$

The subscripts i and b refer to the interface and the bulk of the gas respectively. Figure 2.1 represents this situation.

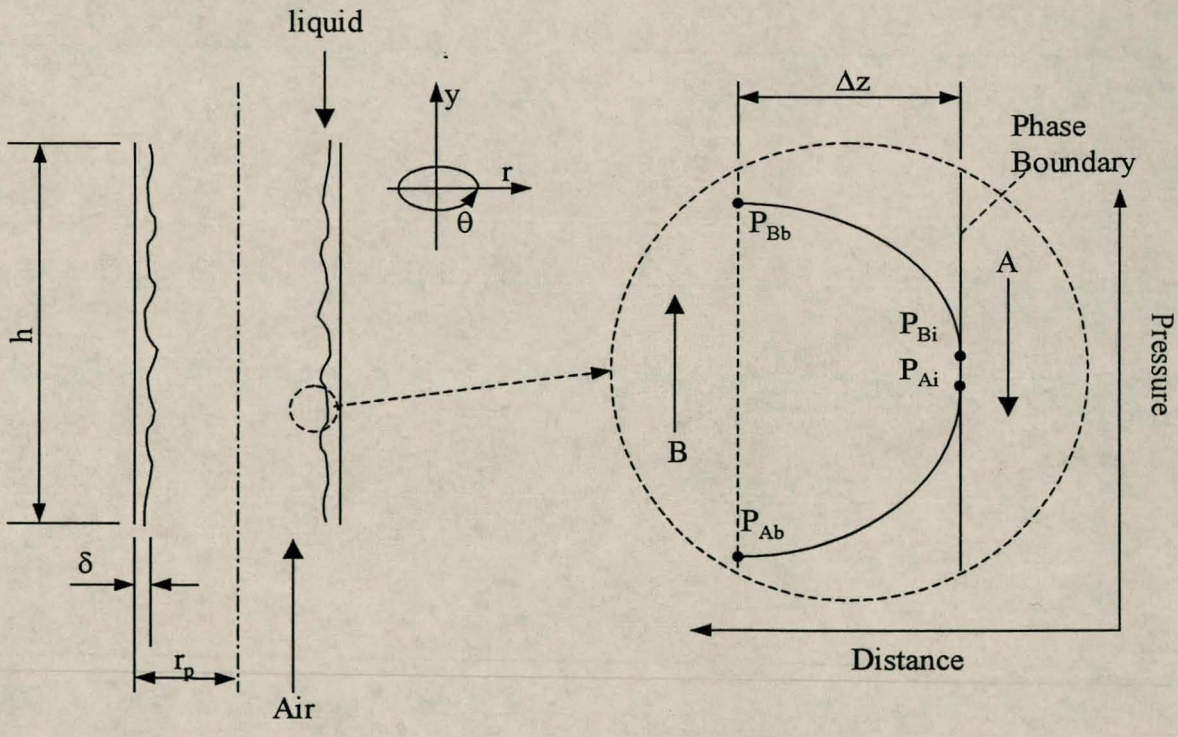

Figure 2.1 Diffusional sublayer in a wetted wall column

Δz is the thickness of the diffusional sublayer and since it is difficult to measure or correlate, a mass transfer coefficient is introduced:

$$N_A = k_g \frac{P}{P_{Bm} RT}(P_{Ai} - P_{Ab}) \tag{2.19}$$

To obtain the total rate of mass transfer from a liquid film on the inside of a pipe wall, the following integration has to be done:

$$n = N_A A = \int_0^h \int_0^{2\pi} \left[k_g \frac{P}{P_{Bm} RT}(P_{Ai} - P_{Ab}) \right] r d\theta dy \tag{2.20}$$

If it is assumed that

- The variables are independent of θ
- The pressure drop is negligible
- k is independent of y

equation 2.20 is simplified to:

$$n = 2\pi r k_g P \int_0^h \frac{1}{RTP_{Bm}}(P_{Ai} - P_{Ab}) dy \tag{2.21}$$

If isothermal operation is assumed, i.e. evaporative cooling is considered to be negligible, it is not necessary to numerically integrate equation 2.21. For short columns this is a good approximation. If pure B enters the column and the mass transfer rate of A is small, (P_{Ai}-P_{Ab}) will vary more between the inlet and the outlet of the column than P_{Bm}. An arithmetic mean between the inlet and outlet values of P_{Bm} will be adequate. A logarithmic average of the inlet and outlet of the partial pressure driving force is used:

$$\Delta P_A = \frac{(P_{Ai} - P_{Ab})_{inlet} - (P_{Ai} - P_{Ab})_{exit}}{\ln\left(\frac{(P_{Ai} - P_{Ab})_{inlet}}{(P_{Ai} - P_{Ab})_{exit}} \right)} \tag{2.22}$$

The molar transfer rate is calculated by substituting ΔP_A into equation 2.21 and integrating over the height of the column:

$$n = A_i \frac{k_g P_t \Delta P_A}{RTP_{Bm}} \tag{2.23}$$

In the calculation of the interfacial area the thickness of the liquid film is taken into account, $r = r_p - \delta$ (see figure 2.1):

$$A_i = 2\pi r h \tag{2.24}$$

The calculation of the liquid film thickness and the interfacial velocity are shown in appendix A. The gas phase mass transfer coefficient for the evaporation of pure liquids in a wetted wall column is calculated by using equation 2.23.

2.2.3 Experimental

Experimental setup

As mentioned earlier, it was decided to use a short wetted wall column in contrast to longer columns used by previous investigators. To operate the column as close to isothermal conditions as possible, the whole wetted wall column assembly was submerged in a constant temperature water bath. Figure 2.2 show the wetted wall column assembly.

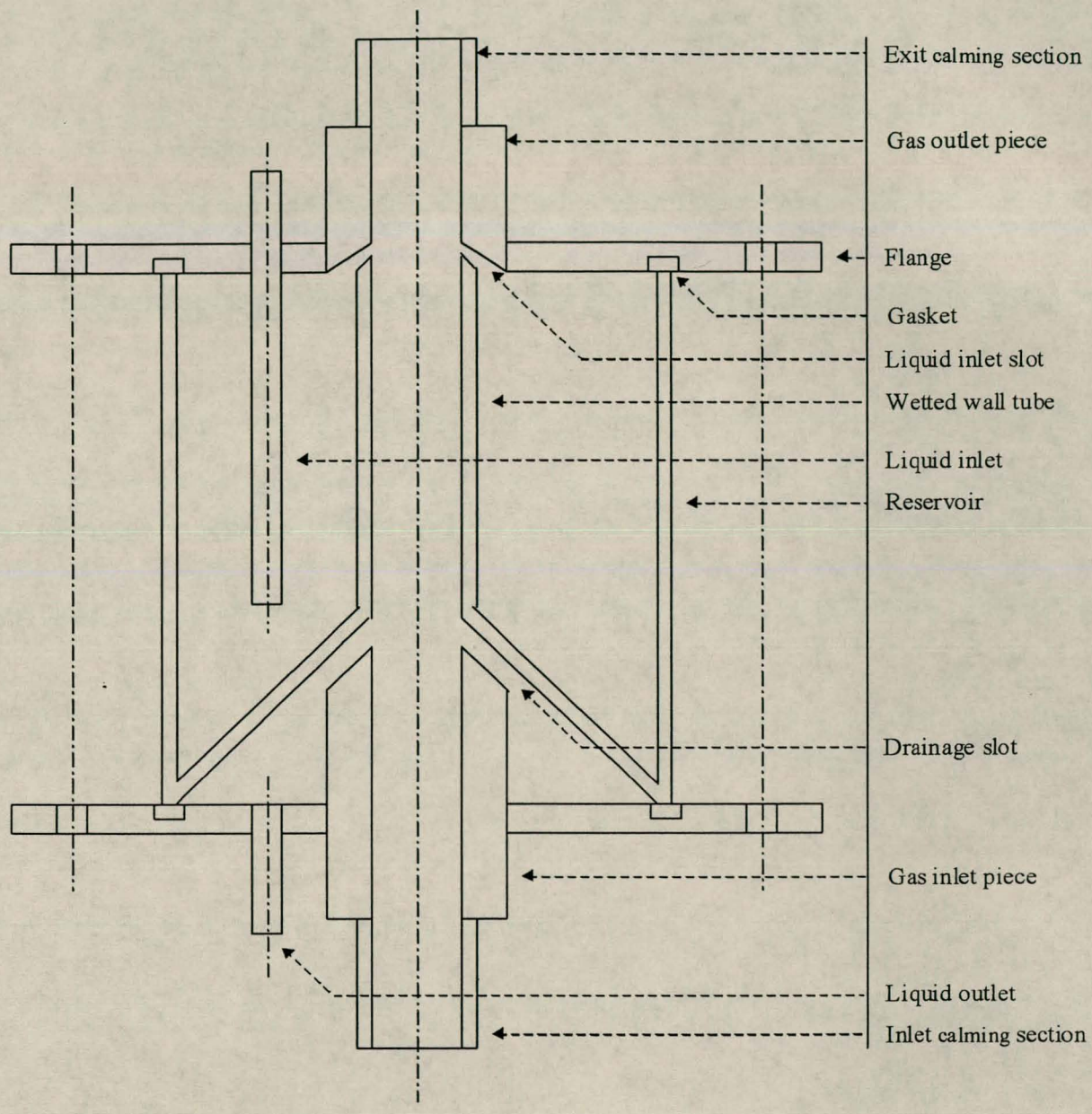

Figure 2.2 Wetted-wall column

The center tube in the assembly is the wetted-wall section. This section is a precision glass tube with an inside diameter of 25.5 mm and a length of 111 mm. At the bottom end the wetted-wall tube is flared at an angle of 45° and fused to the bottom end of a 110 mm glass tube which forms a reservoir around the wetted wall tube. The top end of the wetted-wall tube is ground at an angle of 45°. The top end of the wetted-wall tube protrudes approximately 5 mm above the reservoir's. The gas inlet piece is 145 mm in

length, has an outer bevel of 45° and forms a drainage slot of approximately 3 mm with the bottom of the wetted-wall column. The gas outlet piece is 75 mm in length, has an inner bevel of approximately 20° and forms a drainage slot of approximately 2 mm with the bottom of the wetted wall column. This drainage slot is adjustable to ensure smooth wetting of the wetted-wall column. Gas inlet- and outlet calming sections are used. The inlet calming section is 475 mm long and the outlet calming section is 205 mm. Both sections have a 25 mm internal diameter which is smaller than the 25.5 mm of the wetted-wall tube. This compensates for the thickness of the liquid film flowing down the wetted wall column. The inlet- and outlet calming sections as well as the inlet and outlet pieces are made from phosphor bronze.

The inlet- and outlet pieces fits into two stainless steel flanges, 10 mm thick. The glass wetted-wall/reservoir unit is clamped between the flanges by means of three tie rods. Neoprene gaskets are used to form a seal between the glass and the steel. The distance between the two flanges is measured with a vernier calliper to ensure that the two flanges are parallel. During assembly the wetted-wall tube is carefully aligned with the gas inlet- and outlet pieces.

A flow diagram of the experimental setup is shown in figure 2.3. The unit shown in figure 2.2 is submerged in a glass water bath. The water in this bath is heated and circulated with a MGW Lauda constant temperature bath and circulating pump. The liquid feed to the wetted wall column is pumped from a calibrated reservoir with a small centrifugal pump. The flow rate is measured through a rotameter and controlled with a valve at the pump outlet. The liquid is heated to the temperature of the water bath through a heating coil that is submerged in the constant temperature bath (6 m of ¼ inch copper tubing). The liquid fills the reservoir and flows through the liquid inlet slot into the wetted-wall tube. The liquid exits the tube through the drainage slot and flows under gravity through a valve back to the calibrated reservoir where it is recirculated. A liquid level is allowed to build up in the space between the bottom flange and the drainage slot and is controlled by the valve on the exit line.

Compressed air is dried in a dryer with silica gel. The flow rate is measured through a rotameter and controlled with a valve. The air is heated in an electric heater and enters the wetted-wall tube through the inlet calming section. After exiting the column through the outlet calming section, it is vented to the atmosphere. The temperature of the air is controlled by varying the electric power to the heater with a Variac variable transformer.

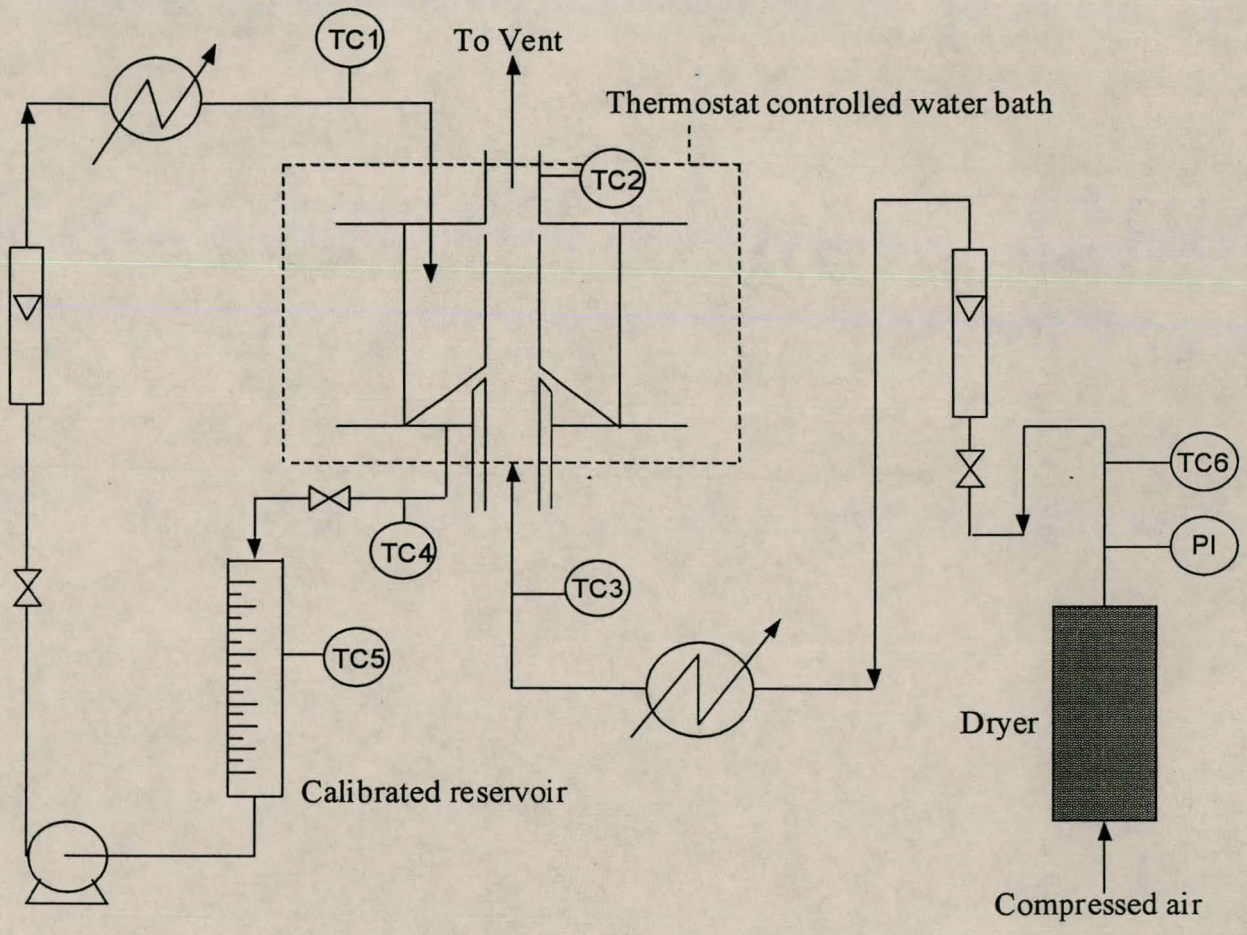

Figure 2.3 Flow diagram: Wetted-wall column

The liquid rotameter was calibrated for each working fluid and temperature with a stopwatch and measuring cylinder. The air flow rotameter was calibrated for low flow rates by measuring the volume of compressed air flowing through it with a Parkinson Cowan measurement turbine gas totalizer. For high flow rates the mass loss from a cylinder of compressed nitrogen was measured over time.

The following temperatures were measured :

- Air at inlet to air flow rotameter
- Air at inlet- and exit of wetted wall column
- Liquid at inlet- and exit of wetted wall column
- Liquid in calibrated reservoir

The temperatures were measured with type K thermocouples and the temperature readings registered on a Yokogawa HR1300 hybrid recorder. The thermocouples are accurate to within 0.2 °C. The pressure of the air at the inlet to the air flow rotameter were also measured.

Experimental procedure

Before starting experimental work, the apparatus is thoroughly cleaned and dried. The apparatus is filled with the desired liquid through the calibrated reservoir and pumped to the reservoir in the wetted wall assembly. The air flow rate and temperature of the water bath is adjusted to the desired values. The temperature of the air is adjusted to the operating temperature by varying the power to the electric heater. The apparatus is then left until the temperatures have stabilized. Before starting experimental work the liquid is circulated until it reaches operating temperature.

The evaporation rate of a liquid is measured at combinations of different air- and liquid flow rates. The evaporation rate is calculated by measuring the volume decrease in the calibrated reservoir during a run. This is done by noting the level in the reservoir before and after a run. The flow rate of the liquid is adjusted by means of the valve in the pump outlet line. The level of liquid between the bottom flange and the bottom of the wetted-wall tube is controlled by the valve in the exit line of the wetted-wall assembly. At the end of a run the valve that controls the liquid flow rate is closed and the valve that controls the level at the bottom of the wetted-wall tube is opened completely. This allows all the liquid in this space to drain to the calibrated reservoir before the level is noted. The average duration of a run was approximately 6 minutes and during this time 30- 70 ml of

liquid was evaporated, depending on the working liquid and the temperature. The temperatures are registered 2 to 4 times during an experimental run, depending on the length of run, and the average is used in the calculations.

2.2.4 Results

The results are plotted in terms of a dimensionless flow number (Re_g or Re_l) and a dimensionless mass transfer number (Sh_g). The formal definitions of the various dimensionless groups are given in table 2.1. Figure 2.4 show the experimental results for six pure components at different air flow rates.

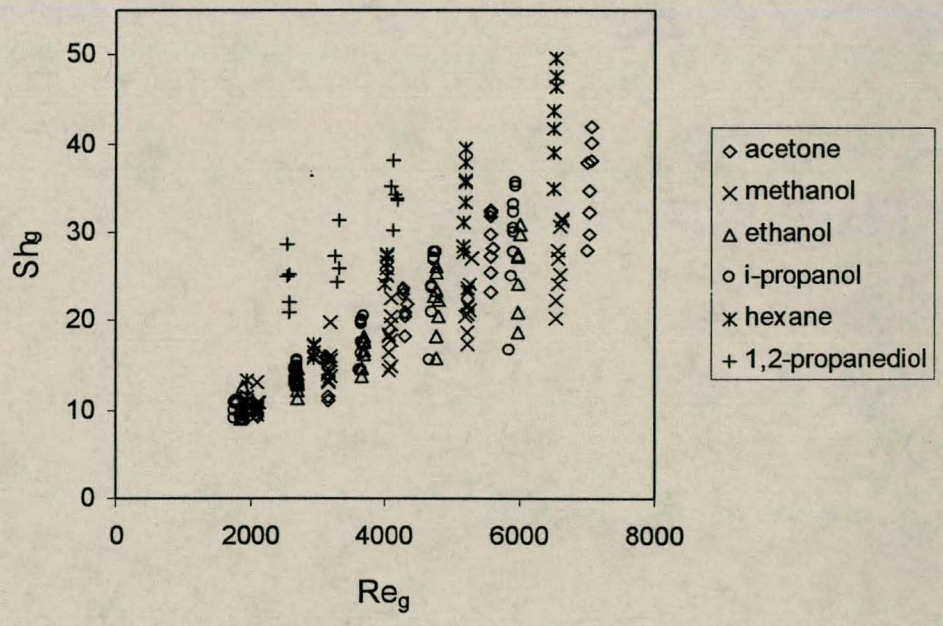

Figure 2.4 Sh_g vs Re_g for different pure components.

The range for various dimensionless numbers and some important properties are as follows:

Sh_g	: 10-50	σ (N/m)	:	0.016-0.028 [N/m]
Re_g	: 1800-7000	μ (Pa.s)	:	2.51-14.7 10^{-4} [Pa.s]
Sc_g	: 0.97-2.02			
Re_l	: 6-330			

Figure 2.5, 2.6 and 2.7 show the influence of the liquid flow rate on the gas phase Sherwood number for three of the pure components studied.

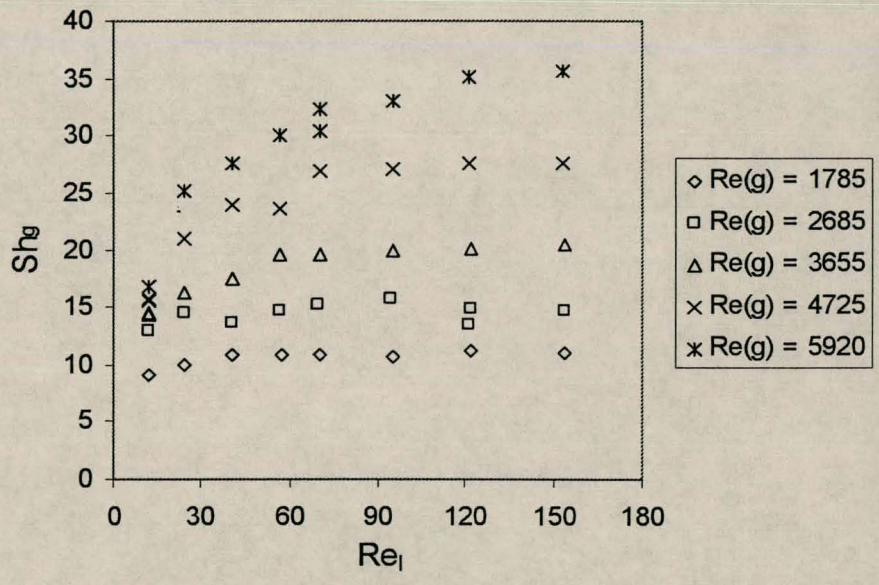

Figure 2.5 Sh_g vs Re_l for i-propanol. Re_g=1785-5920, Re_l=12-153

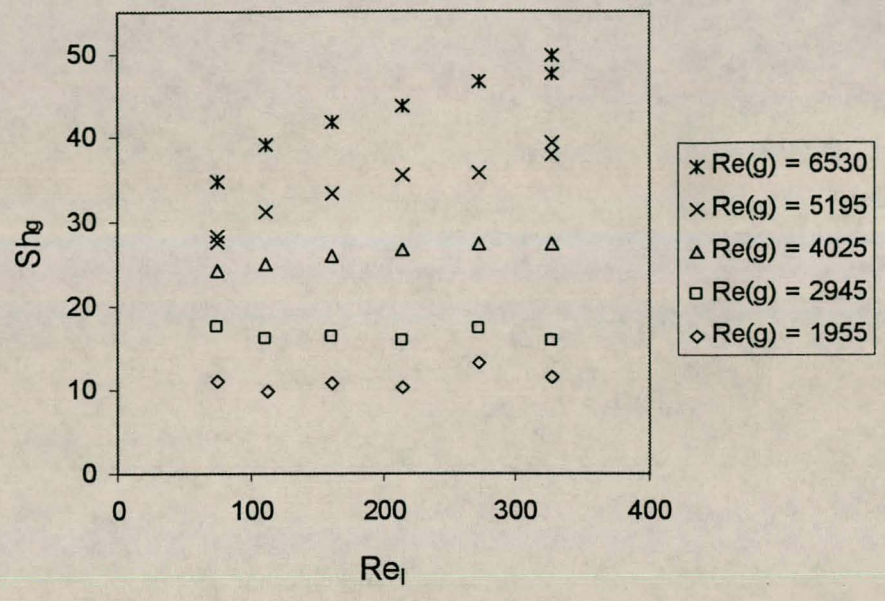

Figure 2.6 Sh_g vs Re_l for n-hexane. Re_g=1955-6530, Re_l=75-327.

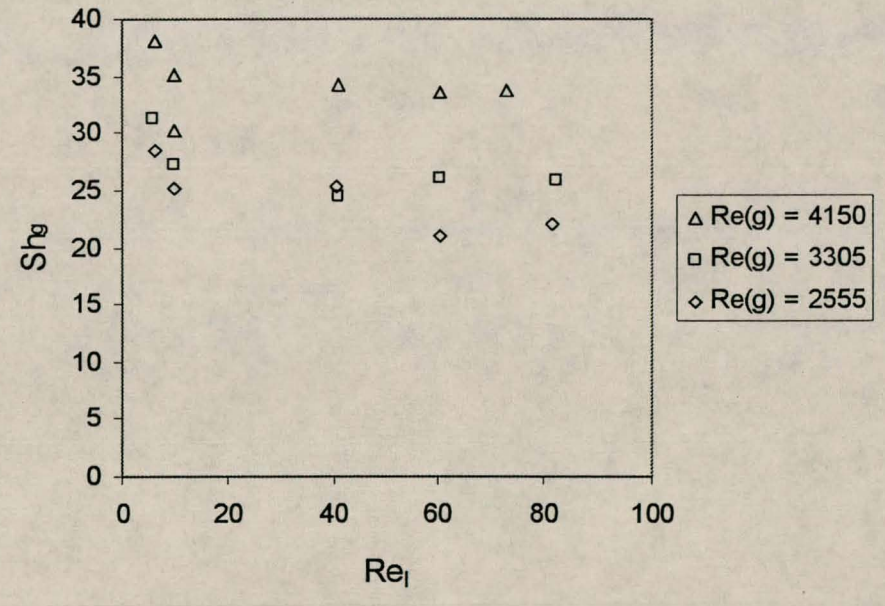

Figure 2.7 Sh_g vs Re_l for 1,2-propanediol. Re_g=2555-4150, Re_l=6-82.

The remaining three pure components showed the same trend as in figure 2.5. Al the results are given in appendix C. The methods and correlations which were used in the estimation of physical properties are shown in appendix B.

The results are compared to the correlations developed by previous investigators in figures 2.8 to 2.10.

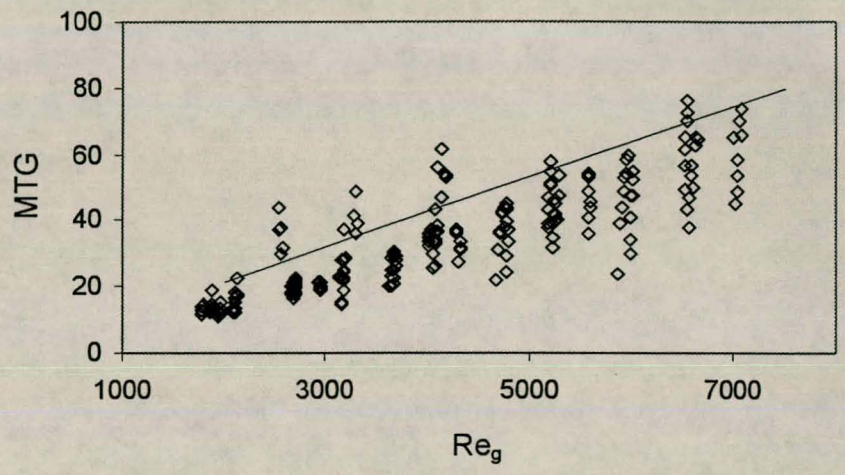

Figure 2.8 Experimental values (◇) compared to that predicted by Sherwood and Gilliland [1934] (solid line). MTG is defined as $\left(\frac{Sh}{Sc^{0.44}}\right)^{\frac{1}{0.83}}$

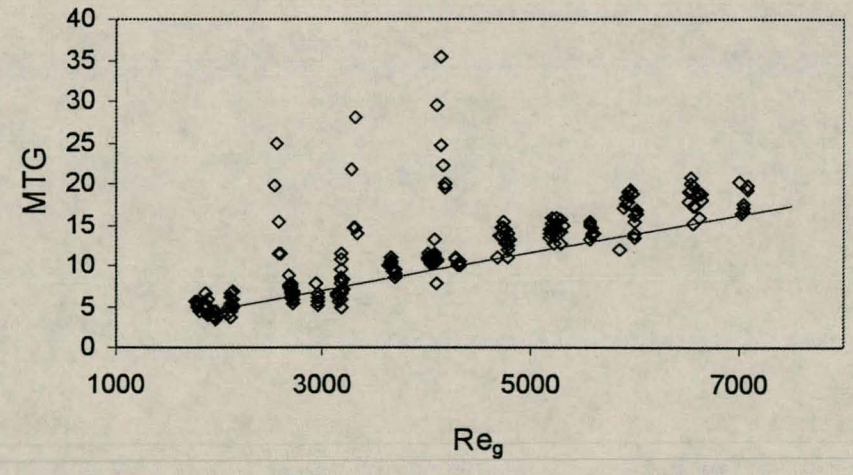

Figure 2.9 Experimental values (◇) compared to that predicted by Kafesjian et al. [1961] (solid line). MTG is defined as $\left(\frac{Sh}{Sc^{0.44}\,\mathrm{Re}_l^{\,0.15}}\right)^{\frac{1}{0.83}}$

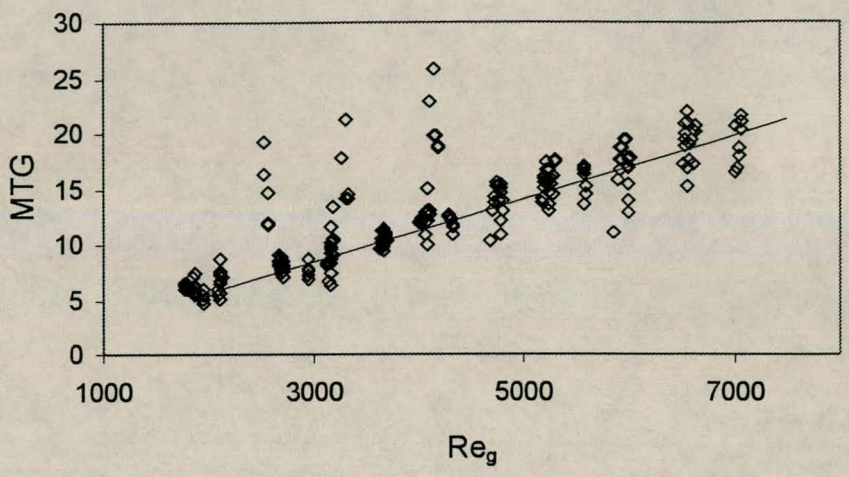

Figure 2.10 Experimental values (◇) compared to that predicted by Crause [1998] (solid line). MTG is defined as $\left(\frac{Sh}{Sc^{0.5}\,\mathrm{Re}_l^{\,0.08}}\right)$

In figure 2.8 most of the experimental points lie below the solid line. The correlation developed by Sherwood and Gilliland [1934] therefore tends to over predict the gas phase mass transfer rate. The correlation proposed by Kafesjian et al. [1961] (figure 2.9) gives a good fit at low Re_g, but tends to under predict the mass transfer rate at higher Re_g. From figure 2.10 it is clear that the correlation developed by Crause [1998] gives a reasonable fit to the data, but there is a few of the data points that lie well below the predicted value. This suggests that Re_l had a larger influence on the gas phase mass transfer rate in the present work than observed in the work by Crause [1998]. In al three of the above figures, there are a few points where the mass transfer rate lie well above that predicted by the different correlations. These points represent the gas phase mass transfer rate of 1,2-propanediol.

The experimental gas phase mass transfer rates for the different pure components were correlated by using a power law series similar to that used by previous investigators. Combinations of different dimensionless numbers were used in the correlating procedure. This was done in order to assess the influence that the different physical properties have on the mass transfer rate. Non linear least square minimization of the squared sum of the

differences between calculated and experimental Sh_g was used to calculate the constants in the correlation. Table 2.1 defines the different dimensionless numbers used.

Table 2.1 Dimensionless numbers [Incropera & De Witt, 1990]

Dimensionless group	Definition	Interpretation
Sherwood number Sh_g	$\frac{k_g \delta}{D_{AB}}$	Dimensionless concentration gradient at surface
Gas phase Reynolds number : Re_g	$\frac{\rho_g u_g (D-2\delta)}{\mu_g}$	Ratio of inertia and viscous forces
Gas phase Scmidt number : Sc_g	$\frac{\mu_g}{\rho_g D_{AB}}$	Ratio of momentum and mass diffusivities
Liquid Reynolds number : Re_l	$\frac{\rho_l u_l \delta}{\mu_l}$	Ratio of inertia and viscous forces
Bond number : Bo	$\frac{g(\rho_l - \rho_g)\delta^2}{\sigma}$	Ratio of gravitational and surface tension forces
Liquid Weber number : We_l	$\frac{\rho_l u_l^{\,2} \delta}{\sigma}$	Ratio of inertia to surface tension forces
Liquid Capillary number : Ca_l [1]	$\frac{\sigma}{u\mu}$	Ratio of surface tension and viscous forces
Liquid Froude number : Fr_l	$\frac{u_l^{\,2}}{g\delta}$	Ratio of inertia and gravity forces

(1) Dimensional analysis

Relative few experimental points were measured for 1,2-propanediol, because of wetting problems at low liquid flow rates. It is also uncertain whether the available correlations for the binary diffusion coefficient are accurate for 1,2-propanediol/air at the experimental conditions. It was therefore decided not to include this data set in the training set.

Table 2.2 shows the results for the different combinations of dimensionless numbers. In correlation 2.25 and 2.29 $Re_{g,r}$ was used. The velocity used in $Re_{g,r}$ is the velocity of the gas phase relative to the liquid surface: $u_{g,r} = u_g + u_{l,i}$.

Table 2.2 Results of different correlations

Correlation	a	b	c	d	e	RMS error	r^2
2.25 $Sh_g=aRe_g^bSc_g^c$	0.0044	0.992	0.583	N/A	N/A	3.175	0.873
2.26 $Sh_g=aRe_{g,r}^bSc_g^c$	0.0008	1.172	0.547	N/A	N/A	2.461	0.924
2.27 $Sh_g=aRe_g^bSc_g^cRe_l^d$	0.0030	0.959	0.485	0.145	N/A	2.024	0.949
2.28 $Sh_g=aRe_g^bSc_g^cWe_l^d$	0.0047	0.992	0.537	0.111	N/A	1.734	0.962
2.29 $Sh_g=aRe_{g,r}^bSc_g^cBo^d$	0.0011	1.188	0.579	0.120	N/A	2.057	0.947
2.30 $Sh_g=aRe_g^bSc_g^cFr_l^d$	0.0036	0.958	0.485	0.146	N/A	2.024	0.949
2.31 $Sh_g=aRe_g^bSc_g^cCa_l^d$	0.0069	1.034	0.623	-0.174	N/A	2.456	0.924
2.32 $Sh_g=aRe_g^bSc_g^cRe_l^dBo^e$	0.0040	0.990	0.533	0.115	0.104	1.732	0.962

$$\text{RMS error} = \sqrt{\frac{\left(Sh_{experimental} - Sh_{predicted}\right)^2}{n}}$$

2.2.5 Discussion of results

From Table 2.2 it is clear that the correlations that do not have a term to describe the liquid phase, similar to that used by Sherwood, fail to correlate the data obtained in this work. All the correlations with liquid flow terms (correlations 2.27, 2.28, 2.30, 2.31, 2.32) performs better than those with no liquid flow term (correlation 2.25, 2.26, 2.29) This is also evident from figure 2.5 and 2.6 which show that Sh_g is influenced by the liquid flow rate. This phenomenon will be explained at the end of this section.

The correlations where the liquid flow term (or terms) incorporate the velocity of the film and the surface tension, give the best fit on the experimental data (correlations 2.28 and

2.32). This is in contrast to previous investigators' findings [Crause, 1998, Kafesjian, 1961], who used the Re_l to characterize the influence that the liquid film has on the gas phase mass transfer. In figure 2.11 the mass transfer rate for water, measured by Crause [1998] in the same apparatus, is compared to that predicted by correlations 2.27 and 2.28. The surface tension of water is approximately 3 times higher than the liquids used to fit the correlation (0.062 N/m). It is clear from figure 2.11 that correlation 2.28 (containing We_l) predicts the mass transfer rate accurately and more so than correlation 2.27 (containing Re_l). It must be mentioned that the liquid flow rate was not varied considerably in these experiments due to the risk of incomplete wetting.

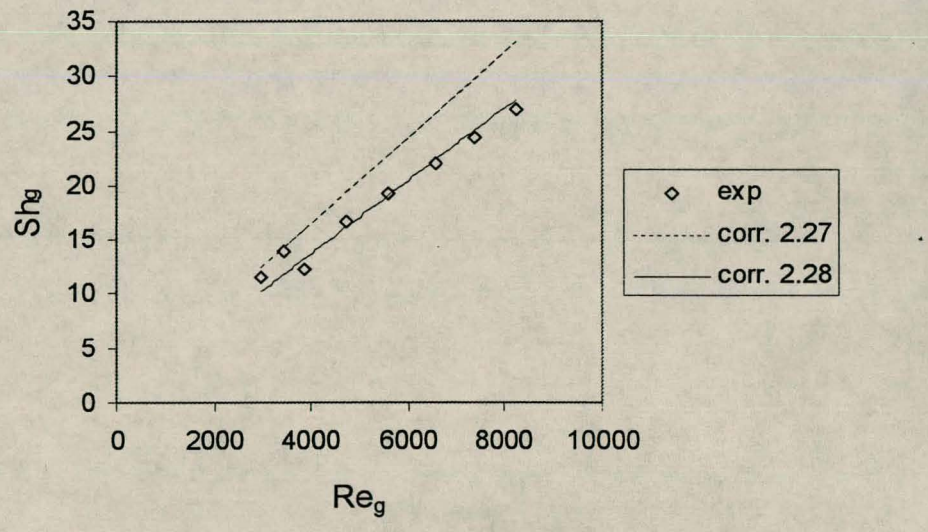

Figure 2.11 Comparison between experimental (◇) and predicted (-) Sh_g values for water [Crause, 1998].

The effect that the surface tension has on the gas phase mass transfer is not fully understood yet. Peramanu et al. [1998] links the surface tension to the instability of a falling liquid film. They found that for a decrease in surface tension there is an increase in the amplitude of the waves on the surface of the film. This might have the effect of inducing more turbulence in the gas layer close to the interface and thereby enhancing the rate of mass transfer.

One can however not ignore the effect that the viscosity of the liquid phase has on the mass transfer rate. Figure 2.4 show that the mass transfer rate for 1,2-propanediol is higher than for the other pure liquids. If it is assumed that this is not due to experimental error or inaccuracies in the estimation of the binary gas phase diffusion coefficient (see appendix B), then the following analysis can be done.

The viscosity of 1,2-propanediol is almost twice that of the highest pure liquid viscosity in the training set ($1.47.10^{-3}$Pa.s compared to $7.65.10^{-4}$Pa.s). The surface tension is 25% higher than the highest surface tension (0.028 N/m compared to 0.023N/m). To verify that it is the viscosity, and not the surface tension, that causes the enhanced mass transfer rate, experimental data for liquids having surface tensions higher than the liquids in the training set are compared with correlation 2.28 in figure 2.12. The viscosity of these liquids falls within the experimental range. The data were obtained from Crause [1998].

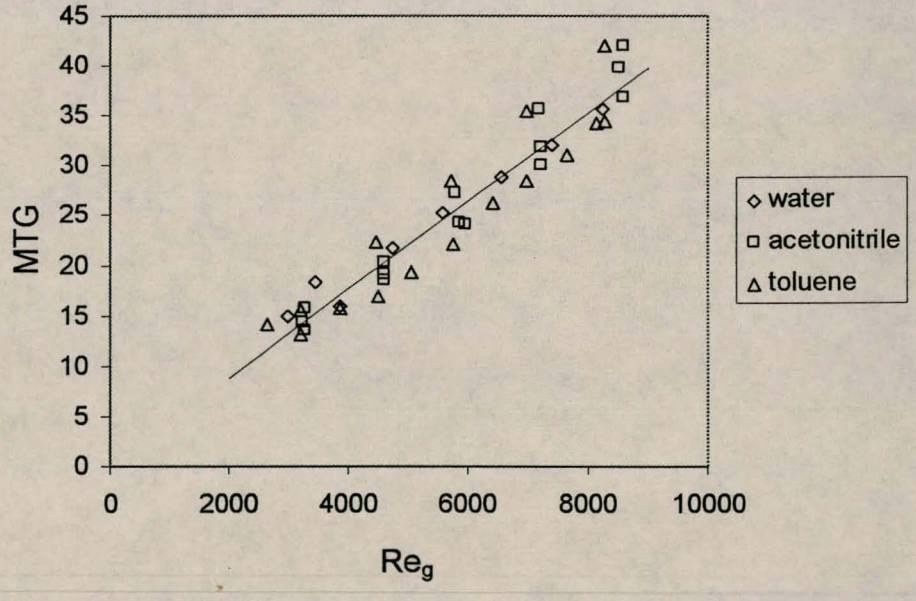

Figure 2.12 Plot of experimental data for water (σ=0.065N/m, μ=$4.55.10^{-4}$Pa.s), acetonitrile (σ=0.028N/m, μ=$3.06.10^{-4}$Pa.s) and toluene (σ=0.024N/m, μ=$4.03.10^{-4}$Pa.s) with correlation 2.28 (—).

Figure 2.12 shows an excellent fit of correlation 2.28 on the experimental data. The conclusion can be made that the viscosity has a definite effect on the mass transfer rate. More experimental work needs to be done in order to investigate this phenomenon. It is however clear that the correlation developed in this work does not extrapolate well to liquids having a viscosity higher than that of the liquids in the training set. It does extrapolate well to liquids having surface tensions substantially higher, but with viscosity falling within the experimental range.

Although correlation 2.32 gives the best fit to the data, it contains four terms compared to the three terms of correlation 2.28. There is also no substantial difference in the error value between these two correlations. It is therefore assumed that correlation 2.28 best describes the mass transfer data of this work. This correlation is plotted with the experimental data in figure 2.13.

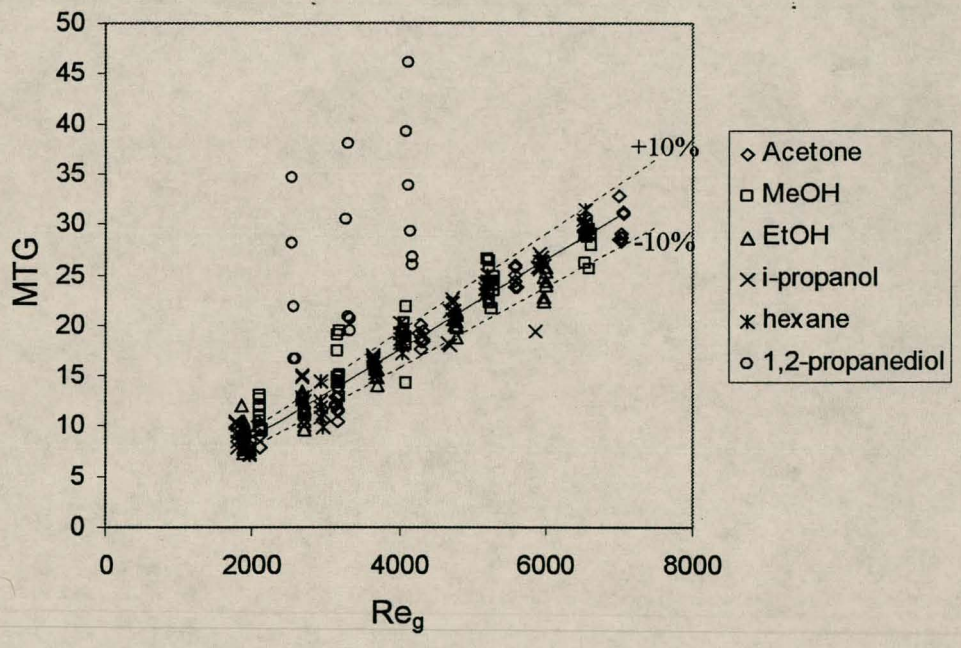

Figure 2.13 Plot of experimental data and correlation 2.28 (—). MTG is defined as $\left(\frac{Sh_g}{Sc_g^{0.537} We_l^{0.111}}\right)^{\frac{1}{0.99}}$. Confidence interval is also shown.

For the sake of simplicity it is proposed that the exponents in correlation 2.28 be rounded to give the following correlation, without increasing the rms error substantially:

$$Sh_g = 0.0044\,\mathrm{Re}_g\, Sc_g^{0.5} We_l^{0.111} \qquad (2.33)$$

The exponent of the gas phase Reynolds (0.99≈1) number is the same as the correlation developed by Crause [1998]. This is to be expected since the same column was used in the experimental work. This exponent is substantially higher than the exponent reported by previous investigators, 0.8-0.83 [Sherwood, 1934, Barnet & Kobe, 1934, Kafesjian, 1961]. The difference can be contributed to the length of the column [Crause, 1998]. The length of the column used in this work (0.1 m) is shorter than that used by previous investigators (0.5-1.8 m). Entrance effects in a column shorter than 6 pipe diameters can be expected to dominate [Crause, 1998]. As mentioned earlier, it is expected that entrance effects will have an influence on the mass transfer in structured packing, where the flow profile is never completely developed due to the geometry of the packing. The exponent compares favorably to values reported in literature for structured packing of about 1 [Weiland et al., 1993], which supports this view. It is slightly higher than the 0.8 proposed by Spiegel and Meier [1987] for gauze packing.

The exponent of the gas phase Schmidt number was rounded to 0.5 because it (0.537) compares favorably to this theoretical value. Dudukovic [1996] has shown that the widely used exponent of 1/3 is not applicable to mass transfer from a falling liquid interface but rather to the mass transfer from a stationary interface.

The exponent of the liquid phase dimensionless number is higher than that found by Crause [1998]. This can be expected since the mass transfer was investigated at lower flow rates than that used by Crause [1998]. It was found that as the flow rate is decreased from that used by Crause [1998] the line of wave inception, or the point where they can be visually observed, moves up the column. Figure 2.14 show the percentage area of the column covered in surface waves as a function Re_l for n-hexane. The values are based on visual observation.

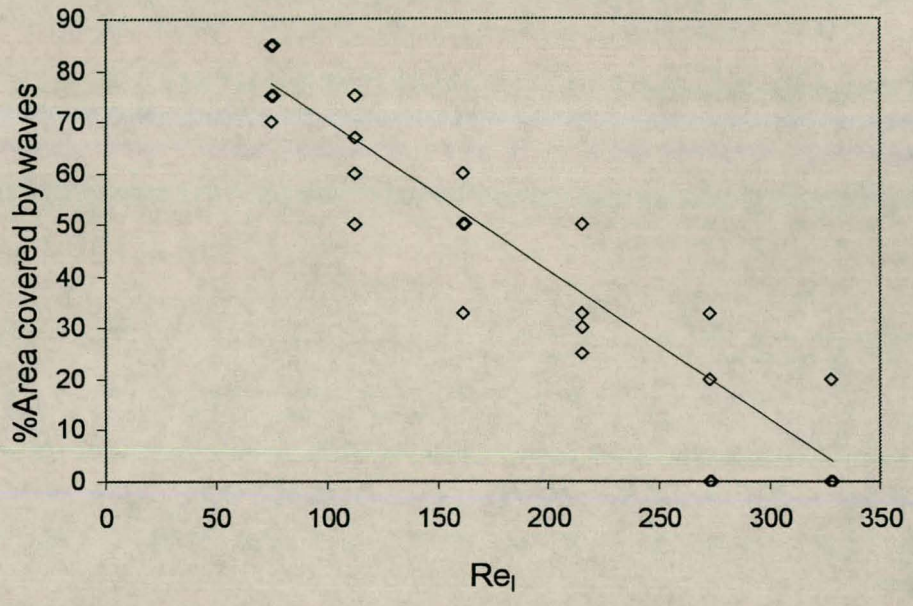

Figure 2.14 % area covered by waves vs. Re_l for n-hexane. Re_g=1950-6540.

Figure 2.14 show that at low flow rates almost the entire surface of the liquid is covered with surface waves. This observation is supported by literature [Tailby & Portalski, 1960, Portalski & Clegg, 1972]. The influence that these waves have on the mass transfer rate is not fully understood yet. Some investigators contribute it to an increase in the surface area [Reker et al., 1966], while others argue that it increases interfacial turbulence [Crause, 1998]. Everybody agrees though that it does have an effect on the mass transfer rate. It is therefore not surprising that for an increase in the area covered by visually observable surface waves, there is an increase in the exponent of the liquid phase dimensionless number. Like previously stated, it was found that in the viscosity range of the experimental work, the We_l gave a better fit than Re_l.

2.2.6 Conclusions

- The mass transfer rate is lower than predicted by the correlation developed by Sherwood and Gilliland [1934]. The correlation of Kafesjian et al. [1961] under

predicts at high Re_g, while the correlation proposed by Crause [1998] gave a reasonable fit.

- It was found that by using the We_l instead of the Re_l, there was an improvement in the correlation of the data.
- The proposed correlation extrapolates well to liquids having surface tensions substantially higher than the experimental range, provided their viscosity lie within the experimental range.
- The exponent of the gas phase Reynolds (0.99) number compares well to that of Crause [1998] (1) and Weiland et al. [1993] (1.03) for structured packing. It is higher than that of Sherwood and Gilliland [1934] (0.83) and other investigators (0.8-0.83) who used longer wetted wall columns.
- The exponent of the gas phase Schmidt number (0.537) compares well to the theoretical value of 0.5 [Dudukovic, 1996].
- In general it was found that the liquid phase has a higher influence on the gas phase mass transfer than reported by Crause [1998]. This is due to the lower flow rates of the liquid phase and the increase in the area covered in visual observable waves which accompanies it. The effect is seen in the higher exponent of the liquid dimensionless number, We_l.
- The exponent of the gas phase Reynolds number and the gas phase Schmidt number were rounded for the sake of simplicity without increasing the error substantially. The proposed correlation is as follows:

$$Sh_g = 0.0044\,\mathrm{Re}_g\, Sc_g^{0.5} We_l^{0.111}$$

and is valid for $1800 < Re_g < 7000$ and $6 < Re_l < 330$

2.3 Complex surface

2.3.1 Literature review

To the authors knowledge there is no literature that deals specifically with mass transfer from a liquid film flowing over a complex surface into a countercurrent air stream. There are a few that deal with the mass transfer in structured packing segments in distillation columns and are reviewed in chapter 4. Most of the literature is focussed on trying to compute the velocity and surface profile, i. e. the hydrodynamics of the liquid flowing over the complex surface [Wang, 1981; Dassori et al., 1982; Pozrikidis, 1988; Zhao & Cherro, 1992]. It is important to know what these profiles look like, but one must be able to use this knowledge to predict the mass transfer rate. Since there is no certainty even in the case of a smooth surface what enhancement effect the surface profile will have on the mass transfer rate, it was decided to also use the smooth surface hydrodynamic model for the complex surface. A short summary of the literature on flow over complex surfaces follows.

Wang [1981] was one of the first to investigate the film thickness and velocity profile of a film flowing down a 'wavy' surface mathematically. The results are not supported with any experimental work. It was found that the amplitude and the phase shift depends on the surface tension and the wave length and orientation of the wavy striations.

Dassori et al. [1982] studied the effect that a second phase will have on the surface of a liquid flowing slowly through a sinusoidal channel. Their work is not supported by any experimental work.

Another paper dealing with this type of flow from a theoretical point of view is by Pozrikidis [1988]. For a sinusoidal wall he found that at low flow rates the surface profile will closely follow that of the wall. For high flow rates the sinusoidal wall only causes a slight deflection on the free surface. It is mentioned that flow reversal may occur at certain flow rates which will influence the transfer processes from such a film. This may

be significant in the mass transfer process from liquid films flowing down the complex surface used in this work. Surface tension was also found to influence the profile of the liquid interface compared to that of the wavy solid wall.

The first paper that deals with the experimental characterization of film flow over complex surfaces is by Zhao and Cerro [1992]. They used highly viscous fluids and measured the film thickness at different liquid flow rates for a variety of complex surfaces. The film thickness was measured by using a precision translator. In the case of low electrical conductivity a video camera, zoomed in on the surface, was used to detect the position where the needle touched the surface. For solutions with higher conductivity the surface was detected through electrical conductance. They found that their experimental work could be correlated by using the Nusselt film thickness, the Reynolds number and the Capillary number. They concluded that compared to a smooth surface the liquid flowing over a complex surface has a larger average film thickness and a smaller average free surface velocity. This causes a larger liquid hold up and longer residence times compared to smooth surfaces. The film is also less prone to breakup.

Shetty and Cerro [1993] attempted to model the experimental results obtained by Zhao and Cerro [1992]. They used a two dimensional streamline function to compute the velocity field and reduce the equations of motion to a single differential equation. A perturbation solution for small film thickness was developed. Their model was accurate at small values of δ, the ratio of Nusselt film thickness to solid surface amplitude. At higher values of δ their model is not accurate and they contribute it to inertia and capillary effects.

Kang and Chen [1995] studied the steady two-dimensional flow of two liquid films down a slightly wavy sinusoidal plane. They followed a perturbation approach in their mathematical model and restricted it to steady flows. They found that interfacial- and surface tension affect the amplitude of the interface and free surface.

In their theoretically based model Bontozoglou and Papapolymerou [1997] considered laminer gas-liquid flow. They performed a linear analysis which lead to ordinary differential equations with non-homogeneous boundary conditions. They calculated a resonance phenomenon, leading to an amplification of the wall corrugations on the liquid film surface.

Trifonov [1998] examined the experimental results obtained by Zhao and Cerro [1992] theoretically by solving Navier Stokes and integral equations. He concluded that at low liquid Reynolds numbers the flow is controlled significantly by surface tension forces, while at higher Reynolds numbers the flow is influenced mainly by inertia forces. For low viscosity liquids stagnation points were found to exists in certain ranges of Re_l. These points form in the bottom of a valley between two peaks. The liquid in these stagnation points tend to recirculate. Liquids having a higher viscosity did not form stagnation points (recirculation zones).

2.3.2 Theory

Because of the complex nature of the flow of a liquid phase over a complex surface, let alone countercurrent air flow, it was decided to use the hydrodynamic model for smooth surfaces as described in appendix A. The theory for mass transfer is the same as in section 2.2 of this chapter.

2.3.3 Experimental

The same experimental setup was used as described in section 2.2. The wetted-wall-tube-and-reservoir glass unit was replaced with another unit having a slightly larger diameter glass tube. A sheet of Sulzer 350Y packing material (without holes) was cut and rolled to fit into the glass tube. The bottom and top ends of this sheet was flattened to be able to clamp it onto the inside of the glass tube. A stainless steel ring was machined to fit into the top end of the glass tube and held the packing sheet in place. This ring also ensured uniform wetting of the packing surface. Silicone cement was used to paste the sheet onto

the inside of the glass tube. At 27.3 mm, the diameter of this packing wetted wall column is slightly larger than its smooth counterpart. The inside diameter of the bottom air inlet piece was machined to this diameter. The total length of this column was 106 mm. Two configurations of the microstructure of the packing surface were used. Most of the experimental work was carried out on a staggered configuration while one set of data was obtained using an inline configuration. The two different configurations are shown in figure 2.15. The characteristic dimensions of the surface micro structure are as follows :

Wavelength : 3.75 mm
Amplitude : 0.6 mm

The experimental procedure is the same as discussed in section 2.2.

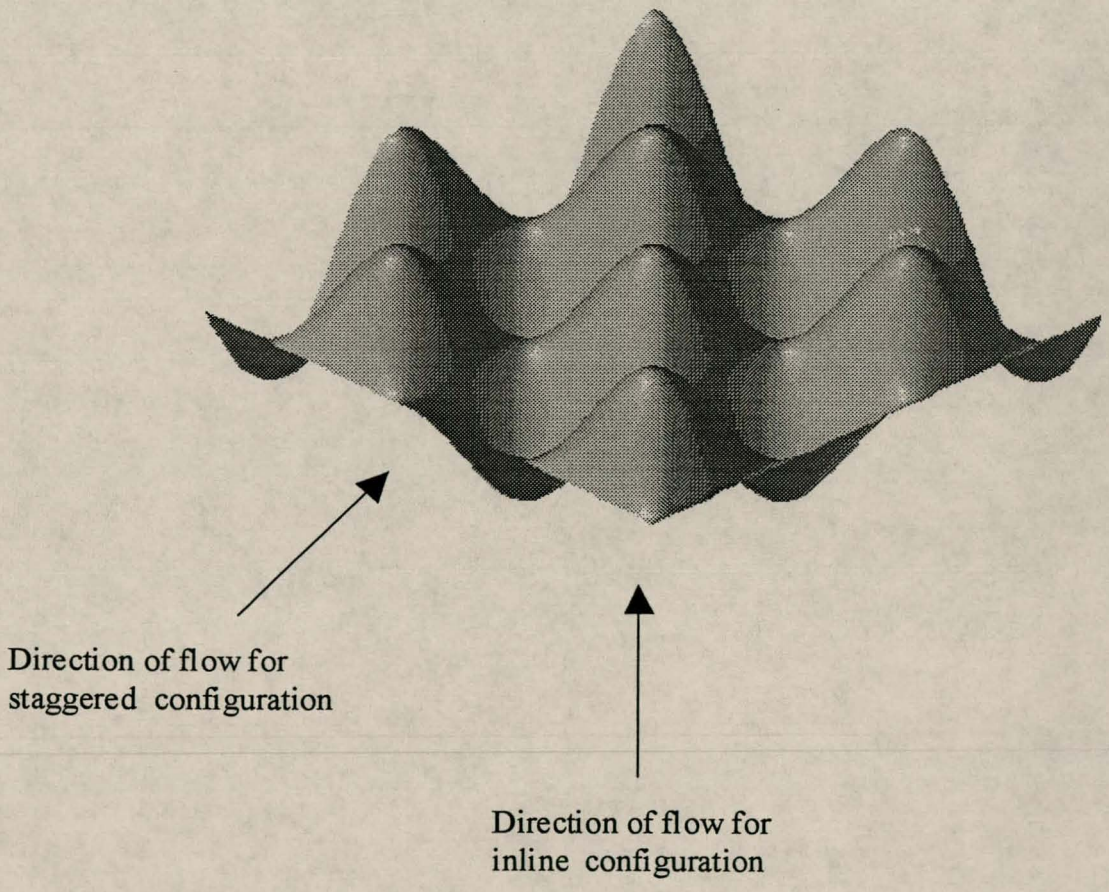

Figure 2.15 Configurations for flow over microstructure of packing

2.3.4 Results

Figure 2.16 show the results for the three pure components used.

The range for various dimensionless numbers and some important properties are as follows :

Sh_g	:	7-50	σ (N/m)	:	0.017-0.021 [N/m]
Re_g	:	1650-6050	μ (Pa.s)	:	$2.61\text{-}5.54\ 10^{-4}$ [Pa.s]
Sc_g	:	0.97-1.93			
Re_l	:	50-200			

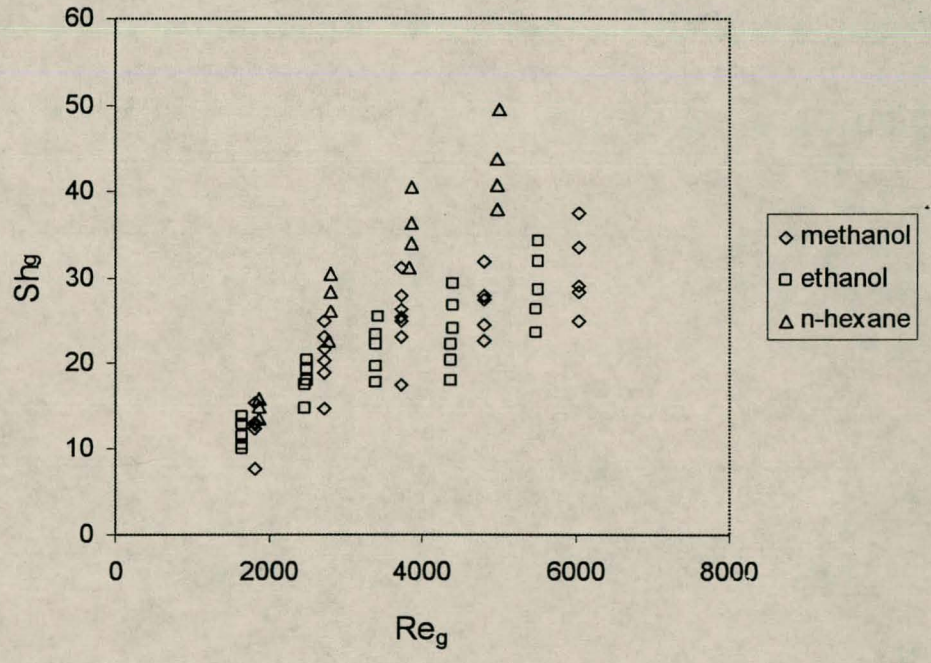

Figure 2.16 Sh_g vs Re_g for different pure components, complex surface (staggered configuration).

The effect that the liquid flow rate has on the rate of mass transfer is shown in figure 2.17. The same trend was observed for the other liquids. Figure 2.18 show the results for the inline- and staggered flow configurations.

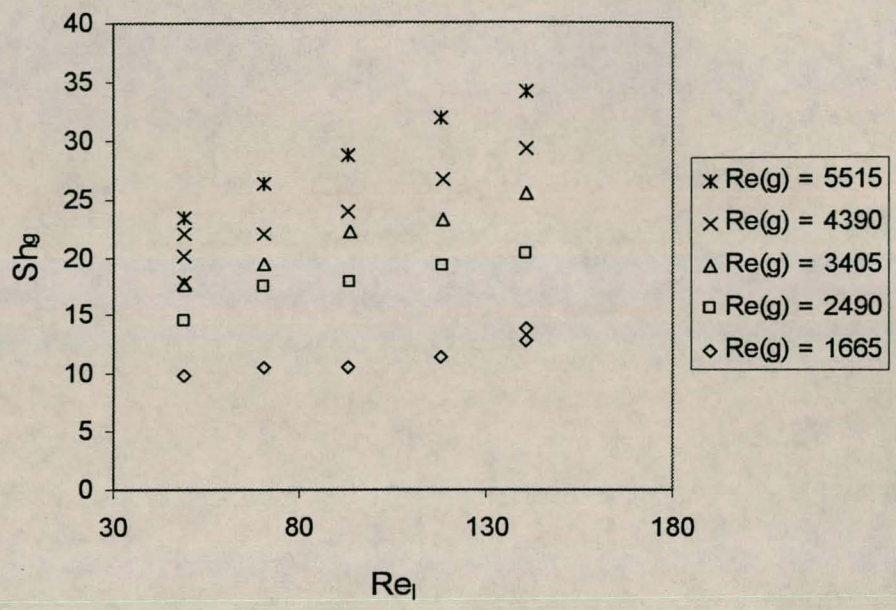

Figure 2.17 Sh_g vs Re_l for ethanol, complex surface (staggered configuration). Re_g=1665-5515, Re_l=50-140.

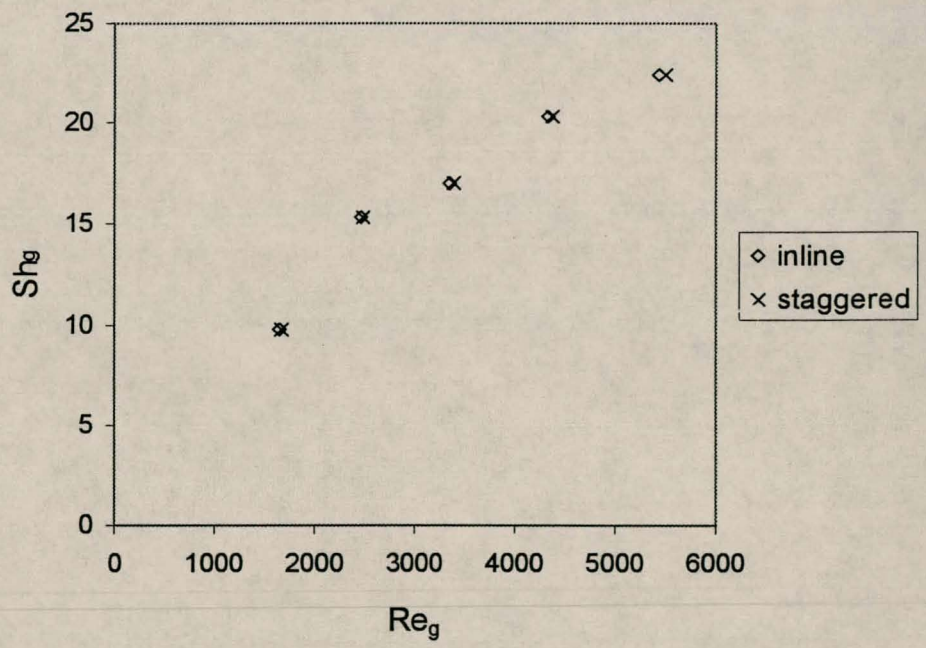

Figure 2.18 Comparison of Sh_g vs Re_g for inline- and staggered configurations for ethanol, Re_l=50.

There is no difference in the rate of mass transfer between these two configurations. It was however found that the surface of the liquid became unstable and breakaway droplets formed for the inline configuration at high liquid flow rates (Re_l>100). For the staggered configuration the liquid flow rate could be increased to $\pm Re_l$=140 without the formation of breakaway liquid droplets.

The correlation developed for smooth surfaces is compared to the experimental data in figure 2.19

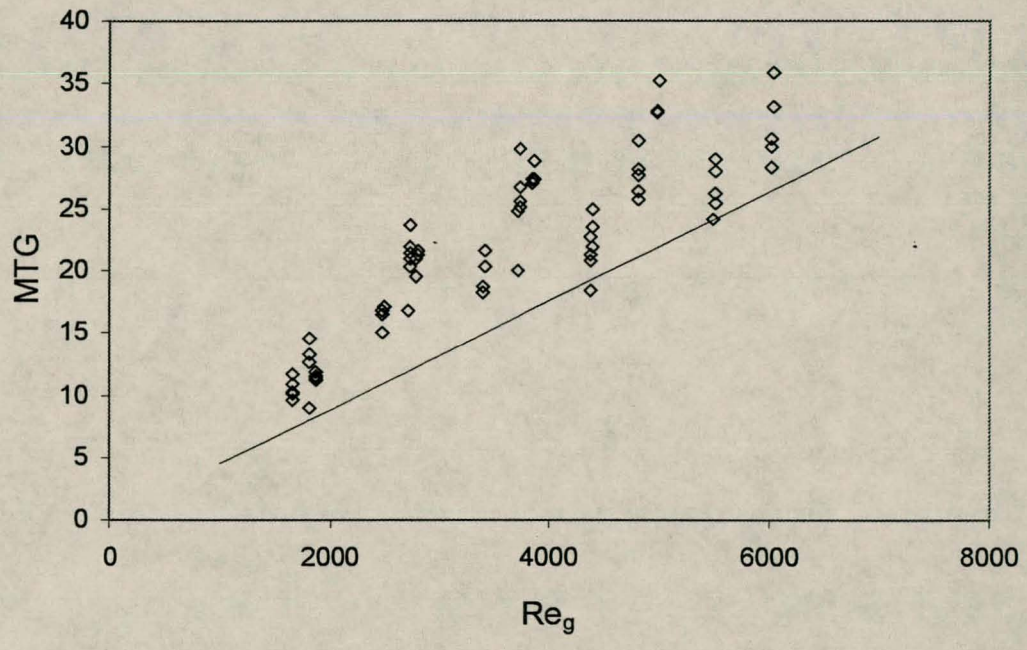

Figure 2.19 Experimental values for complex surface (◇) compared to that predicted by corr. 2.33 (solid line). MTG is defined as $\left(\frac{Sh_g}{Sc_g^{0.5} We_l^{0.111}}\right)$

Figure 2.19 show that correlation 2.33 under predicts the mass transfer rate.

The experimental data was correlated in the same manner and by using the same dimensionless numbers discussed in section 2.3 (see Table 2.1). The capillary number

was included in the correlating procedure because of various investigators' [Shetty & Cerro, 1993; Trifonov, 1998] claim that capillary forces will have an effect on the surface profile of the liquid. The capillary number used in this work is defined as the ratio of surface tension forces to viscous forces and is defined as:

$$Ca = \frac{\sigma}{u\mu} \tag{2.34}$$

The velocity used in the calculation of Ca is the average velocity of the liquid phase, defined by equation A1.12 (see appendix A).

Table 2.3 Results for different correlations, complex surface.

Correlation	a	b	c	d	e	RMS error	r^2
2.35 $Sh_g=aRe_g^bSc_g^c$	0.0413	0.761	0.576	N/A	N/A	4.417	0.738
2.36 $Sh_g=aRe_{g,r}^bSc_g^c$	0.0069	0.958	0.615	N/A	N/A	3.744	0.812
2.37 $Sh_g=aRe_g^bSc_g^cRe_l^d$	0.0067	0.772	0.618	0.364	N/A	2.158	0.937
2.38 $Sh_g=aRe_g^bSc_g^cWe_l^d$	0.0375	0.776	0.755	0.21	N/A	2.968	0.882
2.39 $Sh_g=aRe_{g,r}^bSc_g^cBo^d$	0.0776	0.769	0.720	0.184	N/A	4.198	0.763
2.40 $Sh_g=aRe_g^bSc_g^cFr_l^d$	0.0099	0.772	0.619	0.365	N/A	2.158	0.937
2.41 $Sh_g=aRe_g^bSc_g^cRe_l^dBo^e$	0.0047	0.752	0.547	0.393	-0.099	2.069	0.943
2.42 $Sh_g=aRe_g^bSc_g^cCa_l^d$	0.095	0.769	0.720	-0.184	N/A	4.196	0.764
2.43 $Sh_g=aRe_g^bSc_g^cRe_l^dCa_l^e$	0.0078	0.781	0.645	0.355	-0.038	2.240	0.933

$$\text{RMS error} = \sqrt{\frac{\left(Sh_{experimental} - Sh_{predicted}\right)^2}{n}}$$

2.3.5 Discussion of results

It was again found that Sh_g is dependant on the liquid flow rate. Figure 2.17 shows that quite clearly. It was also found that the liquid flow rate influences the mass transfer rate at lower Re_g than for the smooth surface. For the smooth surface the slope of Sh_g vs Re_l is smaller at low Re_g (<2700) than for the complex surface (see figure 2.5 and 2.17). A possible explanation for this might be the formation of stagnant and recirculating pockets of air in the valleys between peaks for the complex surface at low Re_g. At higher liquid flow rates these pockets no longer exist due to a flatter surface profile [Zhao & Cerro, 1992]. This will explain the increase in the rate of mass transfer with liquid flow rate. This argument will also be true for the smooth surface were the liquid film surface profile is wavy. It must be remembered however that the wavy interface extends for the entire length of the column in the case of the complex surface at low flow rates.

Figure 2.20 compares Sh_g vs Re_g for smooth- and complex surfaces. The data is for n-hexane at a constant liquid flow rate (relatively low, $Re_l \approx 70$). The sharp increase of Sh_g with Re_g for the complex surface, above that measured for smooth surfaces, may be caused by the onset and increase in interfacial turbulence with an increase in Re_g. This has a more profound effect on the complex surface because the surface profile of the liquid film is wavy for the entire length of the column, especially at low liquid flow rates. This waviness is induced and cannot 'fall flat' as in the case of flat surfaces.

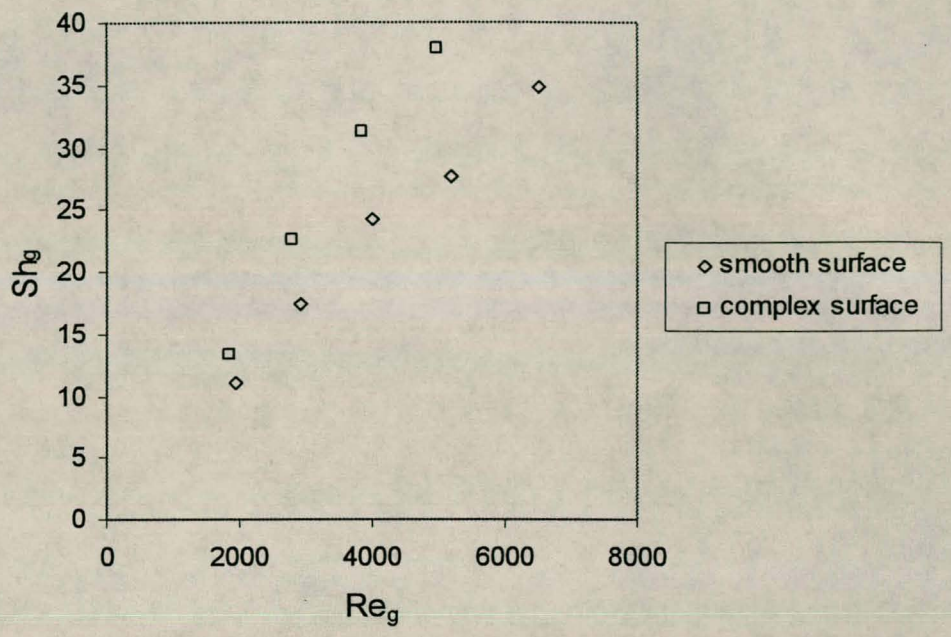

Figure 2.20 Sh_g vs Re_g for n-hexane. Re_l(smooth)=75, Re_l(complex)=67.

The formation of breakaway droplets in the inline configuration at higher Re_l might be explained by the mean film thickness and the average surface velocity of the liquid phase. The mean thickness of the liquid film in this type of configuration is thought to be smaller than in the staggered configuration, with most of the volume of the liquid flowing in the channels between inline peaks (see figure 2.15). The thickness of these films is comparable to that of a smooth surface. The staggered configuration induce liquid spreading and therefore the volume of the liquid film is more uniformly spread over this configuration. The mean thickness of these films is greater than for smooth surfaces and the average free surface velocity is smaller [Zhao & Cerro, 1992]. It follows that for an increase in the liquid flow rate the average surface velocity of the liquid film will reach the critical value for breakaway sooner in the inline configuration than in the staggered configuration.

It is apparent from figure 2.19 and 2.20 that there is a definite increase in the rate of mass transfer compared to that predicted for smooth surfaces. This is thought to be caused by both an increase in the effective area for mass transfer and an increase in interfacial

turbulence. Both these phenomena are a direct consequence of the wavy surface profile of the liquid phase induced by the packing surface.

Table 2.3 show that correlation 2.41 gave the best fit on the experimental data. Correlations 2.37 and 2.40 gave the same rms error value. The difference between these two correlations is the liquid flow term. Correlation 2.37 uses the liquid Reynolds number while correlation 2.40 uses the liquid Froude number. In section 2.2 of this chapter it was found that both the viscosity and the surface tension has an effect on the mass transfer rate. Because of the small range in viscosity and surface tension of the experimental liquids, it is not surprising that the Froude number accurately represents the effect of the liquid phase on the mass transfer rate. It is however doubtful that this will be the case with liquids having a viscosity and surface tension outside the range of the liquids used in fitting the correlation.

It was found that a correlation with a dimensionless liquid flow term containing only the surface tension, like the Weber number used in section 2.2, did not accurately fit the data (correlation 2.38). A correlation containing only the Capillary number for the liquid phase did not give a reasonable fit (correlation 2.42). A correlation containing both the liquid Reynolds- and Capillary numbers (correlation 2.43), similar to that used by Shetty and Cerro [1993] in their work on hydrodynamics, gave a reasonable fit. It did however not improve on correlation 2.41.

It is assumed that correlation 2.41 best describes the mass transfer data measured in this work for liquid films flowing down a complex surfaces. This correlation is plotted with the experimental data in figure 2.21.

In figure 2.22 the experimental data is plotted with correlation 2.36. This correlation will be used in chapter 4.

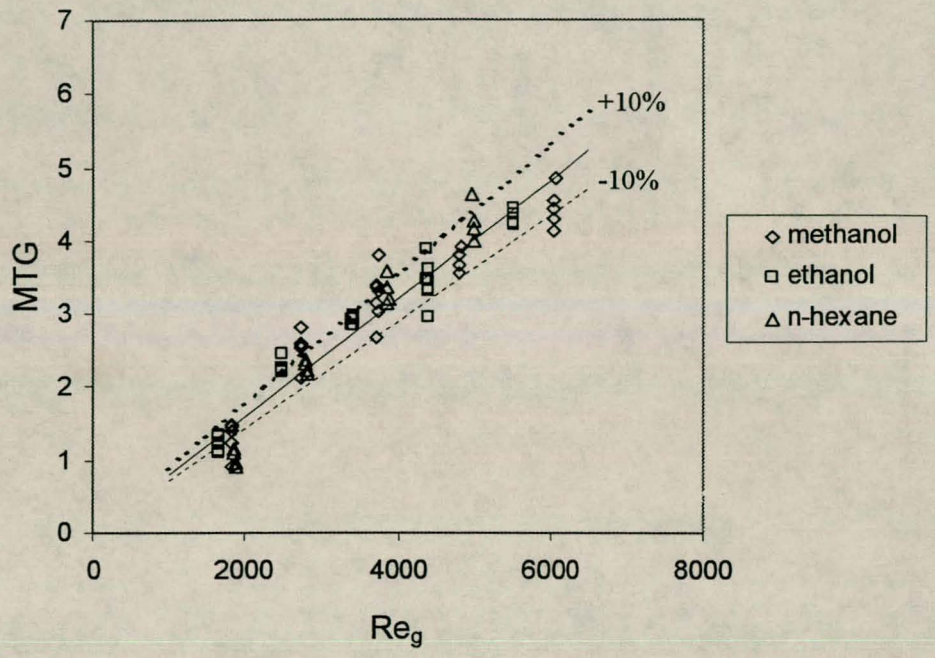

Figure 2.21 Plot of experimental data and correlation 2.41 (—). MTG is defined as $\left(\frac{Sh_g}{Sc_g^{0.547}\,\mathrm{Re}_l^{0.393}\,Bo^{-0.1}} \right)^{\frac{1}{0.75}}$. Confidence interval is also shown.

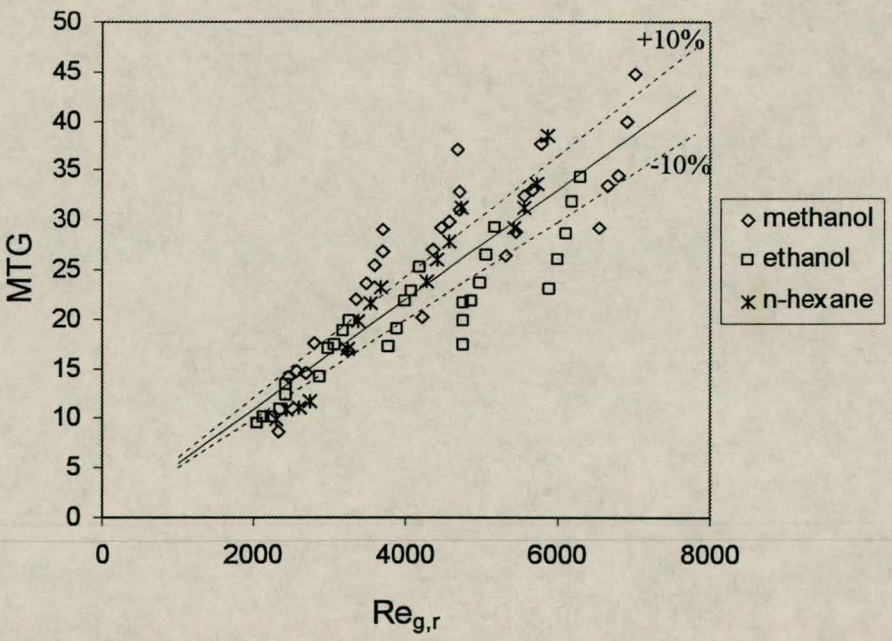

Figure 2.22 Plot of experimental data and correlation 2.36 (—). MTG is defined as $\left(\frac{Sh_g}{Sc_g^{0.615}} \right)^{\frac{1}{0.958}}$. Confidence interval is also shown.

If the exponent of the gas phase Schmidt number in correlation 2.41 is set equal to the theoretical value (0.5), and the remaining of the constants regressed on the experimental data, the error value is not increased by much. The proposed correlation is as follows:

$$Sh_g = 0.0036\,\mathrm{Re}_g^{\,0.76}\,Sc_g^{\,0.5}\,\mathrm{Re}_l^{\,0.41}\,Bo^{-0.13} \qquad (2.44)$$

The exponent of the dimensionless liquid flow terms (Re_l and Bo) is larger than for the smooth surface (section 2.2). This is to be expected since the mass transfer rate was found to be much more dependent on the liquid flow rate. The theoretical view of Trifonov [1998] on the hydrodynamics of the liquid film is supported by the inclusion of both a dimensionless number containing the surface tension and a dimensionless number containing viscosity.

2.3.6 Conclusions

- Higher mass transfer rates were measured than for smooth surfaces. This is caused by both an increase in the effective surface area and interfacial turbulence.
- The effective surface area and the increase in interfacial turbulence is linked to the wavy surface profile of the liquid phase induced by the packing surface. This profile is influenced by the liquid flow rate.
- Both an inline and a staggered configuration of the surface profile were investigated. For the inline configuration it was found that at Re_l>100 the surface became unstable with breakaway droplets forming. No difference in the mass transfer rate was observed for the two configurations
- The mass transfer rate was found to be much more dependent on the liquid flow rate than for smooth surfaces.

- After setting the exponent of the Schmidt number equal to the theoretical value of 0.5, the mass transfer from a liquid film flowing over a Sulzer 350Y type complex surface could be correlated by :

$$Sh_g = 0.0036\,\mathrm{Re}_g^{\,0.76}\, Sc_g^{\,0.5}\, \mathrm{Re}_l^{\,0.41}\, Bo^{-0.13}$$

and is valid for $1650 < \mathrm{Re}_g < 6050$ and $50 < \mathrm{Re}_l < 200$

CHAPTER 3 Liquid phase mass transfer

3.1 Introduction

In most conventional distillation applications the liquid phase resistance to mass transfer is considered to be negligible. The same assumption can not be made in extractive distillation applications where there is usually a substantial difference in the physical properties between the solvent and the solute. This chapter will deal with the problem of estimating this resistance, if any. It will also show that in some instances considerable enhancement of the overall mass transfer coefficient is possible.

3.2 Literature review

Numerous studies have been made in the past on liquid side resistance in mass transfer. In most of the earlier papers [Emmert & Pigford, 1954; Stirba & Hurt, 1955; Vivian & Peaceman, 1956] liquid side mass transfer coefficients were found to be much higher than predicted by penetration theory. This was attributed to the increase in surface area due to surface waves. In the more recent papers [Barrdahl, 1988; Wasden, 1990; Yoshimura, 1996] most of the effort has been concentrated on trying to model the surface waves and their effect on the liquid phase mass transfer rate. This was done with limited success. The study by Yoshimura et al. [1996] was the most successful. They developed a double boundary layer model for controlled wave disturbances. The problem of quantifying the enhanced mass transfer rate caused by irregular distorted three-dimensional waves still remains to be solved. In all these articles most of the experimental work concentrated on the adsorption of sparingly soluble gases in water.

Numerous investigators [Brian, 1971; Imaishi, 1982; Golovin, 1992; Vazquez, 1996; Lu, 1997] have investigated the influence of the Marangoni effect on the liquid phase mass transfer. The Marangoni effect, a special case of interfacial turbulence, is observed when solutes are desorbed from solvents having a substantially higher surface tension.

Little work has been done on determining the liquid side resistance to mass transfer in conventional- and extractive distillation systems. There seems to be a general agreement that the liquid side resistance is negligible in conventional systems [Jackson & Ceaglske, 1950; Spiegel & Meier, 1987]. Bravo et al. [1990] argued that in some instances this resistance is significant.

Crause [1998] investigated the liquid side resistance in extractive distillation systems. This was done by evaporating binary liquid mixtures that consist of a volatile and a non-volatile liquid in a wetted-wall column. No liquid side resistance to mass transfer was observed. A definite overall mass transfer enhancement was observed in most of the binary systems investigated. Although this was attributed to surface tension gradients in the liquid film, no correlation could be obtained between the observed enhancement and the Marangoni number.

In light of the conflicting views of different investigators [Bravo et al., 1990; Spiegel & Meier, 1987] and in order to confirm the conclusions made by Crause [1998] for extractive distillation systems, the liquid side resistance was investigated for binary liquid mixtures with one and both components volatile. This was done for both smooth and complex surfaces.

3.3 Theory

The theory dealing with mass transfer across a phase boundary where the resistance in both phases are significant, is dealt with in chapter 4. The final form of the equation relating the overall mass transfer coefficient to the individual mass transfer coefficient is as follows:

$$\frac{1}{k_{og}} = \frac{1}{k_g} + \frac{m}{k_l} \qquad (3.1)$$

m is the slope of the equilibrium line and is defined as [Nieuwoudt, 1994]:

$$m = \frac{y_A}{x_A}\left(\frac{M_{r,l}}{M_{r,g}}\right)\left(\frac{\rho_g}{\rho_l}\right) \tag{3.2}$$

y_A is calculated as P_{Ai}/P_t. P_{Ai} is the vapour pressure of component A corresponding to the mole fraction of x_A in the liquid phase and is calculated with the NRTL equation. The overall mass transfer coefficient is defined as (see chapter 2):

$$N_A = k_{og}\frac{P_t \Delta P_A}{RTP_{Bm}} \tag{3.3}$$

$$\text{with } \Delta P_A = \frac{(P_{Ai} - P_{Ab})_{inlet} - (P_{Ai} - P_{Ab})_{exit}}{\ln\left(\frac{(P_{Ai} - P_{Ab})_{inlet}}{(P_{Ai} - P_{Ab})_{exit}}\right)} \tag{3.4}$$

P_{Ab} is the free stream partial pressure of component A.

For binary mixtures with only one volatile component, the molar flux is simply the total mass evaporated. In binary mixtures where both components are volatile, the estimation of the molar flux for each component is complicated somewhat. Crause [1998] has shown that for a binary mixture of component A and C evaporating into a gas B, the mole fraction of A (based on the total evaporation rate) that evaporates is given by

$$z_A = \frac{y_{Ai}}{y_{Ai} + Ky_{Ci}} \tag{3.5}$$

K is a ratio of the gas phase diffusion coefficients:

$$K = \left(\frac{D_{CB}}{D_{AB}}\right)^c \tag{3.6}$$

The analysis was done assuming that at low mass transfer rates the fluxes of the two components are independent. The exponent c in equation 3.6 is equal to the exponent of the Schmidt number in the gas phase mass transfer correlation. In this work this exponent is assumed to be equal to the theoretical value of 0.5 (see chapter 2).

In binary systems where there is a substantial difference between the surface tensions of the components, the Marangoni number is often used to correlate the observed enhancement. Imaishi et al. [1982] defines the Marangoni number as:

$$Ma = \frac{(\sigma_i - \sigma_L)}{\mu k_l} \tag{3.7}$$

The surface tension of the liquid at the interface, σ_i, is calculated for the interfacial concentration, C_{li}, calculated from:

$$C_{li} = \frac{C_l}{(1+B)} \tag{3.8}$$

B is a ratio of the mass transfer resistances in the liquid and the gas phases and is given by:

$$B = \frac{mk_g}{k_l} \tag{3.9}$$

The liquid side resistance in equation 3.9 is calculated using the penetration theory of Higbie. For a wetted wall column, the liquid phase mass transfer coefficient is given by [Emmert & Pigford, 1954]:

$$k_l = 2\sqrt{\frac{D_A u_i}{\pi z}} \tag{3.10}$$

The gas phase mass transfer coefficient in equation 3.9 is calculated from equation 2.33 for smooth surfaces and equation 2.36 for complex surfaces.

To investigate whether the liquid side resistance is significant, the experimental overall mass transfer coefficient calculated from equation 3.3 is compared to the predicted value. The gas phase mass transfer coefficient is estimated with equations 2.33 and 2.36 and the liquid phase mass transfer coefficient with equation 3.10. The predicted overall mass transfer coefficient is then calculated with equation 3.1.

It will be assessed whether the observed enhancement, if any, is a function of the Marangoni number (equation 3.7). The observed overall mass transfer coefficient is also compared to the case of zero liquid phase resistance.

3.4 Experimental

The same apparatus described in section 2.2.3 was used in the experimental work. Several binary mixtures were evaporated at low evaporation rates. This was done in order to minimize the change in liquid composition and simplify the analysis. The total volume of liquid in the experimental setup was approximately 1550 ml for the smooth surface wetted wall assembly and approximately 1450 ml for the complex surface wetted wall assembly. The maximum amount of liquid evaporated during a run was approximately 50 ml. The maximum change in liquid concentration for binary mixtures with one volatile component is therefore 10% for the complex surface setup. An average concentration is used in the calculations. In order to maintain a constant liquid concentration for a series of runs, the liquid reservoir was topped up with the volatile component after each run.

The change in composition during an experimental run for binary mixtures with both components volatile are negligible. After each run the liquid reservoir was topped up with the binary mixture used to fill the apparatus at start up. After every second run a sample was drawn from the liquid reservoir. GC analysis provided the composition of these samples. The average composition of the liquid for each experimental run was determined by linear interpolation between the sampling points.

3.5 Smooth surface

3.5.1 Results

The binary mixtures investigated with one volatile component are methanol/ethylene glycol, methanol/1-octanol, ethanol/tridecane, and n-hexane/tridecane. Binary mixtures with both components volatile are methanol/ethanol and acetone/methanol.

Figure 3.1 show the result of the experimental and predicted mass transfer coefficients for the binary system methanol/ethylene glycol. VLE data for this system was obtained from the SIMSCI databank in the simulation package Pro II.

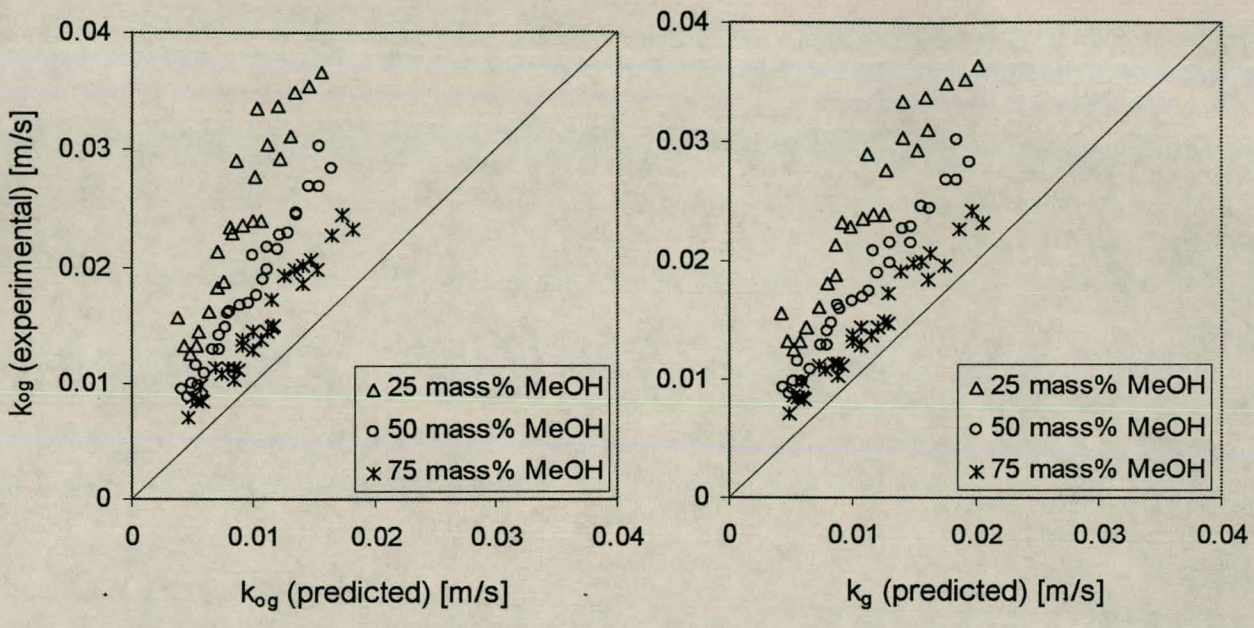

Figure 3.1 Plot of measured k_{og} vs (a) predicted k_{og} and (b) predicted k_g for methanol/ethylene glycol. Re_g=1950-6490, Re_l=6-91.

Figure 3.2 show the same results for the binary system methanol/1-octanol.

In figure 3.3 the results are shown for the system ethanol/tridecane. The tridecane used in these experiments was distilled from a heavy paraffin cut containing approximately 60% tridecane. The final product had a purity of approximately 95% tridecane. Since no experimental VLE data could be obtained in literature for this system, the binary interaction parameters for the NRTL model were estimated by making use of the UNIFAC group contribution method in the simulation package Pro II. This was also done for the system methanol/1-octanol.

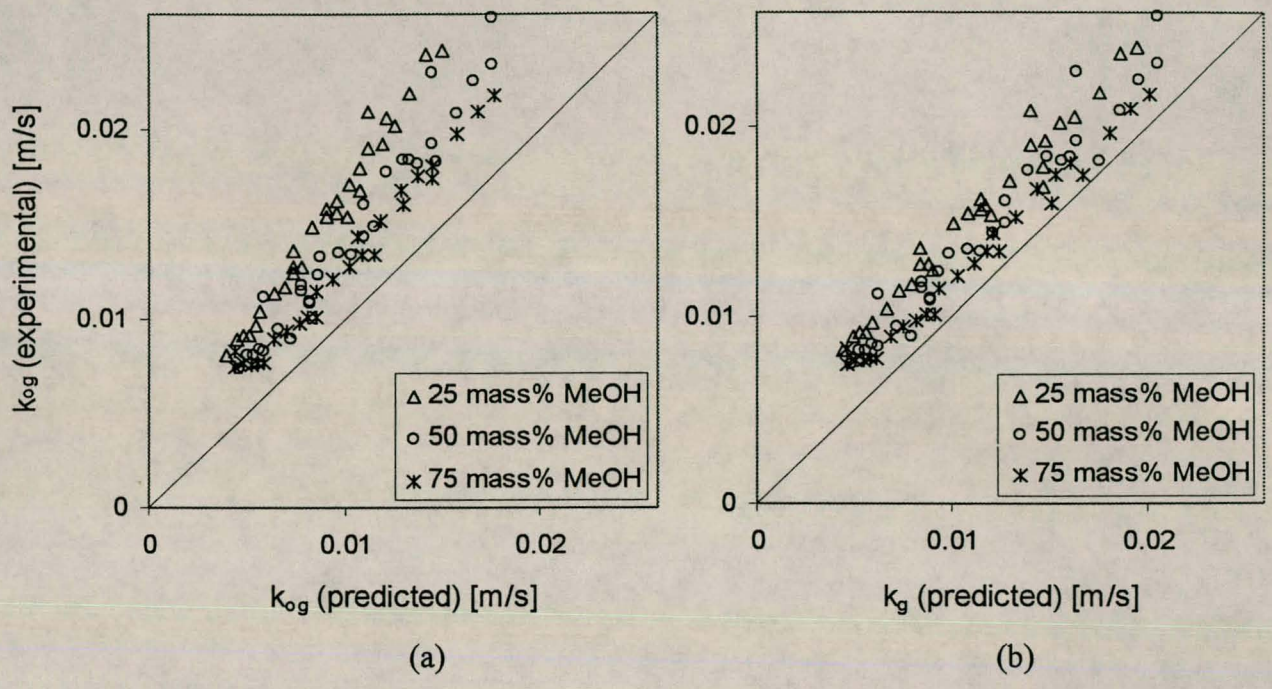

Figure 3.2 Plot of measured k_{og} vs (a) predicted k_{og} and (b) predicted k_g for methanol/1-octanol. Re_g=1950-7240, Re_l=18-142.

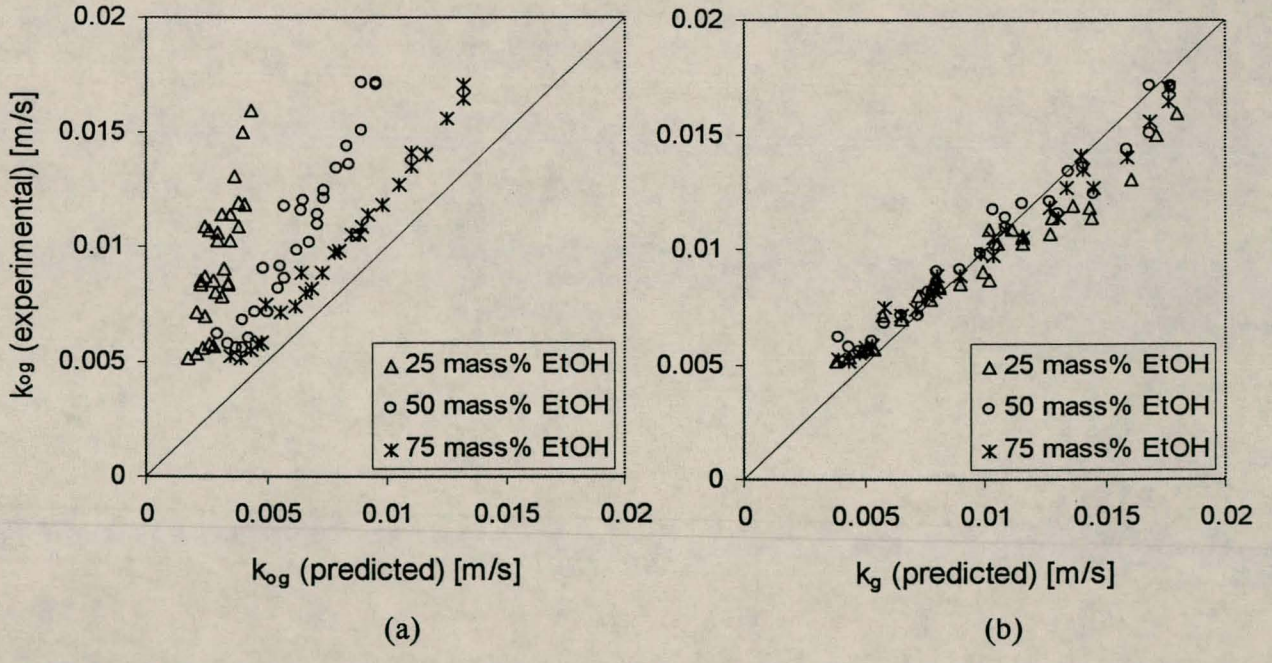

Figure 3.3 Plot of measured k_{og} vs (a) predicted k_{og} and (b) predicted k_g for ethanol/tridecane. Re_g=1945-6480, Re_l=19-103.

Figure 3.4 show the results for the binary system n-hexane/tridecane. The n-hexane used in these experiments was distilled from a light paraffin cut containing approximately 70% n-hexane. The final product had a purity of approximately 98% n-hexane. The tridecane had the same purity as mentioned above. Again no VLE data was available in literature or the SIMSCI databank for this binary system. The binary interaction parameters for the NRTL model were also estimated from the UNIFAC group contribution method in Pro II.

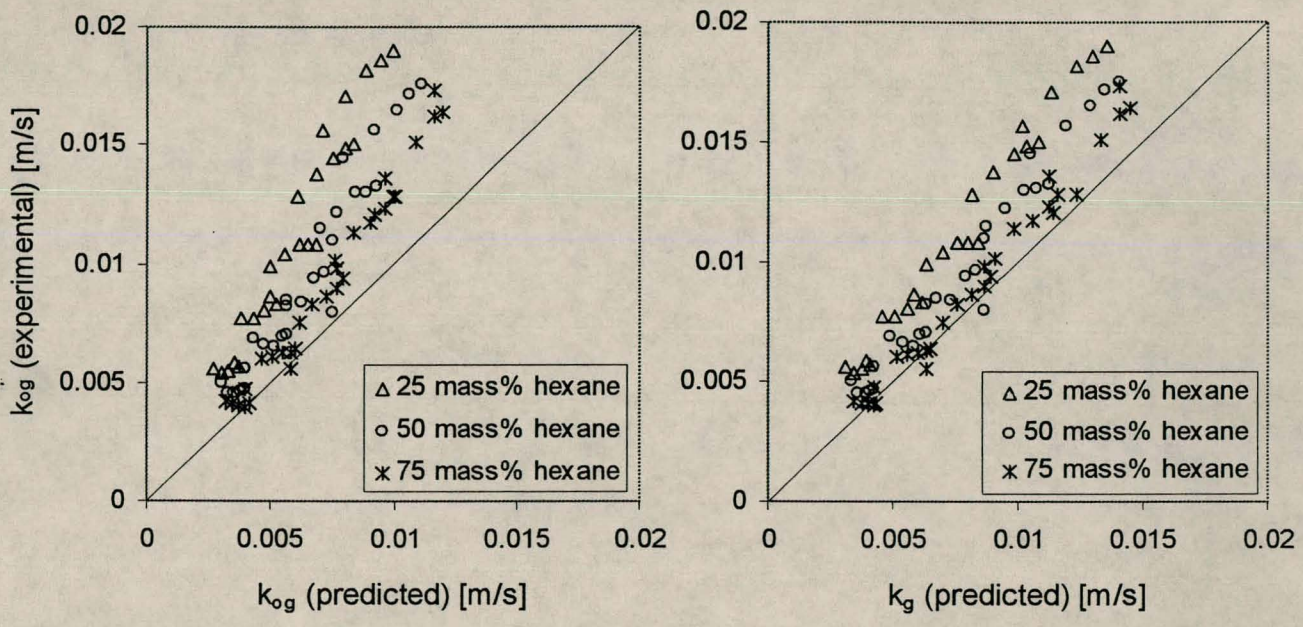

(a) (b)

Figure 3.4 Plot of measured k_{og} vs (a) predicted k_{og} and (b) predicted k_g for n-hexane/tridecane. Re_g=2215-7360, Re_l=15-165.

The results for the binary systems with both components volatile are presented in the same format. Figure 3.5 show the results for the binary system acetone/methanol. The composition in the liquid phase is near to the azeotropic composition (89.5 mole % acetone @ 37.1°C). Since the azeotropic composition is used, the liquid composition does not change and no liquid resistance exists.

Figure 3.6 show the result for the binary mixture methanol/ethanol at an average methanol concentration of 51 mole %.

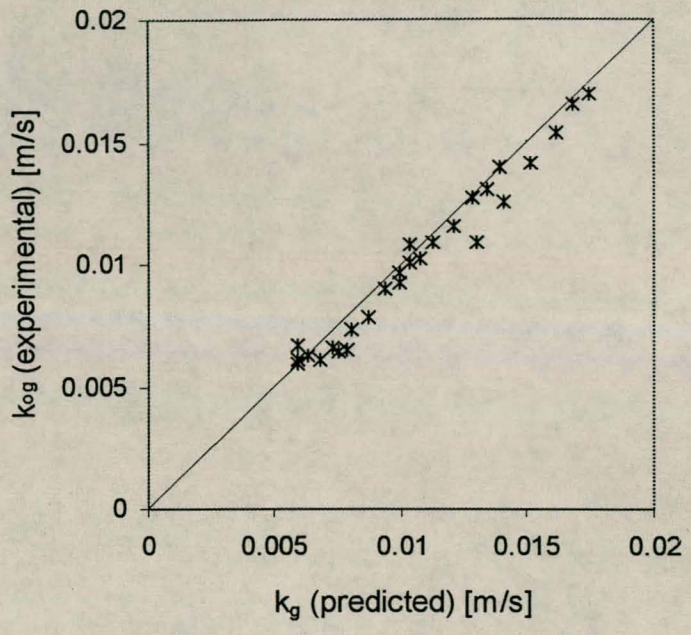

Figure 3.5 Plot of measured k_{og} vs predicted k_g for acetone in a binary mixture of acetone/methanol containing 89.5 mole% acetone. Re_g=3020-6720, Re_l=66-297.

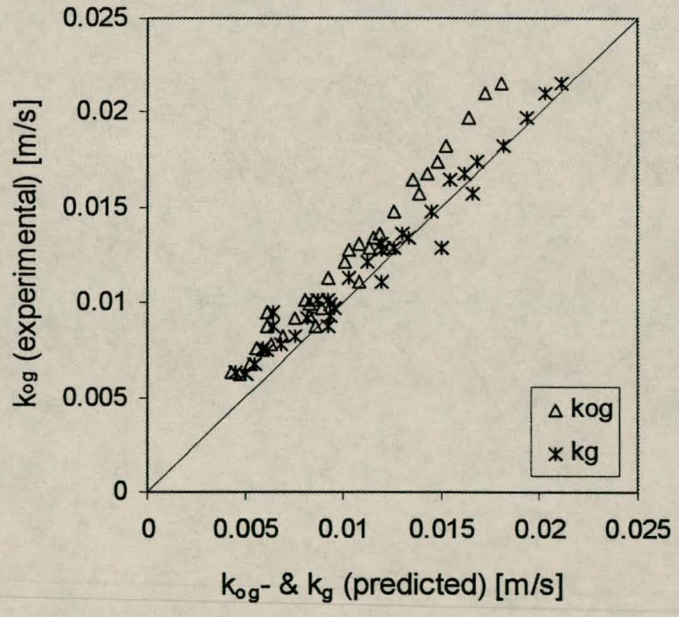

Figure 3.6 Plot of measured k_{og} vs predicted k_{og} and k_g for methanol in a binary mixture of methanol/ethanol containing 51 mole % methanol. Re_g=1870-6180, Re_l=28-155.

A summary of all the experimental results are given in appendix C.

3.5.2 Discussion of results

It is evident from figures 3.1(a) through to figure 3.6(a) that the liquid side resistance, calculated with Higbie's penetration theory, is negligible in the binary systems investigated. This conclusion can be made because in all the plots of k_{og} (experimental) versus k_{og} (predicted) the points lie above the diagonal, i.e. the experimental measured k_{og} is higher than the predicted k_{og} (see section 3.3).

What is surprising to see is that in most of the binary systems with one volatile component, the measured k_{og} is higher than the predicted k_g. Crause [1998] has also observed this phenomena. For the system methanol/ethylene glycol the measured mass transfer coefficient is much higher than the predicted value at low concentrations of methanol (see figure 3.1 (b)). This also seems to be true for the n-hexane/tridecane system (figure 3.4 (b)).

For the system methanol/1-octanol (figure 3.2(b)) there is some enhancement of the measured value over the predicted value, although it is not as composition dependant as in the methanol/ethylene glycol and n-hexane/tridecane systems.

The binary system ethanol/tridecane is an exception. At low mass transfer rates there is good agreement between the measured and predicted mass transfer coefficients (see figure 3.3 (b)). At higher mass transfer rates some liquid side resistance develop, but it is much smaller than predicted by penetration theory. It must however be mentioned that the binary interaction parameters used in the NRTL equation to calculate the volatile component's vapour pressure, were estimated using the UNIFAC method. Experimental vapour/liquid equilibrium data will verify whether the observed resistance is meaningful.

In the binary systems with both components volatile there are close agreement between the measured overall gas phase mass transfer coefficient (k_{og}) and the predicted gas phase mass transfer coefficient (k_g) (figure 3.5 and 3.6). Both these figures are for the component which form the bulk of the evaporating mixture (the more volatile component). The methanol/ethanol system investigated had a liquid phase methanol concentration of 51 mole%. The concentration of methanol in the gas layer next to the interface in equilibrium with the liquid phase is 66 mole% at the experimental conditions. The acetone/methanol system investigated had a liquid phase concentration of approximately 89.5 mole% acetone. Since this concentration is close to the azeotropic point the concentration of the acetone in the gas layer next to the interface is almost the same. In both instances the concentration of the more volatile component (methanol, acetone) is much higher than that of the less volatile component (ethanol, methanol). It is therefore a good approximation to assume the flux of the more volatile component independent of the flux of the less volatile component. The opposite is however not true. In order to evaluate the gas phase mass transfer coefficient for the less volatile component, the molar flux of the two components will have to be coupled. This falls outside the scope of this work and the reader is referred to the literature [Taylor & Krishna, 1993].

A mass transfer enhancement factor is defined to try and correlate the observed enhancement with some physical property(s). The enhancement factor is defined as:

$$F = \frac{k_{og}(measured)}{k_g(predicted)} \tag{3.11}$$

Table 3.1 shows the enhancement factors for the binary mixtures containing one volatile component.

Table 3.1 Enhancement factors for binary mixtures containing one volatile component (smooth surface).

System	mass % (volatile component)	Viscosity [Pa.s] $\times 10^4$	Surface tension [N/m]	F
Methanol/ ethylene glycol	25	30.1	0.037	2.27
	50	13.5	0.030	1.67
	75	7.1	0.025	1.32
Methanol/ 1-octanol	25	8.3	0.024	1.44
	50	5.4	0.023	1.28
	75	4.6	0.022	1.23
Ethanol/ tridecane	25	6.0	0.021	1.00
	50	5.6	0.021	1.05
	75	5.5	0.020	1.02
n-Hexane/ tridecane	25	7.9	0.022	1.48
	50	5.0	0.020	1.23
	75	3.5	0.018	1.08

The enhancement factors shown in table 3.1 were calculated as the average for a specific composition. The surface tension for the volatile components under the experimental conditions were as follow:

Methanol : 0.021 N/m
Ethanol : 0.019 N/m
n-Hexane : 0.016 N/m

A possible explanation for the enhancement is the Marangoni effect (see section 3.2). Since no liquid side resistance could be detected in the systems investigated, it is believed that the Marangoni effect might enhance the gas phase mass transfer rate by causing interfacial turbulence. No difference could however be detected in the appearance of the liquid surface between different concentrations of the solute, as observed by Crause [1998]. In figure 3.7 the enhancement is compared with the Marangoni number. From this figure it is clear that there is no correlation between the observed enhancement and Ma.

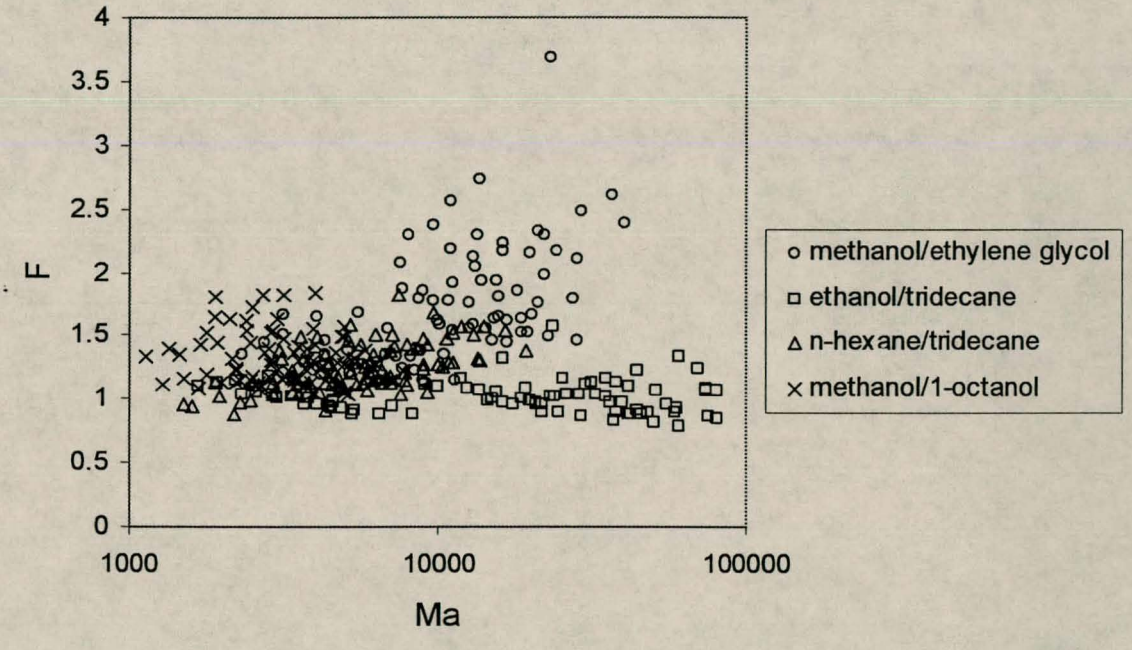

Figure 3.7 Plot of enhancement (F) vs Ma for different binary mixtures.

There are however some difficulties involved when calculating the Marangoni number [Crause, 1998]:

- The liquid side resistance was calculated using Higbie's penetration theory which was developed for laminer flow. No correlation exists for turbulent conditions. (The logic behind the use of Higbie's theory is that it will estimate k_l within an order of magnitude for the different systems.)

- The liquid phase diffusion coefficient is required. The accuracy of existing correlations is doubtful.
- In order to calculate the interfacial surface tension, the concentration gradient in the liquid phase must be known.

The Marangoni number fails to predict the observed enhancement but there do however seem to be a link between the surface tension and the enhancement. Figure 3.8 show the effect of the quantity ($\sigma_{mixture} - \sigma_{volatile}$) on F (from table 3.1).

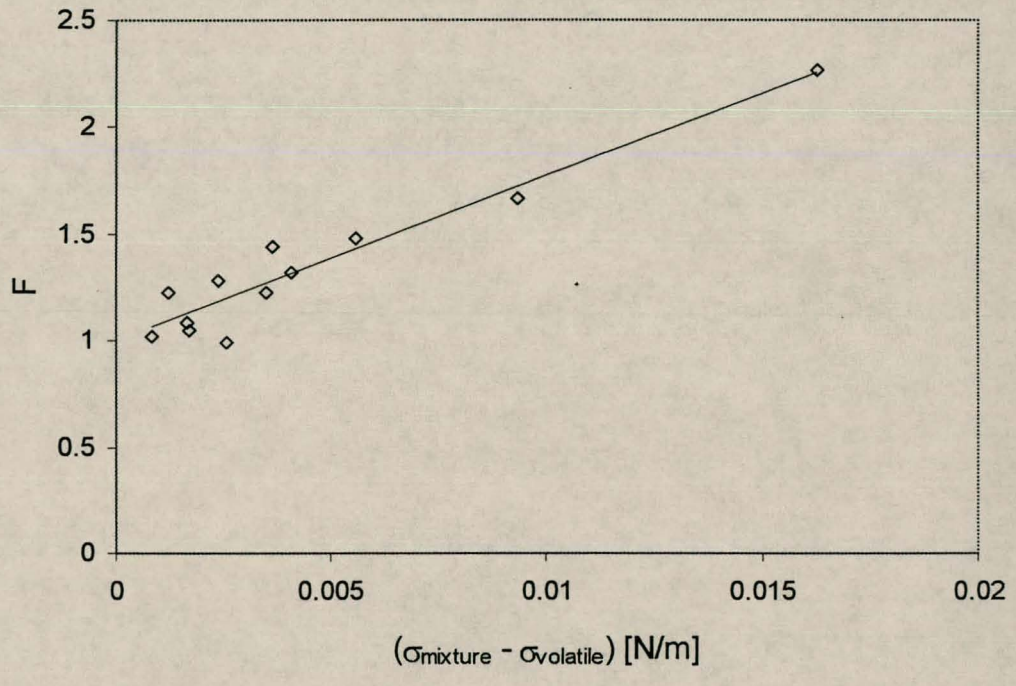

Figure 3.8 Enhancement (F) vs. ($\sigma_{mixture} - \sigma_{volatile}$)

The straight line in figure 3.8 gives a reasonable fit to the data with r^2=0.92. Care must however be taken when evaluating these results. The correlation developed in chapter 2 under predicts the mass transfer rate substantially for 1,2-propanediol. If it is assumed that the binary diffusion coefficient used in calculating Sh for 1,2-propanediol is correct (see chapter 2), then it can be concluded that correlation 2.33 will under predict the mass transfer rate for liquids having a viscosity higher than the experimental range (2.51-7.65 10^{-4}Pa.s). The viscosity of the 25- and 50 mass% methanol/ethylene glycol mixtures fall

well outside the experimental range (see table 3.1). The enhancement calculated for the 25- and 50 mass% methanol/ethylene glycol mixtures will therefore not be solely because of the surface tension gradient. The higher viscosity will also influence the calculated enhancement.

In order to eliminate this uncertainty these two points are eliminated in figure 3.9.

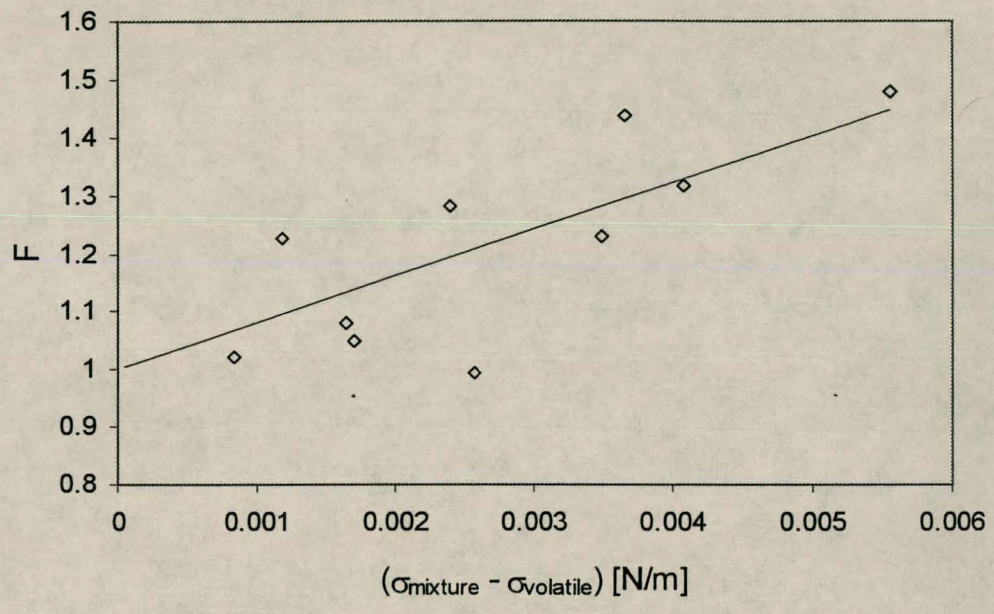

Figure 3.9 Enhancement (F) vs. ($\sigma_{mixture} - \sigma_{volatile}$)

Figure 3.9 show a scatter in the data at low differences in surface tension. For differences higher than 3.5 mN/m there seem to be an upward trend.

The conclusion can be made that the observed enhancement is coupled to the difference in surface tension between the solute and the solvent. It may be that liquid phase mass transfer coefficients calculated with Higbie's penetration theory are faulty and masks this effect (surface tension difference) in the Marangoni number. This is supported by the results obtained for the binary mixtures with both components volatile. Since there is almost no difference in the surface tension of the components in both the

acetone/methanol and methanol/ethanol mixtures, it is expected that F≈1. This was indeed found to be the case with F=1.1 for acetone/methanol and F=1.06 for methanol/ethanol (see figure 3.5 and 3.6).

The reason behind the enhancement observed when there is a substantial difference in the surface tension of solute and solvent is still uncertain. It is believed that this difference will cause some kind of hydrodynamic instability at the interface which will lead to interfacial turbulence in the gas phase. It is possible that this instability will be in the form of surface waves which may also increase the mass transfer area.

3.6 Complex surface

3.6.1 Results

For complex surfaces, the investigation of liquid side resistance was limited to binary mixtures with one volatile component. The mixtures investigated were methanol/ethylene glycol and n-hexane/tridecane. For a summary of the results see appendix C.

Figure 3.10 show the results for the binary mixture methanol/ethylene glycol. Figure 3.11 show the results for n-hexane/tridecane. The predicted gas phase mass transfer coefficient (k_g) is calculated with equation 2.36.

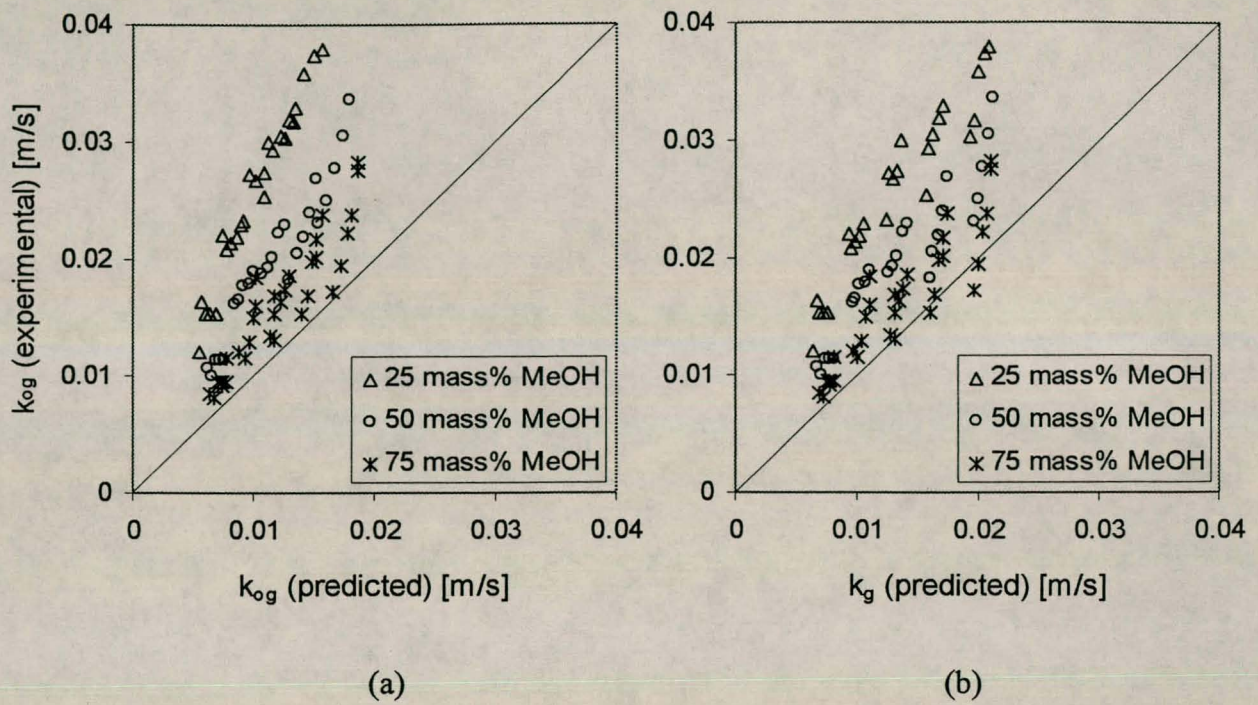

(a) (b)

Figure 3.10 Plot of measured k_{og} vs (a) predicted k_{og} and (b) predicted k_g for methanol/ethylene glycol, complex surface. Re_g=1800-6740, Re_l=5-97.

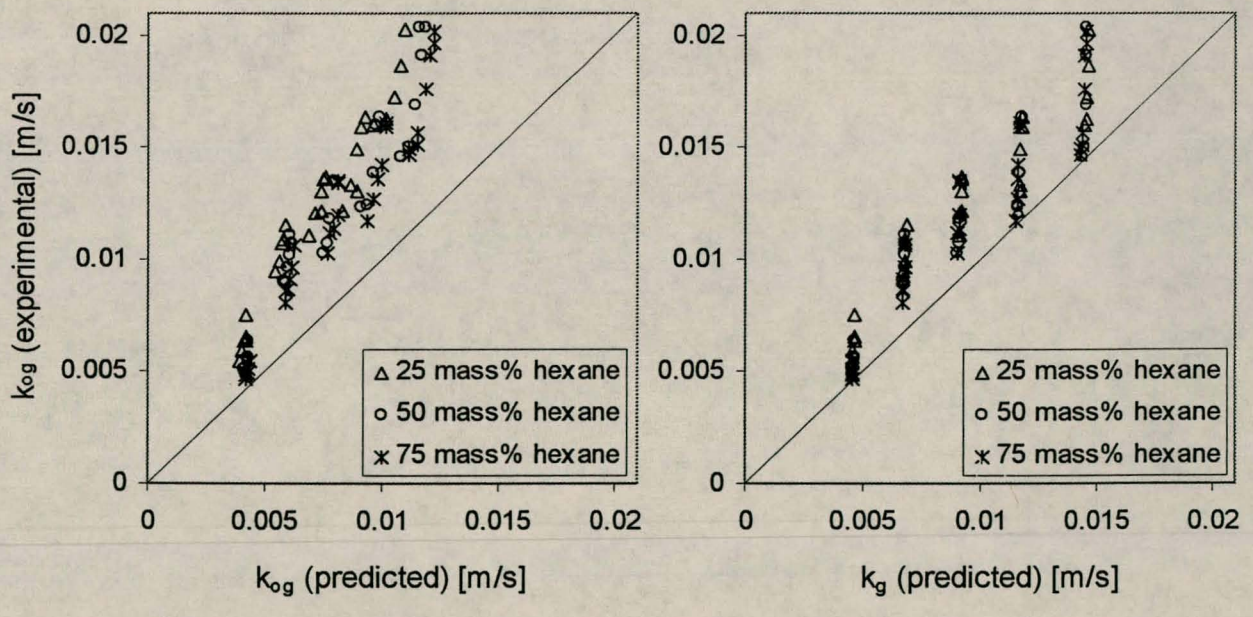

(a) (b)

Figure 3.11 Plot of measured k_{og} vs (a) predicted k_{og} and (b) predicted k_g for n-hexane/tridecane, complex surface. Re_g=2200-7160, Re_l=24-172.

3.6.2 Discussion of results

It is again evident from figure 3.10(a) and 3.11(a) that there is no liquid side resistance to mass transfer. In all these figures the experimental measured k_{og} are higher than the predicted values (the markers lie above the diagonal). The experimental measured k_{og} is also higher than the predicted k_g (see figure 3.10(b) and 3.11(b)), the same as for smooth surfaces. An enhancement factor is defined as in equation 3.11 and the results shown in table 3.2. The correlation used to calculate k_g is correlation 2.36. This was done because correlation 2.44 was fitted in a narrow range of liquid viscosity and only two of the data points would fall inside this range. Correlation 2.36 uses a relative gas phase Reynolds number to account for the influence that the liquid phase has on the mass transfer rate (see chapter 2). It will therefore not be too sensitive to physical properties like viscosity. The enhancement factors calculated with correlation 2.44 are also shown.

Table 3.2 Enhancement factors for binary mixtures containing one volatile component (complex surface).

System	mass% (volatile component)	Viscosity [Pa.s] $\times 10^4$	Surface tension [N/m]	F (corr 2.44)	F (corr 2.36)
Methanol/ethylene glycol	25	29.8	0.038	4.63	2.00
	50	13.4	0.031	2.28	1.48
	75	7.1	0.025	1.48	1.21
n-Hexane/ tridecane	25	8.0	0.021	1.74	1.34
	50	5.1	0.019	1.30	1.28
	75	3.5	0.018	1.16	1.24

A comparison between the two enhancement factors prove that correlation 2.44 is extremely sensitive to the liquid viscosity and surface tension. Where these properties are within the experimental range good agreement are obtained between the two enhancement factors (50 & 75 mass% n-hexane/tridecane).

It is again evident that the enhancement is coupled with the difference in surface tension between the solute (volatile component) and the solvent. No experimental work were done for systems where there is only a small difference in surface tension between solvent and solute, but the same trend is expected as observed for the smooth surface. Since there is some doubt as to the accuracy of correlation 2.36 in calculating k_g (see table 2.3), no comparison between the smooth- and complex surface will be made. This awaits future work.

3.7 Conclusions and recommendations

- In most of the systems investigated the liquid side resistance was found to be negligible.
- The system ethanol/tridecane is an exception. Some liquid side resistance was observed at low concentrations and high mass transfer rates. It was however much less than predicted by Higbie's penetration theory.
- For both the smooth and complex surfaces the experimentally determined overall mass transfer coefficient were found to be higher than the predicted gas phase mass transfer coefficient in most instances (ethanol/tridecane being the only exception).
- This enhancement is coupled to the difference in surface tension between the solvent and solute.
- In binary systems where there is no difference in the surface tension between the components there is no substantial enhancement. (acetone/methanol, methanol/ethanol)
- No correlation could be obtained between the observed enhancement and the Marangoni number. Inaccurate values for the liquid phase mass transfer coefficient may mask the effect.

The results indicate that for mixtures of high viscosity the correlations developed in chapter 2 must be used with caution. It is recommended that the database for these correlations be extended to contain more liquids of high viscosity. This is necessary if it is to be used in extractive distillation applications. There is little or no vapour/liquid equilibrium data available for most of the binary system containing one volatile component. Future studies will have to include the experimental measurement of vapour/liquid equilibrium data.

CHAPTER 4 Binary distillation in structured packing

4.1 Introduction

In the past 20 years structured packing has become increasingly popular for use in a wide variety of applications where gas-liquid contacting is required. The most popular application however remains in the field of distillation. It is widely known that structured packing offer significant capacity and efficiency advantages. It is especially useful for applications where maintaining a low pressure drop is critical [Weiland et al., 1993]. Most of the performance characteristics of this type of packing are reported in terms of the height equivalent to a theoretical plate (HETP) and the overall height of a transfer unit (HTU). These quantities incorporate the mass transfer resistances from both phases. A more fundamental approach would be to determine the mass transfer resistances separately for each phase and reporting the performance characteristics in terms of these resistances. In this chapter this approach will be followed.

4.2 Literature review

Bravo et al. [1985] have done extensive research work on structured packing. In their first paper on the subject, they use a correlation, similar to that developed by Sherwood and Gilliland [1934] for a wetted wall column, to correlate the gas phase mass transfer coefficient in columns containing gauze type structured packing:

$$Sh_g = 0.0338\,\mathrm{Re}_g^{\,0.8}\,Sc_g^{\,0.333} \tag{4.1}$$

The liquid phase mass transfer coefficient is defined as:

$$k_l = 2\sqrt{\frac{D_l u_{l,eff}}{\pi S}} \tag{4.2}$$

The effective area is taken to be equal to the surface area of the packing, i.e. $a_e=a_p$.

The equivalent diameter for the vapour phase is defined as:

$$D_{eq} = Bh\left[\frac{1}{(B+2S)} + \frac{1}{2S}\right] \tag{4.3}$$

In more resent publications [Rocha et al., 1996] the wetted wall analogy has been retained with the following adjustments to the correlation:

$$Sh_g = 0.054\,\mathrm{Re}_{g,r}^{\ 0.8}\, Sc_g^{\ 0.33} \tag{4.4}$$

$$k_L = 2\left(\frac{D_L C_E u_{l,eff}}{\pi S}\right)^{0.5} \tag{4.5}$$

C_E is a discount factor which accounts for parts of the bed that do not encourage rapid surface renewal. It must be mentioned that none of these adjustments are supported by wetted wall experimental work, but is fitted on data were the effective mass transfer area is already estimated by a correlation.

The velocity of the vapour phase relative to the liquid interface is used to calculate the vapour phase Reynolds number. The velocities of the two phases are defined as:

$$u_{g,eff} = \frac{u_{g,\sup er}}{\varepsilon(1-h_L)\sin\theta} \tag{4.6}$$

$$u_{l,eff} = \frac{u_{l,\sup er}}{\varepsilon h_L \sin\theta} \tag{4.7}$$

The characteristic length is taken as the side dimension (S) of a corrugated cross section. For sheet metal packing they recommend that the effective interfacial area be calculated using the correlation developed by Shi and Mersmann [1985]:

$$\frac{a_e}{a_p} = F_{SE} \frac{29.12(We_L Fr_L)^{0.15} S^{0.359}}{\mathrm{Re}_L^{0.2} \varepsilon^{0.6} (1-0.93\cos\gamma)(\sin\theta)^{0.3}} \tag{4.8}$$

For gauze packing the effective area is correlated by:

$$\frac{a_e}{a_p} = 1 - 1.203\left(\frac{u_{l,\sup er}^{\ 2}}{Sg}\right)^{0.111} \tag{4.9}$$

They also propose an extensive set of correlations [Rocha et al., 1993] to calculate liquid holdup, pressure drop and film thickness. Their use of Higbie's penetration model to calculate the liquid side resistance is believed not to be very accurate for liquid flow over complex surfaces [Crause, 1998]. This is supported by the wetted wall experimental work performed in this study (chapter 3) and that of Crause [1998].

Spiegel and Meier [1987] reported a correlation of similar form to calculate the gas phase mass transfer coefficient:

$$Sh_g \propto \mathrm{Re}_g^{0.8} Sc_g^{1/3} \tag{4.10}$$

They did however not provide a constant of proportionality. The characteristic length used in this correlation is the hydraulic diameter of the vapour channels in the packing and is defined as:

$$d_h = \frac{4}{a_p} \tag{4.11}$$

They share the earlier view of Bravo et al. [1985] that the packing surface is completely wetted for gauze type packing. They propose that the effective surface area for metal sheet type packing is proportional to the liquid density and liquid velocity in the following manner:

$$a_e \propto (\rho_l u_{l,\sup er})^{0.2} \tag{4.12}$$

Again no proportionality constant is given. In their analysis the liquid phase mass transfer coefficient is neglected. They found that often $k_L >> k_G$ and almost always $k_L > k_G$. They published an extensive set of efficiency- and pressure drop graphs for the various Mellapak structured packing types.

Nawrocki et al. [1991] developed a mechanistic model for the liquid distribution, effective area and mass transfer. Their mass transfer model is essentially similar too that proposed by Bravo et al. [1985]. They determined the liquid flow and distribution inside a packing element by making use of the amount of intersection points inside a packing element. The distribution of a rivulet entering such an intersection was calculated and by combining al the intersections the liquid flow inside the packing is determined completely.

Weiland et al. [1993] measured mass transfer coefficients and effective interfacial areas for Goodloe and Montz A2 structured packing. They used a similar correlation for the gas phase mass transfer coefficient than previous investigators:

Goodloe $$Sh_g = 0.0567\,\mathrm{Re}_g^{\,1.10}\,Sc_g^{\,1/3} \tag{4.13}$$

Montz A2 $$Sh_g = 0.0373\,\mathrm{Re}_g^{\,1.02}\,Sc_g^{\,1/3} \tag{4.14}$$

They used correlations of the same form to correlate the liquid phase mass transfer coefficient (in contrast to using Higbie's penetration theory):

Goodloe $$Sh_L = 3.4\,\mathrm{Re}_L^{\,-0.08}\,Sc_L^{\,1/2} \tag{4.15}$$

Montz A2 $$Sh_L = 5.2\,\mathrm{Re}_L^{\,-0.04}\,Sc_L^{\,1/2} \tag{4.16}$$

The effective interfacial area were correlated by using a capacity factor:

Goodloe $a_e = 356F^{-0.2}$ (4.17)

Montz A2 $a_e = 265F^{-0.4}$ (4.18)

For the equivalent diameters used in the dimensionless numbers, the reader is referred to the publication.

Crause [1998] modified his wetted wall correlation by introducing a packing factor, F_p.

$$Sh = 0.00283F_p \, \mathrm{Re}_g \, \mathrm{Re}_l^{0.08} \, Sc_g^{0.5} \quad (4.19)$$

This factor characterizes the enhancement of mass transfer in structured packing compared to a wetted-wall column. His work indicated a packing factor of F_p=1.03 for Mellapak 350Y. In his model the flow of the liquid phase was approximated to be vertically down the packing with the vapour phase flowing in the channels. Complete wetting of the packing was assumed.

Various authors published papers on pressure drop and liquid holdup in structured packing [Billet et al., 1993]. Since the aim of this study is to develop a dependable mass transfer model, the reader is referred to the literature.

4.3 Theory

The mass transfer process taking place inside structured packing during distillation can be described mathematically by the two film theory of Whitman [Coulson & Richardson, 1991]. According to this theory there exists a thin film on either side of the phase boundary through which the mass transfer is solely through intermolecular diffusion. The concentration gradients in the bulk of the phases are considered to be negligible. Figure 4.1 represents this situation:

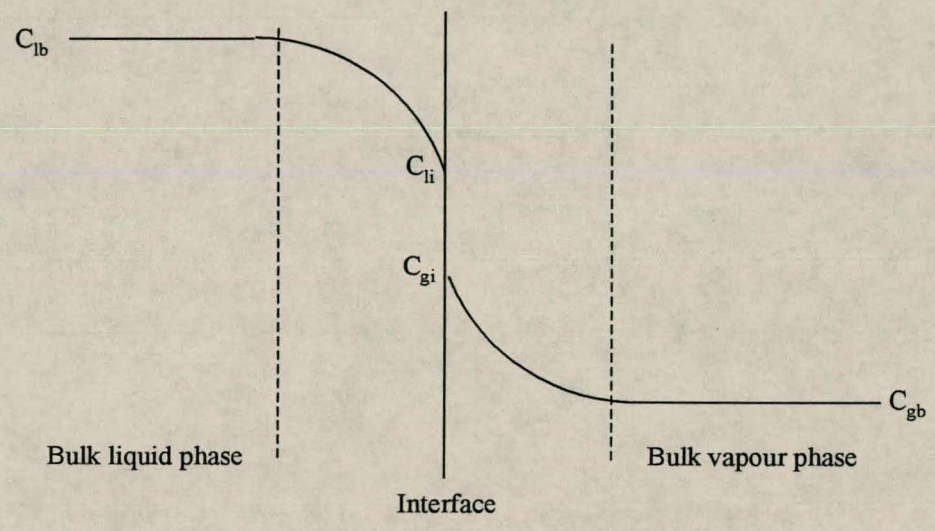

Figure 4.1 Two film theory [Nieuwoudt, 1994]

The rate of transport of a component from the bulk of the liquid phase to the interface is expressed as:

$$N = k_l (C_{lb} - C_{li}) \tag{4.20}$$

The rate of transport to the interface must equal the rate of transport away from the interface because of no net mass accumulation:

$$N = k_l (C_{lb} - C_{li}) = k_g (C_{gi} - C_{gb}) \tag{4.21}$$

The bulk of the vapour phase is in equilibrium with a certain concentration in the liquid phase and is described as:

$$C_{gb} = mC_l^* \tag{4.22}$$

And because of the assumption of equilibrium at the interface:

$$C_{gi} = mC_{li} \tag{4.23}$$

The rate of transfer to and from the interface is therefore:

$$N = k_l\left(C_{lb} - C_{li}\right) = k_g\left(C_{gi} - C_{gb}\right) = mk_g\left(C_{li} - C_l^*\right) \tag{4.24}$$

The bulk of the liquid phase is in equilibrium with a certain concentration in the vapour phase and is described as:

$$C_g^* = mC_{lb} \tag{4.25}$$

Overall transfer coefficients is defined in terms of the concentrations C_l^* and C_g^*:

$$N = k_{ol}\left(C_{lb} - C_l^*\right) \tag{4.26}$$

$$N = k_{og} = \left(C_g^* - C_{gb}\right) \tag{4.27}$$

Eliminating the concentrations C_g^* and C_l^* lead to the following equations:

$$\frac{1}{k_{ol}} = \frac{1}{k_l} + \frac{1}{mk_g} \tag{4.28}$$

$$\frac{1}{k_{og}} = \frac{m}{k_l} + \frac{1}{k_g} \tag{4.29}$$

The slope of the equilibrium line, m, can be written as [Nieuwoudt, 1994]:

$$m = K_i \left(\frac{\rho_v}{\rho_l} \right) \left(\frac{M_r^{liq}}{M_r^{vap}} \right) \tag{4.30}$$

A mass balance between the two phases flowing countercurrent yields the following differential equation [Nieuwoudt, 1994] (in terms of the overall gas phase mass transfer coefficient):

$$-u_{g,\sup er} A dC_g = k_{og} \left(C_g^* - C_{gb} \right) a A dz \tag{4.31}$$

Rearranging and integrating yields:

$$\int_{C_{gl}}^{C_{go}} \frac{dC_g}{\left(C_{gb} - C_g^* \right)} = \int_{z=0}^{z=h} \frac{-k_{og} a}{u_{g,\sup er}} dz \tag{4.32}$$

$$h = \frac{u_{g,\sup er}}{k_{og} a} \int_{C_{gl}}^{C_{go}} \frac{dC_g}{\left(C_g^* - C_{gb} \right)} \tag{4.33}$$

$$h = H_{Tog} \times N_{Tog} \tag{4.34}$$

The height equivalent to a theoretical plate, or HETP, is used in the literature to quantify the performance of a packing material. This concept can be explained by referring to Figure 4.2.

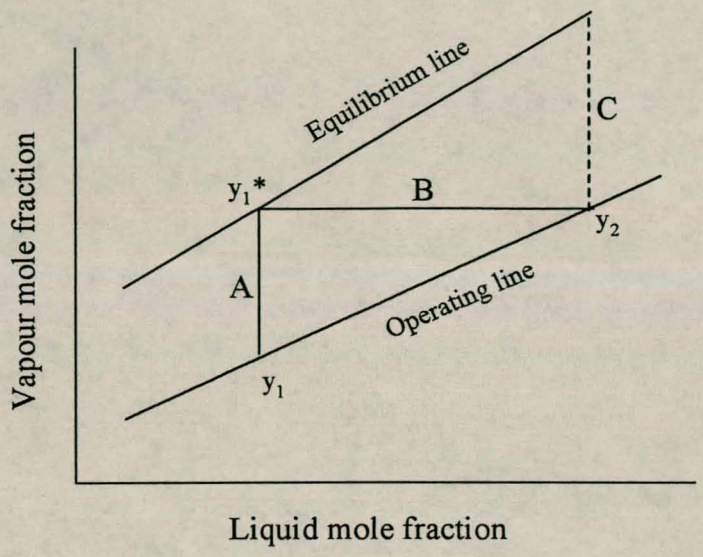

Figure 4.2 Theoretical plate [Nieuwoudt, 1994]

An equilibrium stage, or one theoretical plate, will cause a composition change in the vapour phase from y_1 to y_2 [Foust et al., 1980]. The packing height equivalent to a theoretical stage (HETP) can be determined by calculating the number of transfer units needed to cause this composition change and the height of such a transfer unit.

The equation for the operating line is as follows:

$$d(Gy) = d(Lx) \tag{4.35}$$

If G and L are assumed constant over a theoretical stage, then equation 4.35 can be written as [Nieuwoudt, 1994]:

$$\frac{dy}{dx} = \frac{L}{G} = \frac{A}{B} \tag{4.36}$$

If it is assumed that the equilibrium line is straight over a theoretical stage, it can be shown that [Nieuwoudt, 1994]:

$$K_i = \frac{\Delta y^*}{\Delta x} = \frac{C}{B} \tag{4.37}$$

From equation 4.36 and 4.37 follows that:

$$C = \left(\frac{G}{L}\right) K_i A \tag{4.38}$$

The number of transfer units from equation 4.33 are:

$$N_{Tog} = \int_{C_{gI}}^{C_{go}} \frac{dC_g}{\left(C_g^* - C_{gb}\right)} \tag{4.39}$$

Equation 4.39 can be written in terms of mole fraction:

$$N_{Tog} = \int_{y_1}^{y_2} \frac{dy_i}{\left(y_i^* - y_{ib}\right)} \tag{4.40}$$

This equation can be approximated with [Foust et al., 1980]:

$$N_{Tog} = \frac{\left(y_2 - y_1\right)}{\left(y^* - y\right)_{LM}} \tag{4.41}$$

where

$$(y^* - y)_{LM} = \frac{(y_1^* - y_1) - (y_2^* - y_2)}{\ln \frac{(y_1^* - y_1)}{(y_2^* - y_2)}}$$
$$= \frac{(A - C)}{\ln\left(\frac{A}{C}\right)} \qquad (4.42)$$
$$= \frac{A\left(\frac{G}{L}K_i - 1\right)}{\ln\left(\frac{G}{L}K_i\right)}$$

Substituting into equation 4.41 leads to:

$$N_{Tog} = \frac{\ln\left(\frac{G}{L}K_i\right)}{\left(\frac{G}{L}K_i - 1\right)} \qquad (4.43)$$

Equation 4.43 gives the number of transfer units in a theoretical stage. The height equivalent to a theoretical stage (HETP) is calculated by multiplying the number of transfer units with the height of a transfer unit:

$$HETP = H_{Tog} \times N_{Tog}$$
$$= \frac{u_{g,\sup er}}{k_{og} a_e} \frac{\ln\left(\frac{G}{L}K_i\right)}{\left(\frac{G}{L}K_i - 1\right)} \qquad (4.44)$$

Before the flow patterns of the vapour- and liquid phases are described, it is necessary to first look at the structured packing used in this study, Mellapak 350Y.

The characteristic dimensions of Mellapak 350Y are given in Table 4.1.

Table 4.1 Packing Dimensions

Geometric dimension	Symbol	Value
Crimp height [mm]	h	8.5
Channel base [mm]	B	17.4
Channel side [mm]	S	12.1
Equivalent diameter [mm]	D_{eq}	12.2
Void fraction	ε	0.95
Corrugation angle [°]	θ	45
Wetted perimeter [m^{-1}]	p	350

The equivalent diameter is defined as that for the triangular passage shown in figure 4.5. Only two of the three walls are wetted by the liquid and this is taken into account in defining the equivalent diameter:

$$D_{eq} = \frac{Bh}{S} \tag{4.45}$$

Figure 4.3 show the flow channels inside the packing. Figure 4.4 show the packing dimensions on a single corrugated sheet.

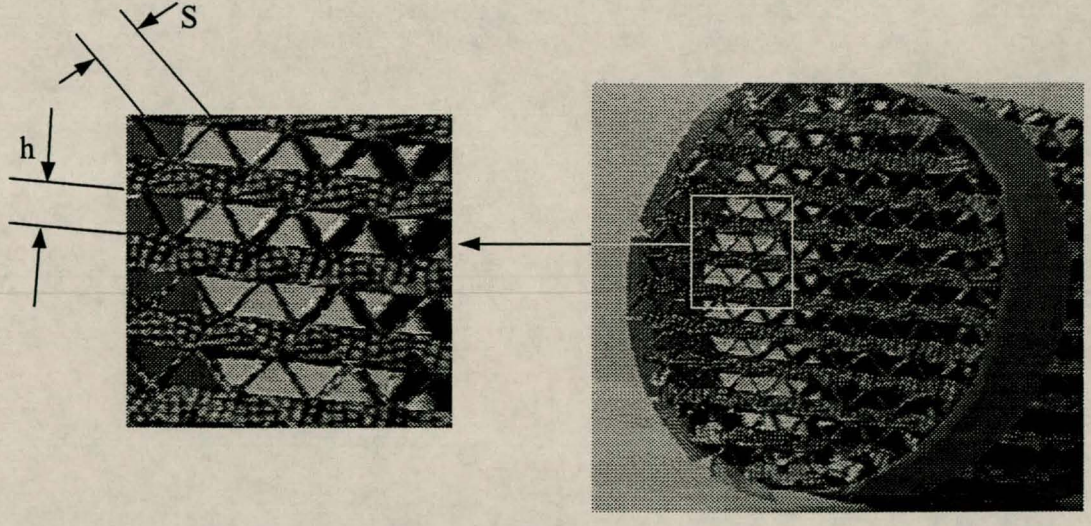

Figure 4.3 Flow channels inside Mellapak 350Y

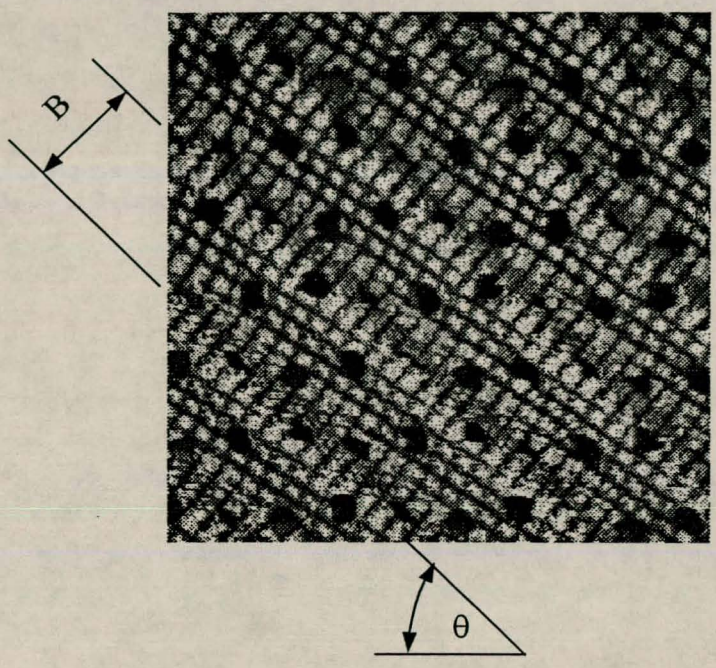

Figure 4.4 Dimensions on single corrugated sheet

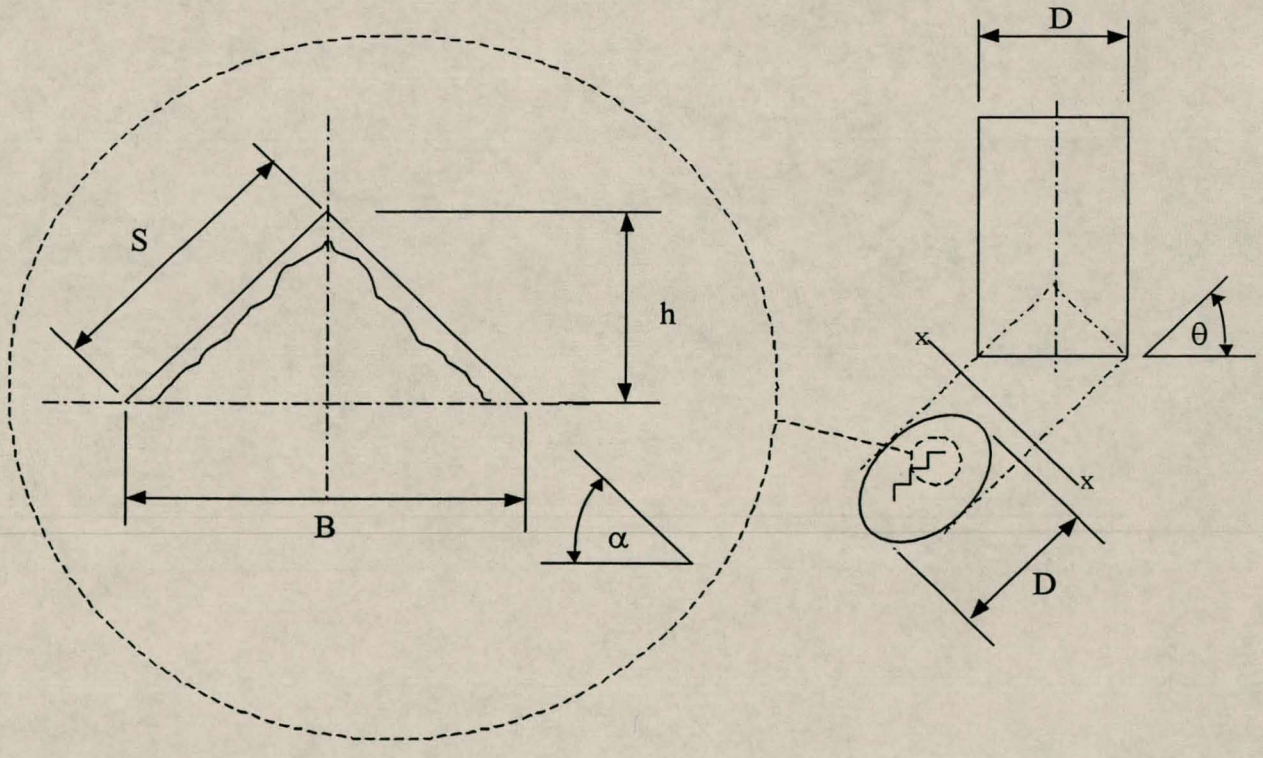

Figure 4.5 Dimensions of a single flow passage

The flow of the liquid and vapour phases can be visualized by looking at a single corrugated sheet (Figure 4.4). The liquid can be approximated to flow down the packing at an angle θ to the horizontal in the triangular passages. The walls of the triangular passages are completely wetted by the liquid. The vapour phase flow countercurrent to the liquid phase in these passages. A different approach to that suggested by Nieuwoudt [1994] and Crause [1998] was followed in applying the mass transfer model. In order to promote a better understanding of the problem, the total flow rate of vapour and liquid were divided among the total number of channels in the packing. The number of channels in the packing is calculated as follows (see figure 4.5):

$$n = \frac{A_{Total}}{A_{Channel}} \tag{4.46}$$

The total area for flow (A_{Total}) must be the area perpendicular to the flow direction. This area is the column area projected perpendicular to the flow direction, as shown in figure 4.5. The void fraction is taken into account when calculating the flow area:

$$A_{Total} = \varepsilon \frac{\pi}{4} D^2 \sin\theta \tag{4.47}$$

The area of a flow channel is calculated with:

$$A_{Channel} = \frac{1}{2} Bh \tag{4.48}$$

The velocity and thickness of the liquid film can be calculated by applying the momentum equation in two dimensions. The reader is referred to appendix A for a complete derivation and the assumptions made. The liquid film thickness (δ) is calculated from the following implicit equation:

$$\frac{(\rho_l - \rho_g)\delta^3 g \sin\theta}{3\mu} + \frac{\tau}{\mu}\left[\frac{\delta^2}{2} - \frac{4\delta^3}{3(D_{eq} - 2\delta)}\right] - \delta u_{avg} = 0 \tag{4.49}$$

The interfacial velocity is calculated from:

$$u_i = \frac{(\rho_l - \rho_g)g\delta^2 \sin\theta}{2\mu} + \frac{\tau}{\mu}\left[\delta - \frac{2\delta^2}{(D_{eq} - 2\delta)}\right] \tag{4.50}$$

The pressure drop over the column is caused by interfacial drag at the liquid-vapour interface and the static pressure drop of the vapour phase. Since the pressure drop is measured, the interfacial shear stress is calculated from [Nieuwoudt, 1994]:

$$\tau_i = \frac{(\Delta P_{measured} - \Delta P_{static})}{\frac{\Delta h}{\sin\theta}} \frac{D_{eq}}{4} \tag{4.51}$$

The equivalent diameter is defined as that for the triangular passage shown in figure 4.5. Only two of the three walls are wetted by the liquid and this is taken into account in defining the equivalent diameter:

$$D_{eq} = \frac{Bh}{S} \tag{4.52}$$

The average velocity of the liquid phase is calculated as follows:

$$u_{l,avg} = \frac{Q_l}{2n\delta\left(S - \frac{B\delta}{2h}\right)} \tag{4.53}$$

The hydraulic model and gas phase mass transfer correlations developed in chapter 2 are combined in the following manner.

The observed separation is simulated by making use of a simulation package (Pro Π). The stagewise composition-, temperature- and flow profiles are used in the hydraulic model to calculate the liquid film thickness and interfacial velocity. The gas phase mass transfer correlations where a relative vapour phase Reynolds number are used make use of the interfacial velocity to calculate the relative vapour velocity:

$$u_{g,r} = u_{g,eff} + u_{l,i} \tag{4.54}$$

The liquid film thickness and the composition-and temperature profiles (used to calculate physical properties) are in turn used in the gas phase mass transfer correlations developed in chapter two to determine the gas phase Sherwood number and therefore k_g

The Reynolds numbers for the vapour- and liquid phases in the structured packing are defined as:

$$\mathrm{Re}_g = \frac{\rho_g u_{g,eff} D_{eq}}{\mu_g} \tag{4.55}$$

$$\mathrm{Re}_l = \frac{\rho_l u_{l,avg} \delta}{\mu_l} \tag{4.56}$$

For the relative vapour phase Reynolds number $u_{g,r}$ is used as defined in equation 4.54. The effective velocity of the vapour phase is calculated from:

$$u_{g,eff} = \frac{Q_g}{\frac{n}{2}\left(B - \frac{2\delta}{\sin\alpha}\right)\left(h - \frac{\delta}{\sin\alpha}\right)} \tag{4.57}$$

The resistance to mass transfer in the liquid phase is assumed to be negligible compared to the resistance in the gas phase (see chapter 3). Equation 4.29 therefore reduces to:

$$k_{og} = k_g \tag{4.58}$$

The flow and composition profiles are used in equation 4.37 to calculate stagewise Ki values. Before equation 4.44 can be used to calculate the HETP, the height of a transfer unit must be calculated for a triangular channel. It can be shown that:

$$H_{Tog} = \frac{u_{g,\sup er}\left(\frac{Bh}{2}\right)}{k_g 2\left(S - \frac{B\delta}{2h}\right)} \tag{4.59}$$

Complete wetting of the packing is assumed in equation 4.59:

The HETP$^{\#}$ values calculated in this manner must be corrected for the packing geometry. The model was developed on the assumption that the liquid and vapour phases flow countercurrent in the channels which are inclined at an angle θ to the horizontal. Therefore:

$$HETP = HETP^{\#} \sin\theta \tag{4.60}$$

The total height of structured packing needed for the observed separation is calculated by the summation of the HETP values:

$$h = \sum_{0}^{j} HETP_j \tag{4.61}$$

4.4 Experimental

The proposed model was validated by making use of total reflux binary distillation data. (See appendix D for the distillation data.)

4.4.1 Column description

The distillation column used is specifically set up for total reflux distillation experimental work. The column has an internal diameter of 200 mm and contains three sections packed with Sulzer Mellapak 350Y. Each section contains 4 packing segments and each segment has a height of 210 mm. The total packed height of the column is therefore 2.52 m. Between each packed section the liquid is redistributed with chimney type distributors having a drip point density of 795 m^{-1}. The packed sections are insulated with ceramic wool and polyethylene foam.

A thermosyphon type reboiler with no baffle in the sump is used. The bottoms product is drawn from the sump. The overhead vapour is condensed in a total condenser which is operated under atmospheric pressure. The distillate product is drawn at a collection point underneath the condenser.

The following temperatures are measured:

- Reboiler return temperature
- Temperature below the packing
- Temperature at the top of each packed segment
- Cooling water inlet and outlet of the condenser

The pressure drop over the column as well as the cooling water- and condensate flowrates are also measured.

A process flow diagram for the distillation column is shown in Figure 4.6.

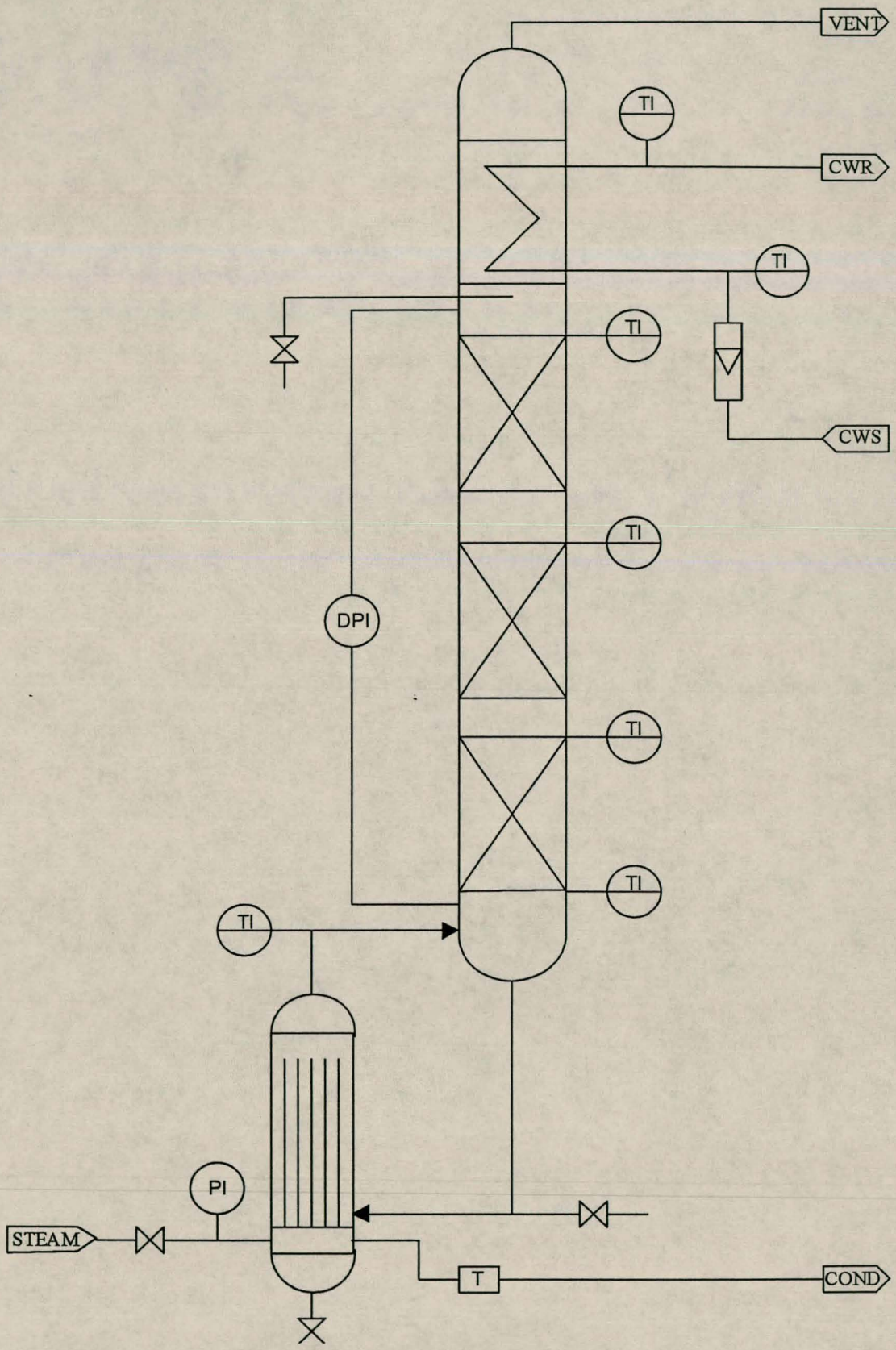

Figure 4.6 PFD for total reflux distillation column

4.4.2 Distillation runs

Total reflux distillation was done on five binary systems. The vapour and liquid load in the column were varied by adjusting the reboiler duty. The column was operated in the following manner :

After the desired mixture has been loaded into the reboiler and start up, the reboiler duty was set to the desired value and the column left for a period of time to stabilize. Stable operation was assumed when there were no changes in the temperatures. Samples were then drawn at the two sampling points and analyzed by means of gas chromatography.

4.5 Results

Total reflux distillation runs were done with four binary systems. These systems were:

- ethanol/i-propanol
- ethanol/methanol
- methanol/acetone
- methanol/i-propanol

For the ethanol/i-propanol system two sets of runs were done at different starting concentrations. For each binary system multiple runs were done at different reboiler duties, i.e. different reflux rates. The conditions for one of the ethanol/i-propanol sets are shown in table 4.2. For a complete set of all the experimental data see appendix D. An input- and output file for the simulation package Pro Π are shown in appendix E. Physical property estimation techniques are listed in appendix B.

Table 4.2 Conditions for ethanol/i-propanol total reflux distillation runs

Run	Ethanol concentration [mass %]		Reflux rate [kg/h]	Average over column :		
	Bottoms	Distillate		Re_g	Re_l	Sc_g
1	12.21	34.27	292.5	5117	27.0	0.545
2	12.05	35.09	291.8	5069	26.7	0.544
3	12.11	34.72	287.1	4949	26.1	0.545
4	12.67	34.49	273	4671	24.6	0.547
5	12.95	34.37	261.6	4443	23.5	0.547
6	12.82	34.71	239.7	4045	21.3	0.547
7	12.73	33.85	231.4	3884	20.5	0.547
8	12.87	33.67	207.7	3462	18.2	0.544
9	14.11	35.16	162.8	2685	14.2	0.548

The calculated packed height using the correlations fitted in chapter 2 and 3 are shown in table 4.4. The values for the packed height are taken as the average for a binary system. The calculated packed height for all the runs are shown in appendix D. For the correlations where it was not already done, the exponent of the Schmidt numbers was rounded to the theoretical value of 0.5 and non-linear regression was done using the exponents of the remaining dimensionless numbers, as described in chapter 2. The constants used in the correlations in table 4.4 are shown in table 4.3.

Table 4.3 Regressed constants for correlations used in table 4.4

Correlation	a	b	c	d	E
2.26 $Sh_g=aRe_{g,r}{}^bSc_g{}^c$	0.0008	1.17	0.5	N/A	N/A
2.27 $Sh_g=aRe_g{}^bSc_g{}^cRe_l{}^d$	0.0030	0.96	0.5	0.14	N/A
2.33 $Sh_g=aRe_g{}^bSc_g{}^cWe_l{}^d$	0.0044	1	0.5	0.11	N/A
2.36 $Sh_g=aRe_{g,r}{}^bSc_g{}^c$	0.0081	0.94	0.5	N/A	N/A
2.37 $Sh_g=aRe_g{}^bSc_g{}^cRe_l{}^d$	0.0085	0.75	0.5	0.357	N/A
2.44 $Sh_g=aRe_g{}^bSc_g{}^cRe_l{}^dBo^e$	0.0036	0.76	0.5	0.41	-0.13

Table 4.4 Average calculated packing height

System	Average packed height [m] according to correlation: 2.26	2.27	2.33	2.36	2.37	2.44	Crause[1]
Ethanol/ i-propanol (1)	3.92	4.45	4.75	2.68	4.57	4.39	3.52
Ethanol/ i-propanol (2)	3.22	3.81	3.94	2.33	3.99	3.82	2.88
Ethanol/ Methanol	4.50	4.66	5.36	2.70	4.52	4.16	3.53
Acetone/ Methanol	3.73	4.06	4.72	2.41	3.98	3.56	3.15
Methanol/ i-propanol	4.03	4.22	4.79	2.46	4.10	3.81	2.97
Average	3.88	4.24	4.71	2.52	4.23	3.95	3.21

(1) As described in Crause [1998]

4.6 Discussion of results

Table 4.4 shows that the average of the packed height calculated by using correlation 2.36 is equal to the experimental packed height of 2.52 m. The correlations fitted on the mass transfer data from complex surfaces (corr. 2.36, 2.37 and 2.44) gave a better fit than the correlations fitted on the data for smooth surfaces (corr. 2.26, 2.27 and 2.33). The correlations for the smooth surface tend to over predict the packed height substantially more than the correlations for the complex surface. This can also be seen in figures 4.7 and 4.8. Figure 4.7 compares the predicted packed height and the actual height with the average vapour phase Reynolds number for the smooth surface correlations. Figure 4.8 compares the same variables for the complex surface correlations. All the experimental data are shown in these plots.

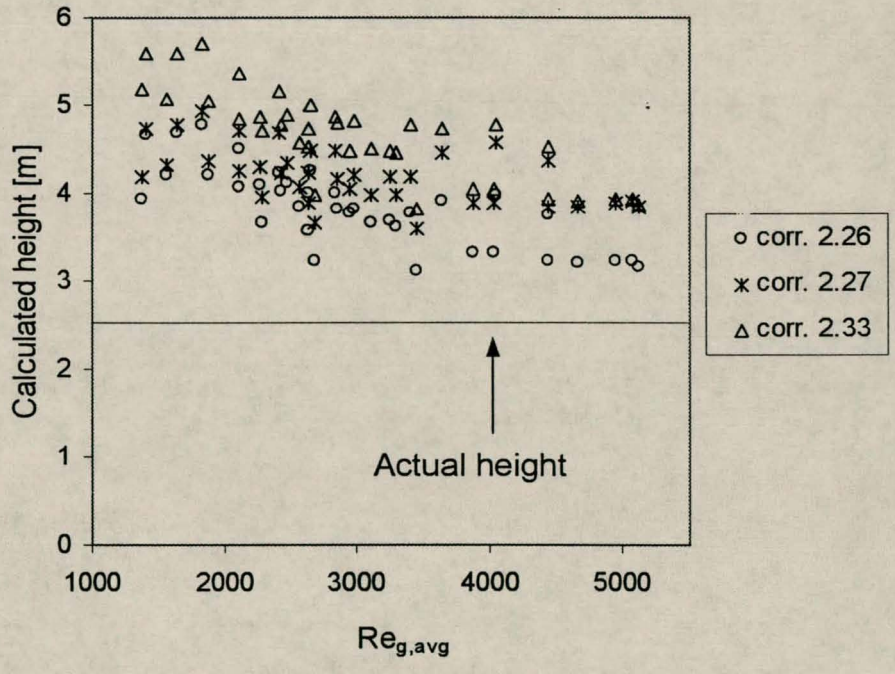

Figure 4.7 Calculated packed height vs $Re_{g,avg}$ for smooth surface correlations.

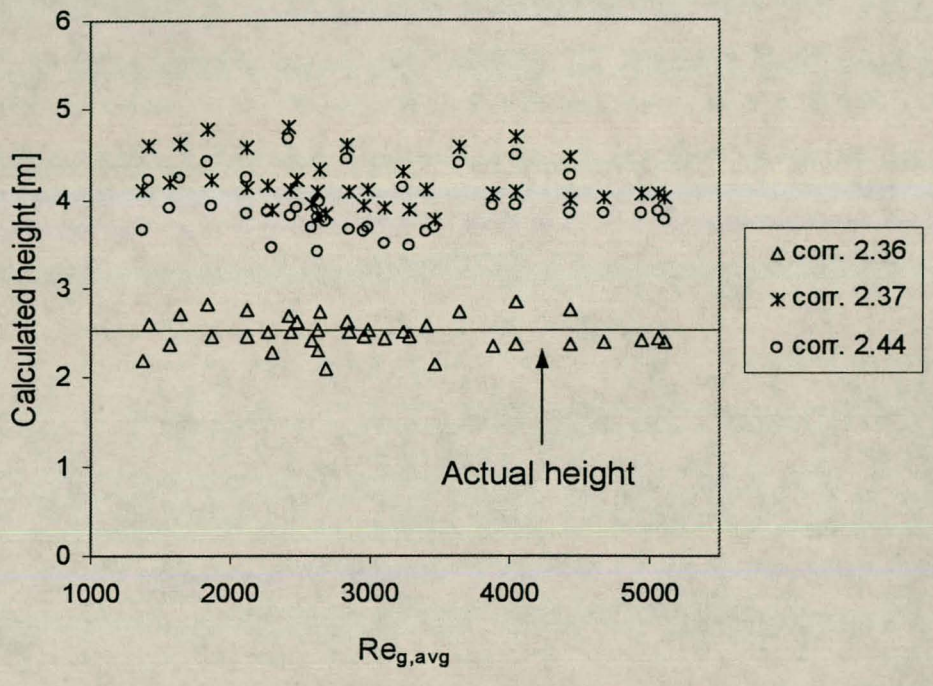

Figure 4.8 Calculated packed height vs $Re_{g,avg}$ for complex surface correlations

Figure 4.7 shows that for the smooth surface correlations there is a upward trend in the predicted packed height for $Re_{g,avg}$ ≤2500. All the correlations follow this trend. This trend is not observable in figure 4.8. In both figures the correlations that contain no liquid flow number (corr. 2.26 and 2.36) perform better than those with liquid flow numbers (corr. 2.27, 2.33 and corr. 2.37, 2.44).

The over prediction in both instances for the correlations containing liquid flow numbers, can be attributed to the lower liquid flow rate on the structured packing compared to that in the wetted wall column. The liquid Reynolds number in the wetted wall column varied between 12-330 with an average of 135 for the smooth surface. For the complex surface the liquid Reynolds number varied between 50-200 with an average of 122. In the structured packing the flow rate was substantially lower. The liquid Reynolds number varied between 10-27 with an average of 19. Extrapolating these mass transfer correlations for the wetted wall column to lower liquid flow rates in the structured packing does not seem to yield satisfactory results. This is especially true in the case of

the smooth surface correlations and in particular corr. 2.33. Correlation 2.33 uses the Weber number to characterize the influence of the liquid film flow on the mass transfer rate. In this dimensionless number the velocity of the liquid phase is squared. It is to be expected that this correlation will not extrapolate well to lower liquid flow rates, i.e. lower liquid velocities, and will predict substantially lower mass transfer rates than expected. Since the mass transfer rate is inversely proportional to H_{Tog}, a smaller mass transfer rate will result in a higher H_{Tog} and a higher calculated packed height.

The fact that the correlations for the complex surface predict the packed height better than the correlations for the smooth surface are in good agreement with the findings in chapter 2. The remainder of this section will deal with these correlations unless stated otherwise.

To ascertain whether the liquid flow rate do indeed influence the mass transfer rate and therefore the packed height, correlation 2.36 is compared to correlation 2.35 in figure 4.9. The difference between these two correlations lies in the vapour phase Reynolds number. In correlation 2.35 the velocity of the vapour phase relative to the packing surface is used in Re_g. In correlation 2.36 the velocity relative to the liquid surface is used.

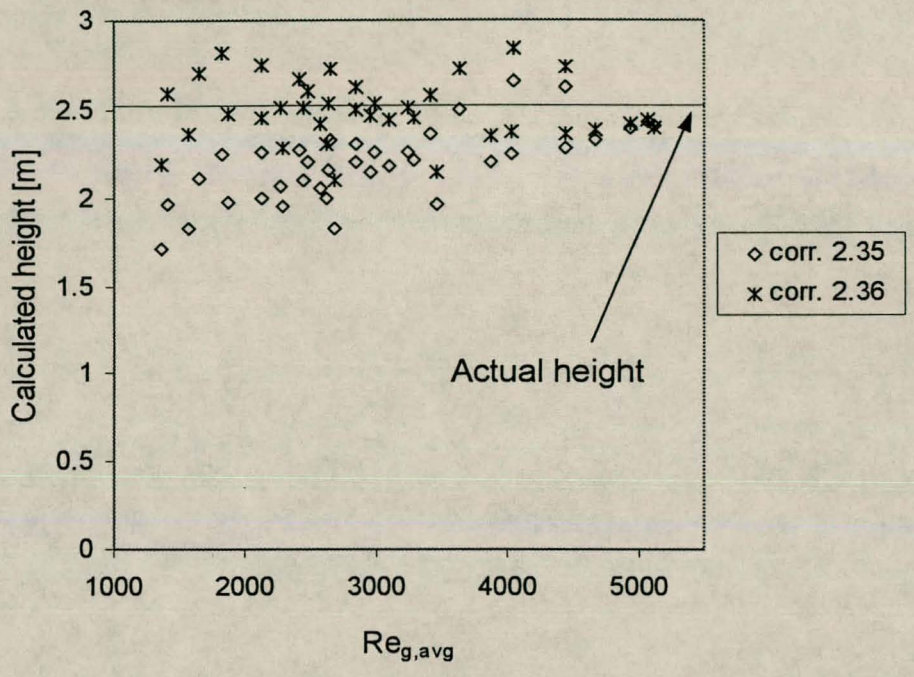

Figure 4.9 Packed height vs $Re_{l,avg}$ for correlations 2.35 and 2.36

For correlation 2.35 there is a clear slope in the data points for an increase in $Re_{l,avg}$. There is quite a scatter in the data points for correlation 2.36, but there is no clear slope. The average of these points are equal to the packed height (see table 4.4). This confirms that the liquid flow rate do indeed influence the mass transfer rate and therefore the packed height.

It is assumed, based on the above arguments, that correlation 2.36 combined with the proposed model, best describes the mass transfer in the structured packing used in this work (Mellapak 350Y). The average error of this correlation in the prediction of the packed height is 0.14 m or 5.7%. The model proposed by Crause [1998] is compared to the proposed model and correlation 2.36 in figure 4.10.

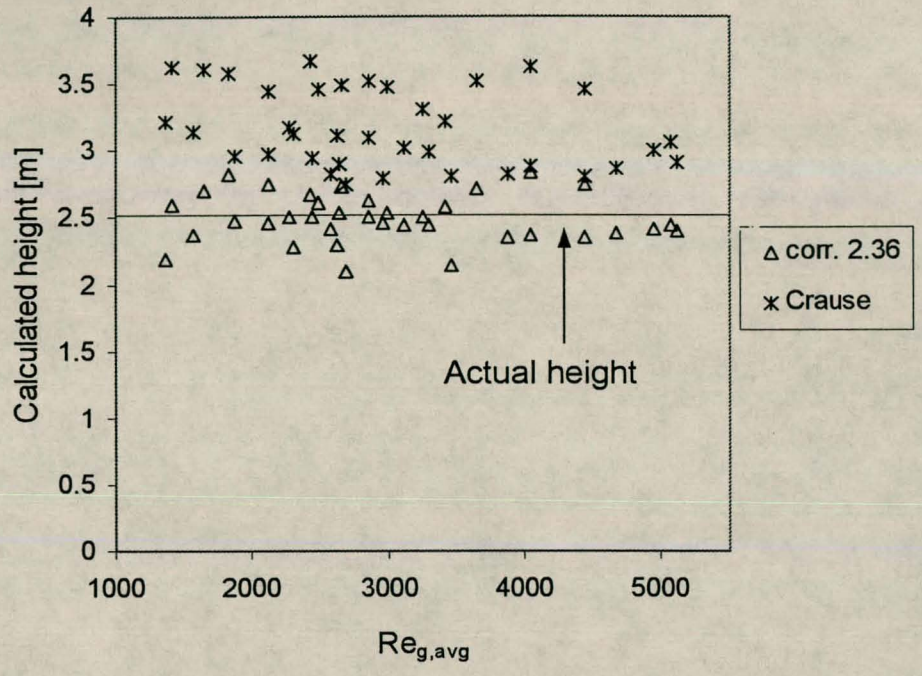

Figure 4.10 Comparison between corr. 2.36 and proposed model with that of Crause [1998].

Figure 4.10 show that the proposed model predicts the packed height more accurately than that of Crause [1998]. The average error for his model is 0.65 m or 25.8%. There is also one major discrepancy in the model proposed by Crause [1998]. In his wetted wall studies a characteristic length for the liquid phase Reynolds number was chosen as the thickness of the liquid film, or more correctly, the hydraulic radius of the film. In the liquid Reynolds number used in his distillation model the equivalent diameter was used. The equivalent diameter is equal to four times the hydraulic radius [Daugherty, 1977]. This descrepancy will cause his model to predict a higher mass transfer rate in the structured packing than was measured in his wetted wall experimental work. According to his correlation $k_g \propto Re_l^{0.08}$ and since H_{Tog} is inversely proportional to k_g, the calculated packed height is $4^{0.08}=1.117$ times or 11.7% too small.

4.7 Sensitivity analysis

A fact that none of the previous investigators mentioned, is the sensitivity of the model to the accuracy of the binary gas phase diffusion coefficient. There exist quite a few correlations to estimate binary diffusion coefficients (Reichenberg, Wilke & Lee, Brokaw, Fuller, Danner) [Reid & Prausnitz, 1987]. Most of the data on which these correlations were fitted contains a non-condensable gas. A substantial amount of the data is for binary systems containing air. There exist no clear rules as to which correlation to use when one or both components are polar. Although the data points on which the correlation of Brokaw [1969] was fitted contained some polar gasses, Reid and Prausnitz [1987] recommend that the correlation of Fuller et al. be used. Wankat et al. [1997] recommends that the correlation of Brokaw [1969] be used for polar systems. The diffusion coefficients predicted by the different correlations are shown in table 4.5.

Table 4.5 Binary gas phase diffusion coefficients at atmospheric pressure

Binary system	Temp. [K]	$D_{AB} \times 10^6$ [m^2/s]			
		Fuller	Wilke Lee	Brokaw	Danner
Ethanol/i-propanol	353.15	9.09	7.19	6.7	8.24
Methanol/ethanol	343.15	13.38	9.95	9.39	11.51
Acetone/methanol	331.15	10.89	8.3	7.85	9.59
Methanol/i-propanol	346.9	11.37	8.65	8.22	9.95

It is alarming to see that the difference between the two correlations of choice in the literature, the method of Fuller et al. and the method of Brokaw, can differ by as much as 42% for the binary methanol/ethanol and on average 38.8% for the four binaries shown above. Because of the much larger data set on which the correlation of Fuller et al. was fitted, it was decided to use this correlation in the model. Table 4.6 shows the influence that the choice of correlation will have on the predicted packed height. Distillation runs were chosen at random for each binary system. The methods and correlations used to estimate physical properties are given in appendix B.

Table 4.6 Influence of diffusion coefficient on predicted packed height

Binary system	Run no.	Calculated packed height [m] : Brokaw	Fuller
Methanol/i-propanol	5	2.95	2.51
Methanol/ethanol	2	3.11	2.61
Ethanol/i-propanol	3	2.81	2.42
Acetone/methanol	7	2.87	2.44

The average difference between the calculated packed heights for the runs shown in table 4.5 is 17.6%. This is a substantial amount and may lead to significant errors when designing a column to perform a specific separation. This analysis show that it is of primary importance that the correlation of binary mass transfer coefficients, applicable to distillation systems, be investigated.

4.8 Conclusions and recommendations

- The mass transfer correlations that gave the best fit on the wetted wall data in chapter 2 did not extrapolate well to the lower liquid flowrates encountered in structured packing.
- The use of correlation 2.36 with the proposed model predicts the packed height accurately with an average error of 5.7%.
- The model proposed by Crause [1998] overpredicts the packed height with an average error of 25.8%. A discrepancy was found in his definition of a characteristic length for the liquid Reynolds number.
- A sensitivity analysis showed that the model is sensitive to the binary diffusion coefficient and that the predicted packed height may vary by as much as 17.6%, depending on which correlation is used. It is recommended that the correlation of diffusion coefficients, applicable to distillation systems, be investigated.

The mass transfer efficiency of structured packing can be predicted by using the model proposed in this chapter together with the mass transfer coefficient predicted by correlation 2.36. It is recommended that the exponent of the Schmidt number in this correlation be rounded to the theoretical value of 0.5:

$$Sh_g = 0.0081 \mathrm{Re}_{g,r}^{0.94} Sc_g^{0.5}$$

It must be mentioned that in the proposed model the assumptions were made that the liquid side resistance is negligible and that the packing surface is completely wetted. In order to extend the model to systems were these assumptions do not apply, reliable correlations are needed for the effective wetted area and the liquid side resistance. This awaits future research.

CHAPTER 5 Conclusions and recommendations

- The gas phase mass transfer in a short wetted-wall column with a smooth surface was correlated with

$$Sh_g = 0.0044\,\mathrm{Re}_g\, Sc_g^{0.5} We_l^{0.111}$$

- The gas phase mass transfer in a short wetted-wall column with a complex surface, similar to that of the structured packing Mellapak 350Y, was correlated with

$$Sh_g = 0.0036\,\mathrm{Re}_g^{0.76}\, Sc_g^{0.5}\, \mathrm{Re}_l^{0.41}\, Bo^{-0.13}$$

- The liquid film was less prone to breakup in the staggered configuration than in the inline configuration of the complex surface.
- Liquid side resistance is negligible in all the binary systems investigated except the system ethanol/tridecane where a small resistance was found.
- The observed gas phase mass transfer enhancement in the binary systems is linked to the difference in surface tension between solvent and solute.
- The separation efficiency of Mellapak 350Y was predicted by making use of a gas phase mass transfer correlation fitted on wetted-wall data for the complex surface. This correlation extrapolates better to the lower liquid flow rates encountered in the distillation work than the correlations mentioned above:

$$Sh_g = 0.0081\,\mathrm{Re}_{g,r}^{0.94}\, Sc_g^{0.5}$$

- When combined with the proposed mass transfer model, the correlation predicted the separation efficiency with an average error of 6%.

The correlations developed in this work are based on low viscosity liquids. It was found that these correlations under predict the mass transfer rate for highly viscous liquids. It is recommended that the database for these correlations be extended to include highly viscous liquids. This is especially true for the complex surface correlation, which was fitted on data from only 3 pure components.

Since the flow rate of the liquid phase is substantially lower in the distillation column than in the wetted-wall column, it is recommended that the wetted-wall apparatus be

scaled down. The possibility of using triangular flow passages in the wetted wall column, similar to that found in structured packing, should be investigated.

A critical review of existing gas phase diffusion coefficient correlations, based on experimental work, should be made.

The quantification of possible gas phase mass transfer enhancement in binary mixtures where surface tension gradients exists needs further investigation.

REFERENCES

Barnet, W.I. and Kobe, K.A., *Heat and vapour transfer in a wetted-wall tower.* **Ind. Eng. Chem.** 33(4), 1941, 436-442.

Barrdahl, R.A.G., *Mass transfer in falling films: Influence of finite-amplitude waves.* **A.I.Ch.E. J.** 34(3), 1988, 493-498.

Billet, R. and Schultes, M., *Capacity studies of gas-liquid two-phase countercurrent-flow columns.* **I. Chem. E. Symposium Series** (104), 1987, B255-266.

Bontozoglou, V. and Papapolymerou, G., *Laminer film flow down a wavy incline.* **Int. J. Multiphase Flow** 23(1), 1997, 69-79.

Brain, P.L.T., Vivian, J.E. and Mayr, S.T., *Cellular convection in desorbing surface tension lowering solutes from water.* **Ind. Eng. Chem. Fundam.** 10(1), 1971, 75-83.

Bravo, J.L., Rocha, J.A. and Fair, J.R., *Mass transfer in gauze packings.* **Hydrocarbon Processing** (1), 1985, 91-95.

Bravo, J.L., *Select structured packings or trays?*, **Chem. Eng. Progr.** 93(7), 1997, 36-41.

Brokaw, R.S., *Predicting transport properties of dilute gases.* **Ind. Eng. Chem. Process Design Develop.**, 8,1969, 240-253.

Cairns, R.C. and Roper, G.H., *Heat and mass transfer at high humidities in a wetted-wall column.* **Chem. Eng. Sci.** 3, 1954, 97-109.

Chilton, T.H. and Colburn, A.P., *Mass transfer (absorption) coefficients.* **Ind. Eng. Chem.** 26(11), 1934, 1183-1187.

Coulson, J.M., Richardson, J.F., **Chemical Engineering Volume 2**, 4th Edition, New York, Pergamon, 1990, Chapter 12.

Crause, J.C., **A fundamental mass transfer model for an extractive distillation application**, M.Ing thesis, University of Stellenbosch, South Africa, January 1998.

Dassori, C.G., Deiber, J.A. and Cassano, A.E., *Slow two-phase flow through a sinusoidal channel.* **Int. J. Multiphase Flow** 10(2), 1984, 184-193.

Daugherty, R.L. and Franzini, J.B., **Fluid mechanics with engineering applications**, 7th Edition, Tokyo, McGraw-Hill, 1977, Chapter 8.

De Nevers, N., **Fluid mechanics for chemical engineers**, 2d edition, New York, McGraw-Hill, 1991, Chapter 6.

Dudukovic, A., Milosevic, V. and Pjanovic, R., *Gas-solid and gas-liquid mass transfer coefficients.* **A.I.Ch.E. J.** 42(1), 1996, 269-270.

Emmert, R.E. and Pigford, R.L., *Interfacial resistance.* **Chem. Eng. Progr.** 50(2), 1954, 87-93.

Fair, R.F. and Bravo, J.L., *Distillation columns containing structured packing.* **Chem. Eng. Progr.** 86(1), 1990, 19-29.

Foust, A.S., Wentzel, L.A., Clump, C.W., Maus, L. and Andersen, L.B., **Principles of unit operations**, 2d Edition, New York, John Wiley & Sons, 1980, Chapter 16.

Golovin, A.A., *Mass transfer under interfacial turbulence: kinetic regularities.* **Chem. Eng. Sci.** 47(8), 1992, 2069-2080.

Humphrey, J.L., *Separation processes: Playing a critical role.* **Chem. Eng. Progr.** 87(10), 1995, 31-41.

Imaishi, N., Suziki, Y., Hozawa, M. and Fujinawa, K., *Interfacial turbulence in gas-liquid mass transfer.* **Int. Chem. Eng.** 22(4), 1982, 659-665.

Incropera, F.P., De Witt, D.P., **Fundamentals of heat and mass transfer**, 3^{d} Edition, New York, John Wiley & Sons, 1990, Chapter 6

Jackson, M.L. and Ceaglske, N.H., *Distillation, vaporization, and gas absorption in a wetted-wall column.* **Ind. Eng. Chem.** 42(6), 1950, 1188-1198.

Kafesjian, R., Plank, C.A. and Gerhard, E.R., *Liquid flow and gas phase mass transfer in wetted wall-wall towers.* **A.I.Ch.E. J.** 7(3), 1961, 463-466.

Kang, F. and Chen, K., *Gravity driven two-layer flow down a slightly wavy periodic incline at low Reynolds numbers.* **Int. J. Multiphase Flow** 21(3), 1995, 501-513.

Kister, H.Z., **Distillation design**, New York, McGraw-Hill, 1992, Chapter 9.

Kurtz, D.P., McNulty, K.J. and Morgan, R.D., *Stretch the capacity of high-pressure distillation columns.* **Chem. Eng. Progr.** 87(2), 1991, 43-49.

Lu, H., Yang, Y., and Maa, J., *On the induction criterion of the Marangoni convection at the gas/liquid interface.* **Ind. Eng. Chem. Res.** 36, 1997, 474-482.

Lugg, G.A., *Diffusion coefficients of some organic and other vapours in air.* **Analytical Chemistry** 40(7), 1968, 1072-1077.

McCarter, R.J. and Stutzman, L.F., *Transfer resistance and fluid mechanics.* **A.I.Ch.E. J.** 5(4), 1959, 502-505.

Mills, A.F., **Heat and mass transfer**, Chicago, Irwin, 1995, Chaper 9.

Nawrocki, P.A., Xu, Z.P. and Chuang, K.T., *Mass transfer in structured corrugated packing.* **Can. J. Chem. Eng.** 69, 1991, 1336-1343.

Nielsen, C.H.E., Kiil, S., Thomsen, W. and Dam-Johansen, K., *Mass transfer in wetted-wall columns: Correlations at high Reynolds numbers.* **Chem. Eng. Sci.** 53(3), 1998, 495-503.

Nieuwoudt, I., **The fractionation of high molecular weight alkane mixtures with supercritical fluids**, PhD Dissertation, University of Stellenbosch, South Africa, March 1994.

Peramanu, S. and Sharma, A., *Nonlinear instabilities of falling films on a heated vertical plane with gas apsorption.* **Can. J. Chem. Eng.** 76(4), 1998, 211-223.

Portalski, S. and Clegg, A.J., *Interfacial area increase in rippled film flow on wetted wall columns.* **Chem. Eng. Sci.** 26, 1971, 773-784.

Porter, K.E., *Why research is needed in distillation.* **Trans. Instn. Chem. Engrs.** 73(A), 1995, 357-362.

Pozrikidis, C., *The flow of a liquid film along a periodic wall.* **J. Fluid Mech.** 188, 1988, 275-300.

Reid, R.C., Prausnitz, J.M. and Poling, B.E., **The properties of gases and liquids**, 4th Edition, New York, McGraw-Hill, 1987.

Reker, J.R., Plank, C.A. and Gerhard, E.R., *Liquid surface area effects in a wetted-wall column.* **A.I.Ch.E. J.** 12(5), 1966, 1008-1010.

Richter, H.J., *Flooding in tubes and annuli.* **Int. J. Multiphase Flow** 7(6), 1981, 647-658

Rocha, J.A., Bravo, J.L. and Fair, J.R., *Distillation columns containing structured packings: A comprehensive model for their performance. 2. Mass-transfer model.* **Ind. Eng. Chem. Res.** 35, 1996, 1660-1667.

Rocha, J.A., Bravo, J.L. and Fair, J.R., *Distillation columns containing structured packings: A comprehensive model for their performance. 1. Hydraulic models.* **Ind. Eng. Chem. Res.** 32, 1993, 641-651.

Sherwood, T.K. and Gilliland, E.R., *Diffusion of vapors into an air stream.* **Ind. Eng. Chem.** 26(5), 1934, 516-523.

Shetty, S. and Cerro, R.L., *Flow of a thin film over a periodic surface.* **Int. J. Multiphase Flow** 19(6), 1993, 1013-1027.

Shi, M.G. and Mersmann, A., *Effective interfacial area in packed columns.* **Ger. Chem. Eng.** 8, 1985, 87-96.

Spedding, P.L. and Jones, M.T., *Heat and mass transfer in wetted-wall columns: I.* **Chem. Eng. J.** 37, 1988, 165-176.

Spiegel, L. and Meier, W., *Correlations of the performance characteristics of the various Mellapak types.* **I. Chem. E. Symposium Series** (104), 1987, A203-215.

Stirba, C and Hurt, D.M., *Turbulence in falling liquid films.* **A.I.Ch.E. J.** 1(2), 1955, 178-184.

Strumillo, C. and Porter, K.E., *The evaporation of carbon tetrachloride in a wetted-wall column.* **A.I.Ch.E. J.** 11(6), 1965, 1139-1142.

Tailby, S.R. and Portalski, S., *Wave inception on a liquid film flowing down a hydrodynamically smooth plate.* **Chem. Eng. Sci.** 17, 1962, 283-290.

Taylor, R. and Krishna, R., **Multicomponent mass transfer**, New York, John Wiley & Sons, 1993, Chapter 8.

Trifonov, Y., *Viscous liquid film flows over a periodic surface.* **Int. J. Multiphase flow** 24, 1998, 1139-1161.

Vazquez, G., Antorrena, G., Navaza, J.M. and Santos, V., *Effective interfacial area in the presence of induced turbulence.* **Int. Chem. Eng.** 34(2), 1994, 247-254.

Vivian, J.E. and Peaceman, D.W., *Liquid side resistance in gas absorption.* **A.I.Ch.E. J.** 2(4), 1956, 437-443.

Wang, C.Y., *Liquid film flowing slowly down a wavy incline.* **A.I.Ch.E. J.** 27(2), 1981, 207-212.

Wankat, P.C. and Knaebel, K.S., *Mass transfer* in Perry, R.H. and Green, D.W. (ed.), **Perry's chemical engineers' handbook**, 7th Edition, New York, McGraw-Hill, 1997

Wasden, F.K., and Duckler, A.E., *A numerical study of mass transfer in free falling wavy films.* **A.I.Ch.E.J.** 36(9), 1990, 1379-1390.

Weiland, R.H., Ahlgren, K.R. and Evans, M., *Mass transfer characteristics of some structured packing.* **Ind. Eng. Chem. Res.** 32, 1993,1411-1418.

Yoshimura, P.N., Nosoko, T. and Nagata, T., *Enhancement of mass transfer into a falling liquid film by two-dimensional surface waves – some experimental observations and modelling.* **Chem. Eng. Sci.** 51(8), 1996, 1231-1240.

Zhao, L. and Cerro, R.L., *Experimental characterization of viscous film flows over complex surfaces.* **Int. J. Multiphase flow** 18(4), 1992, 495-516.

APPENDIX A Liquid film hydrodynamics

A1.1 Film thickness and interfacial velocity

The velocity and thickness of a liquid film flowing down an inclined channel with countercurrent vapour flow, can be calculated by applying the momentum equation in two dimensions [Incropera & De Witt, 1990]:

$$\frac{\partial[(\rho_l u)u]}{\partial x}+\frac{\partial[(\rho_l v)u]}{\partial x}=\frac{\partial \sigma_{xx}}{\partial x}-\frac{\partial P}{\partial x}+\frac{\partial \tau_{yx}}{\partial y}+X \qquad \text{(A1.1)}$$

The following assumptions are made:

1. The velocity component perpendicular to the surface is negligible:

$$u << v \qquad \text{(A1.2)}$$

2. The liquid is incompressible

3. The change in velocity along the surface is negligible:

$$\frac{\partial u}{\partial y} >> \frac{\partial u}{\partial x} \qquad \text{(A1.3)}$$

4. σ_{xx} is very small (A1.4)

5. The fluid is Newtonian which means that:

$$\tau_{yx}=\mu\frac{\partial u}{\partial y} \qquad \text{(A1.5)}$$

6. The change in pressure is as a result of the gravity of the vapour phase and friction [Taitel, 1983]:

$$\frac{\partial P}{\partial x} = \rho_v g \sin\theta + \frac{4\tau}{D_{eq} - 2\delta} \tag{A1.6}$$

7. The body force acting on a liquid element is due to gravitation:

$$X = \rho_l g \sin\theta \tag{A1.7}$$

Figure A1 shows the coordinate system with the different forces acting on a liquid element:

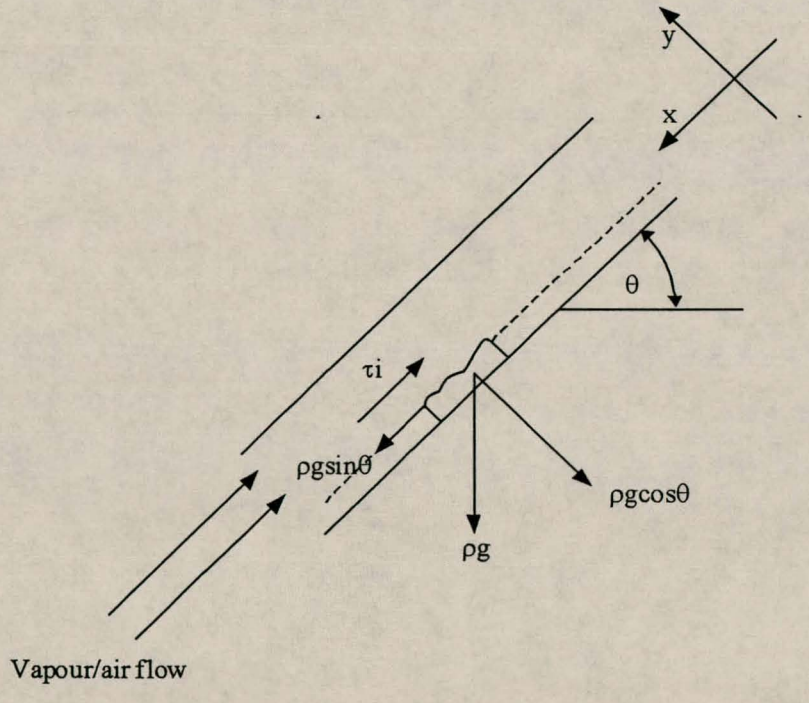

Figure A1 Forces acting on liquid element

By applying the assumptions, expanding the derivatives and applying the continuity equation, equation (A1.1) can be written as:

$$\mu \frac{\partial^2 u}{\partial y^2} = (\rho_v - \rho_l) g \sin\theta + \frac{4\tau}{D_{eq} - 2\delta} \tag{A1.8}$$

The following boundary conditions apply:

At the interface the shear stress is denoted by τ_w

$$\mu_l \frac{\partial u}{\partial y}\Big|_{y=\delta} = \tau_w \tag{A1.9}$$

and it is assumed that there is no slip at the packing surface :

$$u(y)\Big|_{y=0} = 0 \tag{A1.10}$$

Solving equation (A1.8) with the boundary conditions specified in equations (A1.9) and (A1.10) yields:.

$$u(y) = \frac{1}{2}\left[(\rho_v - \rho_l) g \sin\theta + \frac{4\tau}{D_{eq} - 2\delta}\right] y^2 + \left[\tau\left(1 - \frac{4\delta}{D_{eq} - 2\delta}\right) + (\rho_l - \rho_v)\delta g \sin\theta\right] y \tag{A1.11}$$

The average velocity of the liquid can be calculated by means of the following equation:

$$u_{AVG} = \frac{\int_0^\delta u dy}{\int_0^\delta dy} \tag{A1.12}$$

which yields:

$$\frac{(\rho_l - \rho_v)\delta^3 g \sin\theta}{3\mu} + \frac{\tau}{\mu}\left[\frac{\delta^2}{2} - \frac{4\delta^3}{3(D_{eq} - 2\delta)}\right] - \delta u_{avg} = 0 \tag{A1.13}$$

The interfacial velocity is calculated with:

$$ui = \frac{(\rho_l - \rho_v) g \delta^2 \sin\theta}{2\mu} + \frac{\tau\delta}{\mu}\left(1 - \frac{2\delta}{(D_{eq} - 2\delta)}\right) \qquad \text{(A1.14)}$$

A1.2 Interfacial friction

Equations (A1.13) and (A1.14) require the interfacial friction to calculate film thickness and interfacial velocity. Since the pressure drop is measured in the distillation experimental work, the interfacial friction is calculated from equation (4.51). The following applies only to the wetted wall column. The interfacial shear stress is defined as follows:

$$\tau_i = \frac{f_i}{2}\rho_v u^2 \qquad \text{(A1.15)}$$

The friction factor fi is analogous to the Moody friction factor for fluid flow in pipes. The appropriate velocity of the air is the velocity of the air relative to the liquid interface. The analytical expression of Wood [De Nevers, 1991] is used to calculate the friction factor:

$$\begin{aligned} f_i &= a + b\,\mathrm{Re}^{-c} \\ a &= 0.094\left(\frac{\varepsilon}{d}\right)^{0.225} + 0.053\left(\frac{\varepsilon}{d}\right) \\ b &= 88\left(\frac{\varepsilon}{d}\right)^{0.44} \\ c &= 1.62\left(\frac{\varepsilon}{d}\right)^{0.134} \end{aligned} \qquad \text{(A1.16)}$$

The roughness of the interface, e, must however be estimated. Wasden and Duckler [1990] noted that the wave height varied between 2-5 times the film thickness while

Richter [1981] found this value to be between 4 and 6. The roughness of the interface is taken to be 4 times the film thickness in this work.

APPENDIX B Physical property estimation

B1.1 Pure component properties

Liquid density: The Rackett equation was used for all the components with the Rackett constant for acetone, methanol, ethanol, i-propanol, ethylene glycol, tridecane and n-hexane from Reid and Prausnitz [1986] and the Rackett constant for 1,2-propanediol and 1-octanol from the SIMSCI databank. The density of 1,2-propanediol was measured and close agreement was found between the measured and predicted values.

Liquid viscosity: The viscosity correlations for all the pure components were taken from Reid and Prausnitz [1986]. The viscosity of 1,2-propanediol was experimentally measured and was found to be within 3% of the predicted value.

Surface tension: All the pure component surface tension correlations were taken from the extensive compilation by Jasper [1972].

Gas/vapour density: The density of air was calculated using the ideal gas law. The densities of acetone, methanol, ethanol, and i-propanol were calculated with the virial equation. The second virial coefficient were calculated by the method proposed by Vetere [1991].

Vapour pressure: The vapour pressure correlations for all the pure components were taken from the extensive data bank in Reid and Prausnitz [1986].

Gas/vapour viscosity: The viscosity of air was regressed from Incropera and De Witt [1990]. The viscosity of acetone, methanol, ethanol, and i-propanol were calculated with the method of Reichenberg [Reid & Prausnitz, 1986].

B1.2 Mixture properties

Liquid mixture density: The densities of all the liquid mixtures were estimated by making use of the mixing rules proposed by Cheuh and Prausnitz for mixture critical properties. The mixture density was then calculated by using the modified Rackett equation [Reid & Prausnitz, 1986].

Liquid mixture viscosity: The viscosity of all the liquid mixtures were calculated by making use of the method of Grunberg and Nissan [Reid & Prausnitz, 1986].

Liquid mixture surface tension: The surface tension of all the liquid mixtures were calculated with the correlation of Winterfeld et al. [1978].

Liquid phase diffusivity: The liquid phase diffusivity at infinite dilution for all the binary mixtures were calculated using the method of Tyn and Callus [Reid & Prausnitz, 1986]. The Vignes correlation [Reid & Prausnitz, 1986] were used to correct these values for concentration.

Liquid mixture vapour pressure: The NRTL equation [Smith & Van Ness, 1987] was used to calculate the vapour phase composition and vapour pressure for liquid mixtures. Binary interaction parameters from PRO II were used. For the systems n-hexane/tridecane, methanol/1-octanol and ethanol/tridecane the vapour/liquid equilibrium data were estimated with the UNIFAC group contribution method.

Gas/vapour phase diffusivity: The gas- and vapour phase diffusivities of all the components were calculated using the method of Fuller et al. [Reid & Prausnitz, 1986]. Comparison between the calculated value and the published value [Lugg, 1968] for the system 1,2-propanediol/air showed a difference of 8% at 25°. For the system n-hexane/air the constants in the Fuller et al. equation were regressed from data obtained in Reid and Prausnitz [1986] and Lugg [1968]. A sensitivity analysis between the correlations of

Brokaw [1969] and Fuller et al. [Reid & Prausnitz, 1986] showed a difference of 42% for the system methanol/ethanol.

Vapour phase density: The vapour phase density of vapour mixtures was calculated with the virial equation. The second virial coefficient and interaction parameters were calculated with the method proposed by Vetere [1991].

Vapour phase viscosity: The vapour phase mixture viscosity was calculated with the method of Wilke et al. [Reid & Prausnitz, 1986].

APPENDIX C Wetted-wall experimental results

Table C1 Experimental results for pure components – Smooth surface

Run no	Air rate [g/s]	Liquid rate [kg/min]	Evap. rate [ml/min]	T_{avg} (T1-T4) [°C]	T5 [°C]	T6 [°C]	Pt [kPa]	P1 [kPa]	Sh_g	Sc_g	Re_g	Re_l	We_l
Acetone (smooth surface)													
1	1.17	0.315	5.0	30	28.2	22.7	99.46	4.40	10.2	1.46	2092	68	0.152
2	1.17	0.410	5.0	29.9	28.55	22.7	99.46	4.53	9.5	1.46	2093	100	0.290
3	1.17	0.504	5.1	29.9	28.7	22.6	99.46	4.40	10.3	1.46	2110	144	0.529
4	1.61	0.228	7.0	29.3	26.6	21.8	99.46	7.20	9.3	1.46	2113	192	0.862
5	1.60	0.316	7.3	29.6	27.2	21.8	99.39	7.20	15.7	1.46	3129	229	1.155
6	1.61	0.410	7.4	29.6	27.8	21.8	99.46	7.20	15.8	1.46	3136	298	1.792
7	1.61	0.505	7.4	29.8	27.8	21.6	99.46	7.20	16.1	1.46	3140	366	2.535
8	2.09	0.228	8.9	29	25.8	21.3	99.79	10.93	11.5	1.46	3150	68	0.152
9	2.08	0.316	9.6	29.2	26.6	21.7	99.79	10.93	11.0	1.46	3163	100	0.289
10	2.08	0.411	9.9	29.5	27.3	21.8	99.79	10.93	15.7	1.46	3168	143	0.529
11	2.08	0.505	10.0	29.4	27.1	21.9	99.79	11.00	13.7	1.46	3171	192	0.862
12	2.61	0.228	11.1	28.7	25.4	22.5	99.79	16.13	15.3	1.46	3171	192	0.862
13	2.66	0.317	11.3	29	25	19.7	100.73	16.13	18.3	1.46	4313	68	0.152
14	2.65	0.411	12.0	29.2	25.9	19.8	100.66	16.13	20.5	1.46	4320	100	0.289
15	2.66	0.506	12.5	29.2	26.5	19.3	100.59	16.13	20.9	1.46	4322	144	0.529
16	0.80	0.094	3.3	30.5	25.3	17.6	100.59	2.60	21.8	1.46	4328	192	0.862
17	0.80	0.138	3.1	30.7	26.4	17.6	100.59	2.60	23.0	1.46	4287	164	0.666
18	0.81	0.198	3.3	30.5	25.9	15.5	101.13	2.60	23.5	1.46	4284	228	1.154
19	0.81	0.265	3.0	30.5	25.8	16.9	101.13	2.60	23.6	1.46	4293	297	1.789
20	1.21	0.095	3.7	30.5	22.1	17.7	100.99	4.53	23.6	1.46	4294	366	2.533
21	1.22	0.139	3.5	30.4	22.4	15.4	101.19	4.53	23.2	1.46	5572	68	0.152
22	1.22	0.198	5.0	30.4	26.4	15.5	101.19	4.53	25.5	1.46	5584	100	0.289
23	1.22	0.264	4.4	30.5	27.3	15.7	101.19	4.53	27.4	1.46	5590	143	0.529

Table C1 Continued – Acetone (smooth surface)

Run no	Air rate [g/s]	Liquid rate [kg/min]	Evap. rate [ml/min]	T_{avg} (T1-T4) [°C]	T5 [°C]	T6 [°C]	Pt [kPa]	P1 [kPa]	Sh_g	Sc_g	Re_g	Re_l	We_l
Acetone (smooth surface)													
24	1.22	0.265	4.9	30.5	27	15.7	101.19	4.53	28.3	1.46	5598	192	0.861
25	1.66	0.095	5.8	30.3	21.2	16.3	101.06	7.27	29.7	1.46	5570	164	0.664
26	1.66	0.138	6.5	30.3	25.2	16.5	101.06	7.27	31.8	1.46	5573	228	1.152
27	1.66	0.198	6.7	30.5	26	16.6	101.06	7.27	32.2	1.46	5572	297	1.787
28	1.66	0.265	7.0	30.5	26.5	16.6	101.06	7.27	32.5	1.46	5583	365	2.527
29	2.14	0.095	7.4	30.4	22.1	17.1	101.06	11.20	27.9	1.46	7014	68	0.152
30	2.14	0.138	8.1	30.3	24.5	17.2	101.06	11.20	29.7	1.46	7025	100	0.289
31	2.14	0.199	8.7	30.4	23.8	17.3	101.06	11.20	32.3	1.46	7037	143	0.529
32	2.14	0.265	9.0	30.4	25.8	17.4	101.06	11.20	34.6	1.46	7043	192	0.861
33	2.69	0.095	8.8	30.3	20.6	17.2	101.33	16.47	37.8	1.46	7001	163	0.663
34	2.69	0.138	9.4	30.3	24.1	17.3	101.33	16.47	38.1	1.46	7066	227	1.150
35	2.69	0.199	10.2	30.3	23.5	17.5	101.33	16.47	40.1	1.46	7064	296	1.784
36	2.69	0.265	11.0	30.4	25.3	17.6	101.33	16.47	41.9	1.46	7069	364	2.524
Methanol (smooth surface)													
1	0.81	0.310	1.4	30.3	28.6	17.4	100.86	2.67	10.9	0.97	2117	133	0.982
2	0.81	0.405	1.7	30.4	28.3	17.2	100.86	2.67	13.0	0.97	2120	174	1.535
3	0.81	0.508	1.3	30.4	29.1	17.3	100.86	2.67	10.3	0.97	2123	219	2.250
4	0.81	0.614	1.4	30.4	29.3	17.2	100.86	2.67	10.8	0.97	2127	265	3.093
5	0.81	0.083	1.3	30.2	21.5	16.4	100.99	2.67	10.0	0.97	2106	35	0.107
6	0.81	0.132	1.3	30.2	26.4	16.3	100.99	2.67	10.0	0.97	2111	56	0.233
7	0.81	0.192	1.2	30.2	27.4	16.3	100.99	2.67	9.4	0.97	2115	82	0.441
8	0.81	0.258	1.2	30.2	28	16.2	100.99	2.67	9.4	0.97	2119	110	0.721

Table C1 Continued – Methanol (smooth surface)

Run no	Air rate [g/s]	Liquid rate [kg/min]	Evap. rate [ml/min]	T_{avg} (T1-T4) [°C]	T5 [°C]	T6 [°C]	Pt [kPa]	P1 [kPa]	Sh_g	Sc_g	Re_g	Re_l	We_l
Methanol (smooth surface)													
9	1.22	0.083	1.7	30	22.3	15.7	100.99	4.47	13.3	0.97	3163	35	0.107
10	1.21	0.132	2.0	30.1	26.1	16.1	100.86	4.47	15.8	0.97	3164	56	0.233
11	1.21	0.192	1.7	30.2	27.1	16.4	100.86	4.53	13.0	0.97	3168	82	0.441
12	1.21	0.260	1.8	30.2	23.5	17.1	100.86	4.53	14.1	0.97	3174	110	0.721
13	1.21	0.311	1.8	30.3	26	17.6	100.86	4.53	14.0	0.97	3176	133	0.982
14	1.21	0.405	2.5	30.3	28.6	17.8	100.86	4.53	19.9	0.97	3182	174	1.535
15	1.21	0.508	1.8	30.4	28.9	17.8	100.86	4.53	13.8	0.97	3185	219	2.250
16	1.21	0.614	2.1	30.4	29	17.9	100.86	4.53	16.0	0.97	3190	265	3.093
17	1.21	0.405	2.0	30.3	28	17.8	100.86	4.53	15.6	0.97	3182	174	1.535
18	1.65	0.311	4.3	40.7	35.6	17.3	100.86	7.27	17.9	0.97	4087	149	1.063
19	1.65	0.403	5.5	41	37	17.3	100.86	7.27	22.6	0.97	4087	194	1.650
20	1.65	0.515	4.8	41	37.6	17.1	100.86	7.27	19.6	0.97	4094	249	2.485
21	1.65	0.624	5.0	41	38.1	17.1	100.86	7.27	20.4	0.97	4100	302	3.433
22	1.66	0.409	3.6	40.9	27.6	16.6	100.86	7.27	14.9	0.97	4089	194	1.649
23	1.66	0.403	4.8	41	37.4	16.6	100.86	7.27	19.6	0.97	4087	194	1.650
24	1.66	0.084	3.5	40.8	28.5	16.4	100.79	7.27	14.5	0.97	4054	40	0.117
25	1.66	0.131	4.0	40.9	30.8	16.4	100.79	7.27	16.5	0.97	4060	62	0.249
26	1.66	0.193	4.4	40.8	34.4	16.3	100.79	7.27	18.2	0.97	4070	92	0.476
27	1.66	0.259	4.5	40.8	35.4	16.2	100.79	7.27	18.6	0.97	4077	124	0.781
28	2.15	0.084	4.2	40.8	29.2	14.9	100.59	10.93	17.3	0.97	5230	40	0.117
29	2.15	0.131	5.2	40.7	32.1	15.1	100.59	10.93	21.6	0.97	5243	62	0.249
30	2.15	0.193	5.3	40.8	33.7	15.3	100.59	10.93	21.8	0.97	5251	92	0.476
31	2.14	0.259	5.7	41	35	15.5	100.59	10.93	23.2	0.97	5254	124	0.782

Table C1 Continued – Methanol (smooth surface)

Run no	Air rate [g/s]	Liquid rate [kg/min]	Evap. rate [ml/min]	T_{avg} (T1-T4) [°C]	T5 [°C]	T6 [°C]	Pt [kPa]	P1 [kPa]	Sh_g	Sc_g	Re_g	Re_l	We_l
Methanol (smooth surface)													
32	2.11	0.132	4.5	40.8	26.9	20	100.46	10.93	18.6	0.97	5234	62	0.249
33	2.11	0.193	5.1	40.9	34.5	20	100.46	10.93	20.8	0.97	5241	92	0.476
34	2.11	0.192	5.8	40.9	35.4	20	100.46	10.93	23.7	0.97	5241	92	0.476
35	2.11	0.083	5.0	40.8	34.3	19.9	100.46	10.93	20.5	0.97	5223	40	0.117
36	2.13	0.315	5.1	40.8	26.6	17.5	100.79	10.80	21.3	0.97	5276	149	1.063
37	2.13	0.404	5.9	40.9	36.4	17.8	100.79	10.80	24.2	0.97	5282	194	1.649
38	2.13	0.515	6.6	41	37.1	17.8	100.79	10.80	27.0	0.97	5289	249	2.485
39	2.13	0.624	6.6	41	37.6	17.9	100.79	10.80	27.0	0.97	5297	302	3.433
40	2.66	0.315	6.1	40.8	27.4	19.4	100.66	16.13	25.3	0.97	6611	149	1.063
41	2.66	0.404	7.5	41	35.7	19.5	100.66	16.13	30.6	0.97	6615	194	1.650
42	2.65	0.516	7.8	41.1	36.5	19.6	100.66	16.13	31.6	0.97	6623	249	2.487
43	2.65	0.625	7.7	41	37	19.6	100.66	16.13	31.4	0.97	6637	302	3.433
44	2.67	0.084	4.9	40.7	31.2	17.6	100.46	16.27	20.2	0.97	6557	40	0.117
45	2.66	0.131	5.9	40.9	32	17.9	100.46	16.27	24.1	0.97	6563	62	0.249
46	2.66	0.193	6.6	40.9	33.3	18.2	100.46	16.27	27.0	0.97	6576	92	0.476
47	2.66	0.259	6.9	41	34.3	18.2	100.46	16.27	28.1	0.97	6583	124	0.782
48	2.66	0.083	5.5	40.9	33.1	18.3	100.46	16.27	22.4	0.97	6550	40	0.117
Ethanol (smooth surface)													
1	0.80	0.062	2.3	50.3	39	18.1	99.99	2.67	10.0	1.26	1862	19	0.065
2	0.80	0.102	2.1	50.5	41	18.4	99.99	2.67	9.0	1.26	1865	32	0.153
3	0.80	0.159	2.3	50.6	43.9	18.5	99.99	2.67	9.8	1.26	1869	50	0.321
4	0.80	0.225	2.3	50.6	45.4	18.4	99.99	2.67	9.7	1.26	1873	71	0.576
5	0.79	0.266	2.2	50.6	46	18.6	99.79	2.67	9.3	1.26	1871	84	0.762

Table C1 Continued – Ethanol (smooth surface)

Run no	Air rate [g/s]	Liquid rate [kg/min]	Evap. rate [ml/min]	T_{avg} (T1-T4) [°C]	T5 [°C]	T6 [°C]	Pt [kPa]	P1 [kPa]	Sh_g	Sc_g	Re_g	Re_l	We_l
Ethanol (smooth surface)													
6	0.79	0.372	2.5	50.8	48.1	18.8	99.79	2.67	10.4	1.26	1874	118	1.345
7	0.79	0.457	3	50.8	48	18.9	99.79	2.67	12.6	1.26	1877	145	1.901
8	0.79	0.555	2.2	50.7	48.4	18.9	99.79	2.67	9.2	1.26	1882	176	2.634
9	0.79	0.556	2.3	50.7	47.8	18.9	99.86	2.67	9.6	1.26	1883	176	2.634
10	0.79	0.457	2.3	50.8	47.4	19	99.86	2.67	9.6	1.26	1879	145	1.901
11	1.20	0.272	5.3	59.4	54.1	18.3	100.66	4.40	13.2	1.27	2698	98	0.862
12	1.20	0.373	5.5	59.5	54	18.3	100.66	4.40	13.6	1.27	2702	136	1.469
13	1.20	0.462	5.9	59.5	55	18.3	100.66	4.33	14.6	1.27	2707	168	2.106
14	1.20	0.570	5.4	59.6	55.8	18.3	100.66	4.40	13.2	1.27	2711	208	3.001
15	1.20	0.570	5	59.6	55.8	18.4	100.66	4.40	12.2	1.27	2711	208	3.001
16	1.20	0.462	5.7	59.6	55	18.4	100.66	4.40	14.0	1.27	2706	169	2.108
17	1.20	0.061	4.3	58.7	44	18.2	100.59	4.40	11.3	1.27	2684	21	0.068
18	1.20	0.103	4.8	59.1	48.2	18.2	100.59	4.40	12.2	1.27	2684	37	0.168
19	1.20	0.163	5.2	59.4	51.6	18.2	100.59	4.33	12.9	1.27	2687	59	0.366
20	1.20	0.227	5.3	59.4	52.7	18.2	100.59	4.33	13.2	1.27	2692	82	0.635
21	1.65	0.061	5.2	58.6	44.8	16.4	100.66	7.07	13.7	1.27	3672	21	0.068
22	1.65	0.103	5.8	59.1	48.4	16.9	100.66	7.07	14.7	1.27	3671	37	0.168
23	1.65	0.164	6.4	59.2	50.7	17.1	100.66	7.07	16.1	1.27	3678	59	0.365
24	1.65	0.227	6.7	59.3	51.5	17.2	100.59	7.07	16.8	1.27	3682	82	0.634
25	1.64	0.272	7.1	59.4	53.2	17.8	100.46	7.07	17.6	1.27	3679	98	0.862
26	1.64	0.373	7.4	59.4	54.3	17.9	100.46	7.07	18.3	1.27	3688	135	1.467
27	1.64	0.462	7.4	59.5	54.9	18	100.46	7.07	18.2	1.27	3692	168	2.106
28	1.64	0.570	7.3	59.6	55.9	18.2	100.46	7.07	17.8	1.27	3697	208	3.001

Table C1 Continued – Ethanol (smooth surface)

Run no	Air rate [g/s]	Liquid rate [kg/min]	Evap. rate [ml/min]	T_{avg} (T1-T4) [°C]	T5 [°C]	T6 [°C]	Pt [kPa]	P1 [kPa]	Sh_g	Sc_g	Re_g	Re_l	We_l
Ethanol (smooth surface)													
29	2.12	0.272	9.1	59.3	51.8	18.1	100.39	11.07	22.7	1.27	4756	98	0.861
30	2.12	0.374	9.4	59.3	52.6	18.1	100.39	11.07	23.5	1.27	4767	135	1.466
31	2.12	0.463	10.5	59.4	53.8	18.2	100.39	11.07	26.1	1.27	4773	168	2.105
32	2.12	0.571	10.3	59.5	54.7	18.2	100.39	11.07	25.4	1.27	4779	208	2.999
33	2.18	0.061	5.9	58.5	43.4	13.3	101.39	10.87	15.7	1.27	4784	21	0.068
34	2.18	0.104	7	58.8	46.5	13.5	101.33	10.93	18.3	1.27	4785	37	0.168
35	2.17	0.164	7.9	58.9	48.9	13.7	101.26	10.93	20.5	1.27	4791	58	0.365
36	2.17	0.227	8.8	59.2	50.7	14	101.26	10.93	22.4	1.27	4793	82	0.634
37	2.71	0.061	7	58.5	42.2	15.1	101.13	16.13	18.6	1.27	5987	21	0.068
38	2.71	0.104	8.1	58.9	46.5	15.4	101.13	16.13	20.9	1.27	5989	37	0.168
39	2.70	0.164	9.4	59	48.4	15.5	101.06	16.20	24.1	1.27	5997	59	0.365
40	2.70	0.227	10.9	59.3	50.2	15.6	101.06	16.20	27.5	1.27	5999	82	0.634
41	2.70	0.273	10.8	59.1	50.9	14.3	100.66	16.13	27.4	1.27	5989	98	0.860
42	2.70	0.374	11.8	59.2	52	14.6	100.66	16.13	29.7	1.27	6000	135	1.465
43	2.70	0.463	12	59.4	53.5	15	100.59	16.00	29.8	1.27	6000	168	2.105
44	2.69	0.571	12.4	59.4	54.2	15.1	100.59	16.07	30.8	1.27	6011	208	2.996
i-Propanol (smooth surface)													
1	0.81	0.046	3.3	61.2	40.7	17.6	100.99	2.60	9.0	1.51	1772	12	0.040
2	0.81	0.090	3.7	61.1	50.5	18.1	100.99	2.60	10.0	1.51	1779	24	0.128
3	0.80	0.149	4.1	61.3	54.2	18.5	100.86	2.67	10.9	1.51	1779	40	0.300
4	0.80	0.209	4.1	61.4	56.2	18.9	100.86	2.67	10.8	1.51	1783	57	0.534
5	0.80	0.256	4.1	61.3	56.8	18.4	100.86	2.67	10.9	1.51	1786	70	0.747
6	0.80	0.344	4.1	61.5	58.7	18.6	100.86	2.67	10.7	1.51	1788	95	1.238

Table C1 Continued – i-Propanol (smooth surface)

Run no	Air rate [g/s]	Liquid rate [kg/min]	Evap. rate [ml/min]	T_{avg} (T1-T4) [°C]	T5 [°C]	T6 [°C]	Pt [kPa]	P1 [kPa]	Sh_g	Sc_g	Re_g	Re_l	We_l
i-Propanol (smooth surface)													
7	0.80	0.441	4.3	61.6	59.4	18.8	100.86	2.67	11.2	1.51	1791	122	1.879
8	0.80	0.555	4.2	61.5	59.9	19	100.86	2.67	10.9	1.51	1796	154	2.764
9	1.22	0.256	5.7	61.2	56.7	16.2	101.19	4.33	15.2	1.51	2690	70	0.746
10	1.22	0.345	5.9	61.3	57.8	16.4	101.19	4.27	15.7	1.51	2694	94	1.235
11	1.22	0.442	5.1	61.4	58.1	16.6	101.19	4.33	13.4	1.51	2699	121	1.875
12	1.22	0.441	5.7	61.5	58.8	16.9	101.19	4.33	14.9	1.51	2697	122	1.877
13	1.21	0.556	5.6	61.5	59.2	17.1	101.19	4.33	14.6	1.51	2703	154	2.764
14	1.21	0.045	4.5	60.3	44.9	17.5	100.99	4.40	12.9	1.51	2671	12	0.040
15	1.21	0.090	5.3	60.9	50.1	17.7	100.93	4.40	14.5	1.51	2669	24	0.127
16	1.21	0.149	5.1	61.3	53.6	18	100.99	4.40	13.5	1.51	2673	40	0.300
17	1.21	0.210	5.5	61.3	55	18.2	100.99	4.40	14.6	1.51	2679	57	0.533
18	1.66	0.046	5.1	60.5	42.3	15.7	100.93	7.07	14.4	1.51	3644	12	0.040
19	1.66	0.090	6	61	48.5	16.1	100.93	7.07	16.3	1.51	3646	24	0.128
20	1.66	0.149	6.6	61.3	52.4	16.3	100.93	7.07	17.5	1.51	3650	40	0.300
21	1.66	0.210	7.4	61.3	54.9	16.6	100.86	7.07	19.6	1.51	3656	57	0.533
22	1.66	0.045	5.3	60.9	45.9	16.9	100.86	7.00	14.5	1.51	3633	12	0.040
23	1.65	0.256	7.5	61.5	56.1	18.3	100.73	7.07	19.6	1.51	3653	70	0.749
24	1.64	0.345	7.6	61.4	57	18.4	100.73	7.07	19.9	1.51	3663	95	1.236
25	1.64	0.442	7.8	61.6	58.2	18.6	100.73	7.07	20.2	1.51	3667	122	1.879
26	1.64	0.556	7.9	61.6	58.7	18.7	100.73	7.07	20.4	1.51	3675	154	2.767
27	2.15	0.557	10.5	61.4	57.8	16.1	100.99	10.80	27.6	1.51	4769	153	2.761
28	2.14	0.443	10.5	61.4	57.2	16.7	100.99	10.80	27.7	1.51	4758	121	1.875
29	2.14	0.346	10.3	61.5	56.2	16.8	100.99	10.93	27.0	1.51	4746	95	1.238

Table C1 Continued – i-Propanol (smooth surface)

Run no	Air rate [g/s]	Liquid rate [kg/min]	Evap. rate [ml/min]	T_{avg} (T1-T4) [°C]	T5 [°C]	T6 [°C]	Pt [kPa]	P1 [kPa]	Sh_g	Sc_g	Re_g	Re_l	We_l
i-Propanol (smooth surface)													
30	2.14	0.257	10.1	61.3	53.5	16.8	100.99	10.93	26.9	1.51	4739	70	0.747
31	2.13	0.210	8.9	61.3	53.5	18.1	100.79	11.00	23.6	1.51	4723	57	0.533
32	2.13	0.149	9	61.3	51.9	18.3	100.79	10.93	23.9	1.51	4712	40	0.300
33	2.13	0.090	7.8	61.2	48.3	18.4	100.79	10.93	20.9	1.51	4701	24	0.128
34	2.13	0.046	5.8	61.3	41.5	18.3	100.79	10.93	15.5	1.51	4684	12	0.040
35	2.13	0.046	5.9	61.5	40.4	18.5	100.79	10.93	15.6	1.51	4678	12	0.040
36	2.70	0.210	11.3	61.2	52.7	14.6	100.59	16.13	30.1	1.51	5918	57	0.533
37	2.70	0.150	10.3	61.1	50	14.8	100.59	16.13	27.7	1.51	5908	40	0.300
38	2.70	0.090	9.3	61	49.9	15	100.59	16.13	25.1	1.51	5894	24	0.128
39	2.69	0.046	6.4	61.6	41.9	15.3	100.59	16.13	16.7	1.51	5855	12	0.040
40	2.66	0.558	13.5	61.3	57.1	19.1	100.66	16.27	35.7	1.51	5967	153	2.759
41	2.67	0.443	13.3	61.3	56.1	17.8	100.66	16.27	35.2	1.51	5954	121	1.873
42	2.68	0.346	12.6	61.4	56.2	17.3	100.66	16.27	33.1	1.51	5938	95	1.236
43	2.68	0.256	11.5	61.3	54.9	17.1	100.66	16.27	30.4	1.51	5927	70	0.747
44	2.68	0.258	12.3	61.5	51.6	17	100.66	16.27	32.3	1.51	5921	70	0.749
n-Hexane (smooth surface)													
1	0.78	0.091	4.9	41.7	37	25.5	99.93	2.60	11.1	2.02	1950	75	0.226
2	0.78	0.135	4.4	41.8	38.1	25.5	99.93	2.60	9.9	2.02	1953	112	0.441
3	0.78	0.195	4.9	42	39	25.6	99.93	2.60	10.9	2.02	1954	162	0.812
4	0.78	0.258	4.7	42.1	38.6	25.6	99.93	2.60	10.3	2.02	1956	215	1.303
5	0.78	0.327	6.0	42.1	40.2	25.6	99.93	2.60	13.3	2.02	1959	273	1.938
6	0.78	0.393	5.3	42.1	39.5	25.6	99.93	2.60	11.6	2.02	1961	328	2.629
7	1.17	0.091	7.5	41.2	36.3	24.1	100.13	4.60	17.5	2.02	2940	75	0.225

Table C1 Continued – n-Hexane (smooth surface)

Run no	Air rate [g/s]	Liquid rate [kg/min]	Evap. rate [ml/min]	T_{avg} (T1-T4) [°C]	T5 [°C]	T6 [°C]	Pt [kPa]	P1 [kPa]	Sh_g	Sc_g	Re_g	Re_l	We_l
n-Hexane (smooth surface)													
8	1.17	0.136	7.0	41.4	37.2	24.2	100.13	4.60	16.1	2.02	2941	112	0.440
9	1.17	0.195	7.2	41.5	37.6	24.3	100.06	4.60	16.4	2.02	2943	161	0.809
10	1.17	0.258	7.0	41.7	39.1	24.6	100.13	4.60	15.8	2.02	2946	215	1.300
11	1.17	0.327	7.7	41.8	39	24.9	100.13	4.60	17.2	2.02	2949	273	1.934
12	1.17	0.393	7.1	42	38.3	25	100.06	4.60	15.7	2.02	2947	328	2.627
13	1.59	0.091	10.5	41.4	35.2	25.5	100.06	7.20	24.2	2.02	4010	75	0.225
14	1.59	0.136	10.8	41.4	36	25.6	100.06	7.20	25.0	2.02	4017	112	0.440
15	1.59	0.195	11.3	41.6	37.1	25.8	100.13	7.20	25.9	2.02	4022	162	0.810
16	1.59	0.259	11.8	41.7	37.1	26	100.13	7.20	26.7	2.02	4026	215	1.300
17	1.59	0.328	12.2	41.8	38.6	26.1	100.13	7.20	27.5	2.02	4030	273	1.934
18	1.59	0.393	12.3	42	39	26.2	100.13	7.20	27.4	2.02	4030	328	2.627
19	2.05	0.091	12.0	41.4	33.3	27	100.06	11.07	27.7	2.02	5184	75	0.225
20	2.05	0.136	13.6	41.5	35.2	27.2	100.06	11.07	31.2	2.02	5190	112	0.440
21	2.05	0.195	14.6	41.6	36.1	27.3	100.06	11.07	33.4	2.02	5196	162	0.809
22	2.05	0.259	15.7	41.8	37	27.3	100.06	11.07	35.5	2.02	5199	215	1.300
23	2.05	0.328	16.0	42	37.9	27.4	100.06	11.07	35.8	2.02	5200	273	1.937
24	2.05	0.393	17.6	42	38.5	27.4	100.06	11.07	39.4	2.02	5206	328	2.627
25	2.05	0.091	12.4	41.5	34.8	27.3	100.06	11.07	28.4	2.02	5181	75	0.225
26	2.05	0.394	16.8	41.9	37.9	27.4	100.06	11.07	37.8	2.02	5209	327	2.625
27	2.57	0.091	14.9	41.1	33.1	27.6	100.06	16.27	34.9	2.02	6515	75	0.225
28	2.57	0.136	16.9	41.4	33.6	27.9	100.13	16.27	39.1	2.02	6520	112	0.440
29	2.57	0.196	18.1	41.5	35	27.9	100.06	16.27	41.7	2.02	6524	161	0.809
30	2.57	0.259	19.3	41.7	36	28	100.06	16.27	43.8	2.02	6526	215	1.300

Table C1 Continued – n-Hexane (smooth surface)

Run no	Air rate [g/s]	Liquid rate [kg/min]	Evap. rate [ml/min]	T_{avg} (T1-T4) [°C]	T5 [°C]	T6 [°C]	Pt [kPa]	P1 [kPa]	Sh_g	Sc_g	Re_g	Re_l	We_l
n-Hexane (smooth surface)													
31	2.57	0.328	20.6	41.9	36.8	27.9	100.13	16.27	46.5	2.02	6533	273	1.936
32	2.57	0.394	22.0	41.9	37.4	28.1	100.13	16.27	49.7	2.02	6540	327	2.625
33	2.57	0.394	21.0	41.8	36.7	28	100.13	16.27	47.7	2.02	6544	327	2.624
1,2-Propanediol (smooth surface)													
1	1.56	0.282	3.1	132.9	117.2	31	99.79	7.20	25.3	1.64	2561	40	0.447
2	1.56	0.419	2.6	133	119	31	99.79	7.20	20.9	1.64	2569	60	0.866
3	1.56	0.570	2.7	132.7	122.6	31.1	99.79	7.20	22.0	1.64	2580	82	1.443
4	1.56	0.068	3.1	133.2	112.6	31.2	99.79	7.20	25.1	1.64	2534	10	0.041
5	1.56	0.044	3.3	132.2	101.4	31.1	99.79	7.20	28.5	1.64	2540	6	0.020
6	2.02	0.044	3.4	130.7	101.1	31.2	99.79	11.20	31.3	1.64	3306	6	0.020
7	2.02	0.068	3.45	133.6	111.3	31.5	99.79	11.20	27.3	1.64	3269	10	0.042
8	2.01	0.282	3.1	133.5	117.4	31.8	99.79	11.20	24.4	1.64	3302	41	0.449
9	2.01	0.419	3.25	133	125.3	31.9	99.79	11.20	25.9	1.64	3321	60	0.866
10	2.01	0.570	3.25	133.1	121.9	31.9	99.79	11.20	25.9	1.64	3330	82	1.449
11	2.54	0.044	4.35	131.9	98.7	31.6	100.13	16.27	38.1	1.64	4139	6	0.020
12	2.53	0.068	3.65	132.7	106.5	31.9	100.13	16.27	30.3	1.64	4133	10	0.041
13	2.53	0.282	4.3	133.4	116.4	32.4	100.13	16.27	34.3	1.64	4158	41	0.449
14	2.55	0.419	4.15	133	116.9	29.1	99.99	16.27	33.6	1.64	4175	60	0.866
15	2.55	0.504	4.2	133.1	117.9	29.8	99.99	16.27	33.8	1.64	4181	73	1.181
16	2.55	0.068	4.45	133.8	106.8	30.1	99.99	16.27	35.2	1.64	4107	10	0.042

Table C2 Experimental results for pure components – Complex surface

Run no	Air rate [g/s]	Liquid rate [kg/min]	Evap. rate [ml/min]	T_{avg} (T1-T4) [°C]	T5 [°C]	T6 [°C]	Pt [kPa]	P1 [kPa]	Sh_g	Sc_g	Re_g	Re_l	We_l
Methanol (complex surface, staggered configuration)													
1	0.78	0.166	2.1	42.8	37.2	24.2	100.33	2.80	7.8	0.97	1822	77	0.013
2	0.78	0.231	3.3	42.9	38.6	24.7	100.33	2.80	12.4	0.97	1823	107	0.017
3	0.78	0.298	3.5	43.2	39.4	25.1	100.26	2.80	13.0	0.97	1822	138	0.020
4	0.78	0.367	3.5	43.4	40.1	25.5	100.26	2.80	12.8	0.97	1822	171	0.023
5	0.78	0.439	4.1	43.4	40.3	25.8	100.19	2.80	15.3	0.97	1823	204	0.026
6	1.16	0.166	4.0	43.2	36.6	27.0	100.13	4.67	14.7	0.97	2720	77	0.013
7	1.16	0.231	5.1	43.4	37.4	27.3	100.13	4.67	18.9	0.97	2722	107	0.017
8	1.16	0.298	5.5	43.4	38.5	27.4	100.13	4.67	20.3	0.97	2725	138	0.020
9	1.16	0.367	5.9	43.6	39.1	27.4	100.13	4.67	21.7	0.97	2726	171	0.023
10	1.16	0.439	6.7	43.6	39.4	27.4	100.13	4.67	24.8	0.97	2729	204	0.026
11	1.16	0.439	6.2	43.5	39.4	27.4	100.13	4.67	23.0	0.97	2730	204	0.026
12	1.58	0.166	4.8	43.3	36.0	27.6	100.13	7.20	17.4	0.97	3715	77	0.013
13	1.58	0.231	6.3	43.4	37.0	27.6	100.13	7.20	23.1	0.97	3721	107	0.017
14	1.58	0.298	6.8	43.4	37.8	27.6	100.13	7.20	25.0	0.97	3725	138	0.020
15	1.58	0.367	6.9	43.6	38.4	27.6	100.13	7.20	25.4	0.97	3726	171	0.023
16	1.58	0.439	8.4	43.5	38.7	27.6	100.13	7.20	31.2	0.97	3731	204	0.026
17	1.60	0.439	7.0	43.1	38.0	24.9	99.99	7.27	26.3	0.97	3735	203	0.026
18	1.56	0.439	7.4	43.1	38.2	31.2	99.99	7.27	27.9	0.97	3736	203	0.026
19	2.06	0.166	6.0	42.9	35.2	26.2	99.99	11.27	22.6	0.97	4808	77	0.013
20	2.05	0.231	6.6	43.1	35.9	26.5	99.99	11.27	24.5	0.97	4812	107	0.017
21	2.05	0.298	7.4	43.1	37.5	26.7	99.99	11.27	27.5	0.97	4816	138	0.020
22	2.05	0.367	7.6	43.4	37.7	26.9	99.99	11.27	28.0	0.97	4816	171	0.023
23	2.05	0.439	8.6	43.4	38.0	27.0	99.99	11.27	31.8	0.97	4821	204	0.026

Table C2 Continued – Methanol (complex surface)

Run no	Air rate [g/s]	Liquid rate [kg/min]	Evap. rate [ml/min]	T_{avg} (T1-T4) [°C]	T5 [°C]	T6 [°C]	Pt [kPa]	P1 [kPa]	Sh_g	Sc_g	Re_g	Re_l	We_l
Methanol (complex surface, staggered configuration)													
24	2.05	0.439	8.6	43.4	38.0	27.3	99.99	11.27	31.8	0.97	4821	204	0.026
25	2.56	0.166	6.6	42.9	34.6	28.2	99.93	16.60	24.8	0.97	6028	77	0.013
26	2.56	0.231	7.7	43.2	35.5	28.2	99.93	16.60	28.4	0.97	6028	107	0.017
27	2.56	0.298	7.9	43.2	36.2	28.1	99.93	16.60	29.1	0.97	6038	138	0.020
28	2.56	0.367	9.1	43.3	36.9	28.2	99.93	16.60	33.6	0.97	6040	170	0.023
29	2.56	0.439	10.1	43.3	37.1	28.0	99.99	16.60	37.5	0.97	6051	204	0.026
Ethanol (complex surface, staggered configuration)													
1	0.79	0.139	4.3	61.4	52.2	22.9	101.06	2.73	9.9	1.27	1659	49	0.016
2	0.79	0.199	4.6	61.6	54.7	23.1	101.06	2.73	10.5	1.27	1661	70	0.020
3	0.79	0.263	4.7	61.7	55.6	23.5	101.06	2.73	10.5	1.27	1662	93	0.024
4	0.79	0.333	5.1	61.8	57.4	23.6	101.06	2.73	11.5	1.27	1664	118	0.029
5	0.79	0.396	5.7	61.9	57.5	23.9	101.06	2.73	12.8	1.27	1665	141	0.032
6	0.79	0.396	6.2	62.0	58.2	24.1	101.06	2.73	13.8	1.27	1664	141	0.032
7	1.18	0.139	6.4	61.6	50.9	24.5	101.06	4.40	14.6	1.27	2486	49	0.016
8	1.18	0.199	7.6	61.7	53.3	24.6	101.06	4.40	15.2	1.27	2136	122	0.029
9	1.18	0.263	7.9	61.7	54.1	24.6	100.99	4.40	16.0	1.27	2225	128	0.030
10	1.18	0.333	8.6	61.9	56.2	24.6	100.99	4.40	16.9	1.27	2314	135	0.031
11	1.18	0.396	9.0	62.0	55.9	24.6	100.99	4.40	17.7	1.27	2403	142	0.032
12	1.61	0.139	7.7	61.5	50.1	24.6	100.99	7.27	18.5	1.27	2492	149	0.033
13	1.61	0.199	8.6	61.8	51.5	24.8	100.99	7.27	19.3	1.27	2581	156	0.034
14	1.61	0.263	9.8	61.8	54.1	24.7	100.99	7.27	20.1	1.27	2670	162	0.035
15	1.61	0.333	10.3	61.9	54.2	24.7	100.99	7.27	20.9	1.27	2759	169	0.036
16	1.62	0.396	11.3	61.9	55.2	24.7	101.13	7.27	21.7	1.27	2848	176	0.037

Table C2 Continued – Ethanol (complex surface)

Run no	Air rate [g/s]	Liquid rate [kg/min]	Evap. rate [ml/min]	T_{avg} (T1-T4) [°C]	T5 [°C]	T6 [°C]	Pt [kPa]	P1 [kPa]	Sh_g	Sc_g	Re_g	Re_l	We_l
Ethanol (complex surface, staggered configuration)													
17	2.09	0.139	7.8	61.6	47.4	23.7	100.86	11.20	17.9	1.27	4384	49	0.016
18	2.09	0.199	9.8	61.8	51.2	23.9	100.86	11.20	22.1	1.27	4386	70	0.020
19	2.09	0.263	10.6	61.7	52.2	23.9	100.86	11.20	23.9	1.27	4396	93	0.024
20	2.09	0.333	12.0	62.0	53.4	24.0	100.86	11.20	26.7	1.27	4397	118	0.028
21	2.09	0.396	13.1	61.9	54.4	24.1	100.86	11.20	29.3	1.27	4404	141	0.032
22	2.09	0.139	9.7	61.7	49.0	24.2	100.86	11.20	22.0	1.27	4381	49	0.016
23	2.09	0.139	8.9	61.7	48.4	24.2	100.79	11.20	20.2	1.27	4377	49	0.016
24	2.62	0.139	10.2	61.4	47.8	24.4	100.86	16.47	23.4	1.27	5504	49	0.016
25	2.62	0.199	11.6	61.6	50.7	24.5	100.86	16.47	26.3	1.27	5509	70	0.020
26	2.62	0.263	12.6	61.6	51.2	24.6	100.86	16.47	28.7	1.27	5520	93	0.024
27	2.61	0.333	14.1	61.7	52.5	24.8	100.79	16.47	31.8	1.27	5521	118	0.029
28	2.61	0.396	15.3	61.9	53.8	24.8	100.79	16.47	34.2	1.27	5523	141	0.032
Ethanol (complex surface, inline configuration)													
1	0.79	0.086	4.1	62.1	50.6	20.8	100.39	2.80	9.0	1.27	1638	30	0.011
2	0.79	0.116	4.4	62.5	51.8	21.0	100.39	2.80	9.3	1.27	1637	41	0.014
3	0.79	0.150	4.6	62.5	52.9	21.3	100.39	2.80	9.7	1.27	1639	54	0.017
4	0.79	0.186	4.7	62.6	54.1	21.5	100.39	2.80	10.0	1.27	1640	67	0.019
5	0.79	0.214	4.9	62.8	55.5	21.7	100.39	2.80	10.3	1.27	1639	77	0.021
6	1.19	0.086	5.7	62.0	48.1	21.7	100.33	4.47	12.6	1.27	2456	30	0.011
7	1.18	0.116	6.4	62.2	49.3	21.8	100.33	4.47	13.9	1.27	2457	41	0.014
8	1.18	0.150	7.1	62.4	50.4	21.9	100.33	4.47	15.3	1.27	2458	54	0.017
9	1.18	0.186	7.4	62.5	51.6	22.0	100.33	4.47	15.9	1.27	2459	66	0.019
10	1.18	0.214	7.8	62.4	53.2	22.0	100.33	4.47	16.8	1.27	2463	76	0.021

Table C2 Continued – Ethanol (complex surface)

Run no	Air rate [g/s]	Liquid rate [kg/min]	Evap. rate [ml/min]	T_{avg} (T1-T4) [°C]	T5 [°C]	T6 [°C]	Pt [kPa]	P1 [kPa]	Sh_g	Sc_g	Re_g	Re_l	We_l
Ethanol (complex surface, inline configuration)													
11	1.63	0.086	6.1	61.8	45.4	19.5	100.39	7.33	13.7	1.27	3363	30	0.012
12	1.63	0.116	7.3	62.1	47.7	19.7	100.39	7.33	15.9	1.27	3362	41	0.014
13	1.63	0.150	7.8	62.3	48.1	20.0	100.19	7.33	17.0	1.27	3358	54	0.017
14	1.63	0.186	8.8	62.5	50.1	20.1	100.19	7.33	18.8	1.27	3358	66	0.019
15	1.63	0.214	9.3	62.4	50.5	20.1	100.19	7.33	20.0	1.27	3362	76	0.021
16	2.10	0.086	7.7	62.2	45.8	20.2	100.19	11.13	16.7	1.27	4331	30	0.011
17	2.10	0.116	8.5	62.1	46.4	20.2	100.19	11.13	18.6	1.27	4338	41	0.014
18	2.10	0.150	9.4	62.4	47.6	20.3	100.19	11.13	20.3	1.27	4337	54	0.017
19	2.10	0.186	9.9	62.5	49.2	20.4	100.19	11.13	21.2	1.27	4340	66	0.019
20	2.10	0.214	10.5	62.4	49.9	20.4	100.13	11.13	22.5	1.27	4342	76	0.021
21	2.63	0.086	8.6	62.2	41.5	20.5	100.13	16.53	18.9	1.27	5431	30	0.011
22	2.63	0.116	8.6	62.5	45.6	20.5	100.13	16.53	18.4	1.27	5429	42	0.014
23	2.63	0.150	10.4	62.3	47.0	20.5	100.13	16.53	22.4	1.27	5440	54	0.017
24	2.63	0.186	11.6	62.5	48.0	20.6	100.13	16.53	24.8	1.27	5442	66	0.019
25	2.63	0.214	12.1	62.5	49.0	20.6	100.13	16.53	25.8	1.27	5445	77	0.021
n-Hexane (complex surface, staggered configuration)													
1	0.78	0.090	4.8	37.5	31.9	24.8	100.13	2.67	13.4	1.93	1868	67	0.009
2	0.78	0.132	5.3	37.6	33.0	25.1	100.13	2.67	14.8	1.93	1870	99	0.011
3	0.78	0.193	5.4	37.8	33.8	25.3	100.19	2.67	15.0	1.93	1872	145	0.014
4	0.78	0.256	5.8	37.9	34.7	25.5	100.13	2.67	15.9	1.93	1872	193	0.017
5	1.17	0.090	8.3	38.3	31.5	25.9	100.13	4.40	22.6	1.93	2789	68	0.009
6	1.17	0.132	9.6	38.3	32.1	26.0	100.13	4.40	26.1	1.93	2792	100	0.011
7	1.17	0.193	10.3	38.2	33.1	25.6	100.13	4.40	28.4	1.93	2799	146	0.014

Table C2 Continued – n-Hexane (complex surface)

Run no	Air rate [g/s]	Liquid rate [kg/min]	Evap. rate [ml/min]	T_{avg} (T1-T4) [°C]	T5 [°C]	T6 [°C]	Pt [kPa]	P1 [kPa]	Sh_g	Sc_g	Re_g	Re_l	We_l
n-Hexane (complex surface, staggered configuration)													
8	1.17	0.256	11.1	38.3	33.5	25.4	100.13	4.40	30.4	1.93	2802	194	0.017
9	1.62	0.090	10.8	37.1	29.3	21.4	100.39	7.13	31.3	1.93	3848	67	0.009
10	1.62	0.132	11.6	37.0	29.8	21.4	100.39	7.13	34.0	1.93	3855	99	0.011
11	1.62	0.193	12.5	37.1	30.8	21.6	100.39	7.13	36.4	1.93	3860	144	0.014
12	1.62	0.256	13.9	37.1	32.3	21.7	100.39	7.13	40.4	1.93	3865	192	0.017
13	2.09	0.090	13.0	37.0	29.2	22.0	100.39	11.13	37.9	1.93	4977	67	0.009
14	2.09	0.132	13.9	36.9	29.5	22.1	100.39	11.13	40.6	1.93	4987	99	0.011
15	2.09	0.193	15.0	37.1	30.4	22.2	100.39	11.13	43.6	1.93	4990	144	0.014
16	2.09	0.256	17.0	37.1	31.6	22.2	100.39	11.13	49.5	1.93	4996	192	0.017

Table C3 Experimental results binary mixtures – Smooth surface

Run no	Air rate [g/s]	Liquid rate [kg/min]	Evap. rate [ml/min]	T_{avg} (T1-T4) [°C]	T5 [°C]	T6 [°C]	Pt [kPa]	P1 [kPa]	mass% methanol
Methanol/ethylene glycol (smooth surface)									
1	0.77	0.090	1.5	43.5	38.6	29.9	100.19	2.80	25
2	0.77	0.176	1.3	43.7	39.2	30	100.13	2.80	25
3	0.77	0.411	1.3	43.8	41.9	30.3	100.13	2.80	25
4	0.77	0.283	1.2	43.7	41	30.3	100.13	2.80	25
5	1.15	0.090	1.4	43.6	37.5	30.9	100.13	4.40	25
6	1.15	0.176	1.6	43.7	39	31.2	100.06	4.40	25
7	1.14	0.283	1.8	43.9	39.9	31.3	100.06	4.40	25
8	1.14	0.411	1.8	43.9	42.3	31.3	100.06	4.40	25
9	1.14	0.543	2.2	44	42.4	31.3	100.06	4.40	25
10	1.58	0.090	2.0	43	36.1	28.5	99.99	7.20	25
11	1.58	0.176	2.2	43.2	38.6	28.4	99.99	7.20	25
12	1.58	0.283	2.2	43.2	38.7	28.6	99.99	7.20	25
13	1.58	0.411	2.3	43.4	40.2	28.6	99.99	7.20	25
14	1.58	0.543	2.3	43.5	41.5	28.7	99.93	7.20	25
15	2.03	0.090	2.8	43.3	37	29.2	99.93	11.13	25
16	2.03	0.176	2.7	43.6	36.5	29.5	99.93	11.13	25
17	2.03	0.283	2.9	43.7	38.7	29.7	99.93	11.13	25
18	2.03	0.411	2.8	43.7	40.4	29.8	99.93	11.13	25
19	2.03	0.543	3.0	43.7	41.4	30	99.86	11.13	25
20	2.54	0.090	3.2	43.4	36.5	30.3	99.86	16.40	25
21	2.54	0.176	3.3	43.7	36.4	30.6	99.86	16.40	25
22	2.53	0.283	3.4	43.7	38.3	31.5	99.79	16.40	25
23	2.53	0.411	3.4	43.8	40.2	31.7	99.73	16.40	25

Table C3 Continued – Methanol/ethylene glycol (smooth surface)

Run no	Air rate [g/s]	Liquid rate [kg/min]	Evap. rate [ml/min]	T_{avg} (T1-T4) [°C]	T5 [°C]	T6 [°C]	Pt [kPa]	P1 [kPa]	mass% methanol
Methanol/ethylene glycol (smooth surface)									
24	2.52	0.543	3.5	43.8	40.7	31.8	99.73	16.40	25
25	0.77	0.090	1.8	43.2	37.1	27.3	100.06	2.80	50
26	0.77	0.154	1.7	43.3	38	27.5	100.06	2.80	50
27	0.77	0.221	1.9	43.3	38.7	27.7	100.06	2.80	50
28	0.77	0.285	2.2	43.4	39.5	27.9	99.99	2.80	50
29	0.77	0.367	1.9	43.4	40.1	28.2	99.99	2.80	50
30	1.15	0.090	2.2	43.6	36.3	29.9	99.79	4.40	50
31	1.15	0.154	2.6	43.7	37.9	30.3	99.79	4.40	50
32	1.14	0.221	2.6	43.8	38.8	30.5	99.79	4.40	50
33	1.14	0.285	2.9	43.7	39.5	30.5	99.79	4.40	50
34	1.14	0.367	3.2	43.7	40.1	30.5	99.79	4.40	50
35	1.14	0.221	2.8	43.7	38.9	30.5	99.79	4.40	50
36	1.59	0.090	3.0	42.7	35.1	25.8	100.06	7.20	50
37	1.59	0.154	3.2	42.9	35.9	26.3	100.06	7.20	50
38	1.59	0.221	3.2	42.9	37	26.5	100.06	7.20	50
39	1.59	0.285	3.4	43.1	38	26.8	100.06	7.20	50
40	1.59	0.367	3.6	43.1	38.8	27.1	100.06	7.20	50
41	2.05	0.090	4.0	43	35.2	27.8	100.06	11.20	50
42	2.04	0.154	3.9	43.3	35.6	28.2	100.06	11.20	50
43	2.04	0.221	4.4	43.4	36.8	28.3	100.06	11.20	50
44	2.04	0.285	4.4	43.3	37.6	28.5	100.06	11.20	50
45	2.04	0.367	4.7	43.3	38.7	28.6	100.06	11.20	50
46	2.04	0.154	4.2	43.4	36.3	28.8	100.06	11.20	50

Table C3 Continued – Methanol/ethylene glycol (smooth surface)

Run no	Air rate [g/s]	Liquid rate [kg/min]	Evap. rate [ml/min]	T_{avg} (T1-T4) [°C]	T5 [°C]	T6 [°C]	Pt [kPa]	P1 [kPa]	mass% methanol
Methanol/ethylene glycol (smooth surface)									
47	2.54	0.090	4.3	43.5	34.5	30.5	99.99	16.53	50
48	2.54	0.154	4.8	43.5	35.5	30.7	99.99	16.53	50
49	2.54	0.221	5.3	43.6	36.5	30.8	99.99	16.53	50
50	2.54	0.285	5.9	43.6	37.6	30.8	99.99	16.53	50
51	2.54	0.367	5.6	43.6	38.6	31	99.99	16.53	50
52	2.54	0.285	5.3	43.6	37.7	31.1	99.99	16.53	50
53	0.77	0.115	2.1	43	37.5	27.4	99.99	2.80	75
54	0.77	0.173	2.5	43.1	38.4	27.6	99.99	2.80	75
55	0.77	0.241	2.5	43.2	39	27.9	99.99	2.80	75
56	0.77	0.309	2.9	43.4	39.6	28.2	99.99	2.80	75
57	0.77	0.381	2.5	43.5	40	28.4	99.99	2.80	75
58	0.77	0.309	2.5	43.5	39.8	28.6	99.99	2.80	75
59	1.15	0.115	3.3	43.3	37.1	28.8	99.99	4.60	75
60	1.15	0.173	3.2	43.4	37.7	29	99.99	4.60	75
61	1.15	0.241	3.4	43.4	38.6	29.3	99.99	4.60	75
62	1.15	0.309	3.1	43.7	38.7	30.4	99.93	4.60	75
63	1.15	0.381	3.4	43.8	40.1	30.5	99.93	4.60	75
64	1.15	0.309	3.4	43.7	39.8	30.7	99.93	4.60	75
65	1.56	0.115	4.1	43.5	36.8	31	99.93	7.13	75
66	1.56	0.173	3.8	43.4	37.5	31.2	99.93	7.13	75
67	1.56	0.241	4.1	43.5	38.6	31.5	99.93	7.13	75
68	1.56	0.309	4.3	43.4	39.4	31.8	99.86	7.13	75
69	1.56	0.381	4.5	43.8	40	31.8	99.86	7.13	75

Table C3 Continued – Methanol/ethylene glycol (smooth surface)

Run no	Air rate [g/s]	Liquid rate [kg/min]	Evap. rate [ml/min]	T_{avg} (T1-T4) [°C]	T5 [°C]	T6 [°C]	Pt [kPa]	P1 [kPa]	mass% methanol
Methanol/ethylene glycol (smooth surface)									
70	1.56	0.115	4.0	43.6	37.5	31.8	99.86	7.13	75
71	1.56	0.173	4.3	43.5	38.2	31.8	99.86	7.13	75
72	2.04	0.115	4.3	43.1	34.7	29.2	100.13	11.07	75
73	2.04	0.173	5.6	43.1	36.6	29.4	100.13	11.07	75
74	2.04	0.241	5.8	43.2	37.4	29.6	100.13	11.07	75
75	2.03	0.309	5.9	43.3	38.2	29.9	100.13	11.07	75
76	2.03	0.381	6.1	43.4	39.1	30.2	100.06	11.07	75
77	2.03	0.115	5.1	43.2	36	30.3	100.06	11.07	75
80	2.53	0.241	6.7	43.4	36.8	32.2	99.93	16.40	75
81	2.53	0.309	7.1	43.2	38	32.2	99.93	16.40	75
82	2.53	0.381	6.9	43.5	38.8	32.4	99.93	16.40	75
83	2.52	0.173	5.8	43.3	36.5	32.5	99.93	16.40	75
84	2.52	0.115	5.5	43.4	36.1	32.7	99.93	16.40	75

Table C3 Continued – Methanol/1-octanol (smooth surface)

Run no	Air rate [g/s]	Liquid rate [kg/min]	Evap. rate [ml/min]	T_{avg} (T1-T4) [°C]	T5 [°C]	T6 [°C]	Pt [kPa]	P1 [kPa]	mass% methanol
Methanol/1-octanol (smooth surface)									
1	0.78	0.072	1.5	43.1	34.8	25.8	100.06	2.73	25
2	0.78	0.121	1.6	43.4	35.8	26.3	100.06	2.73	25
3	0.77	0.180	1.7	43.5	36.6	26.7	99.99	2.73	25
4	0.77	0.238	1.7	43.5	37.7	26.8	99.99	2.73	25
5	0.77	0.304	1.8	43.6	38.3	27.0	99.99	2.73	25
6	1.16	0.072	1.9	43.4	34.9	27.4	99.99	4.47	25
7	1.16	0.121	2.1	43.7	35.2	27.6	99.99	4.47	25
8	1.15	0.180	2.2	43.7	36.9	28.6	99.93	4.47	25
9	1.15	0.238	2.5	43.8	37.7	28.9	99.93	4.47	25
10	1.15	0.304	2.4	43.9	38.1	29.0	99.86	4.47	25
11	1.15	0.238	2.4	43.8	38.0	29.1	99.86	4.47	25
12	1.57	0.072	2.3	43.5	34.5	29.3	99.86	7.20	25
13	1.57	0.121	2.8	43.6	35.4	29.4	99.86	7.20	25
14	1.57	0.180	2.9	43.7	36.3	29.6	99.86	7.20	25
15	1.57	0.238	3.0	43.8	37.4	29.8	99.86	7.20	25
16	1.57	0.304	2.9	43.8	38.2	29.9	99.86	7.20	25
17	1.57	0.238	2.9	43.8	37.6	29.8	99.86	7.20	25
18	2.04	0.072	2.8	42.7	33.2	29.4	100.06	11.20	25
19	2.04	0.121	3.1	42.9	33.3	28.7	100.06	11.20	25
20	2.04	0.180	3.7	43.0	34.5	28.4	100.06	11.20	25
21	2.04	0.238	3.5	43.1	35.6	28.2	100.06	11.20	25
22	2.04	0.304	3.6	43.1	36.6	28.2	100.06	11.20	25
23	2.04	0.180	3.5	43.3	35.2	28.2	100.06	11.20	25

Table C3 Continued – Methanol/1-octanol (smooth surface)

Run no	Air rate [g/s]	Liquid rate [kg/min]	Evap. rate [ml/min]	T_{avg} (T1-T4) [°C]	T5 [°C]	T6 [°C]	Pt [kPa]	P1 [kPa]	mass% methanol
Methanol/1-octanol (smooth surface)									
24	2.56	0.072	3.1	43.1	32.0	28.5	100.06	16.40	25
25	2.56	0.121	3.8	43.3	33.5	28.7	100.06	16.40	25
26	2.56	0.180	4.0	43.5	34.2	28.9	99.99	16.40	25
27	2.56	0.238	4.4	43.5	35.6	29.0	99.99	16.40	25
28	2.56	0.304	4.4	43.5	36.6	29.0	99.99	16.40	25
29	2.55	0.072	3.3	43.4	33.8	29.4	99.99	16.40	25
30	0.78	0.102	2.0	42.9	36.1	25.5	100.46	2.80	50
31	0.78	0.161	2.2	43.0	36.7	25.8	100.46	2.80	50
32	0.78	0.222	2.2	43.0	37.8	26.0	100.39	2.80	50
33	0.78	0.288	2.3	43.1	38.9	26.2	100.39	2.80	50
34	0.78	0.365	3.0	43.2	39.9	26.4	100.39	2.80	50
35	0.78	0.365	2.3	43.4	39.8	26.7	100.39	2.80	50
36	1.16	0.102	2.7	43.5	35.4	27.9	100.33	4.40	50
37	1.16	0.161	2.5	43.5	36.5	28.0	100.33	4.40	50
38	1.16	0.222	3.3	43.6	37.8	28.2	100.33	4.40	50
39	1.16	0.288	3.1	43.5	38.8	28.2	100.33	4.40	50
40	1.16	0.365	3.5	43.6	39.4	28.2	100.26	4.40	50
41	1.16	0.288	3.1	43.6	38.7	28.2	100.26	4.40	50
42	1.16	0.222	3.2	43.6	37.6	28.2	100.26	4.40	50
43	1.58	0.102	3.7	43.4	35.2	28.3	100.26	7.20	50
44	1.58	0.161	3.7	43.0	35.5	28.3	100.26	7.20	50
45	1.60	0.222	3.7	43.0	35.9	25.1	100.06	7.20	50
46	1.60	0.288	4.0	43.2	37.4	25.4	100.06	7.20	50

Table C3 Continued – Methanol/1-octanol (smooth surface)

Run no	Air rate [g/s]	Liquid rate [kg/min]	Evap. rate [ml/min]	T_{avg} (T1-T4) [°C]	T5 [°C]	T6 [°C]	Pt [kPa]	P1 [kPa]	mass% methanol
Methanol/1-octanol (smooth surface)									
47	1.59	0.365	4.1	43.3	38.2	25.7	100.06	7.20	50
48	2.06	0.102	4.4	43.0	33.2	26.4	100.06	11.20	50
49	2.05	0.161	4.9	43.0	34.4	26.7	100.06	11.20	50
50	2.05	0.222	5.1	43.2	35.5	27.0	100.06	11.20	50
51	2.05	0.288	5.0	43.2	36.8	27.3	100.06	11.20	50
52	2.05	0.365	6.3	43.4	37.7	27.5	99.99	11.20	50
53	2.04	0.365	5.4	43.6	38.0	27.8	99.99	11.20	50
54	2.56	0.102	5.2	43.3	33.8	28.0	99.99	16.33	50
55	2.56	0.161	5.1	43.3	33.8	28.2	99.99	16.33	50
56	2.55	0.222	5.8	43.3	35.1	29.1	99.93	16.33	50
57	2.55	0.288	6.3	43.5	36.6	29.4	99.93	16.33	50
58	2.55	0.365	7.2	43.6	37.5	29.5	99.93	16.33	50
59	2.55	0.365	6.6	43.6	37.3	29.5	99.93	16.33	50
60	0.79	0.119	2.6	42.9	36.6	23.1	100.39	2.73	75
61	0.79	0.177	2.6	43.0	37.7	23.5	100.39	2.73	75
62	0.79	0.240	2.6	43.0	39.3	23.7	100.39	2.73	75
63	0.78	0.307	2.6	43.1	39.8	24.0	100.39	2.73	75
64	0.78	0.072	2.8	43.1	35.9	24.3	100.33	2.73	75
65	0.78	0.072	2.5	43.0	35.2	24.5	100.33	2.73	75
66	1.17	0.072	3.1	43.1	35.8	25.7	100.26	4.40	75
67	1.17	0.119	3.3	43.4	36.1	25.9	100.26	4.40	75
68	1.17	0.177	3.4	43.5	37.5	26.2	100.26	4.40	75
69	1.17	0.240	3.5	43.5	39.1	26.3	100.26	4.40	75

Table C3 Continued – Methanol/1-octanol (smooth surface)

Run no	Air rate [g/s]	Liquid rate [kg/min]	Evap. rate [ml/min]	T_{avg} (T1-T4) [°C]	T5 [°C]	T6 [°C]	Pt [kPa]	P1 [kPa]	mass% methanol
Methanol/1-octanol (smooth surface)									
70	1.17	0.307	3.6	43.7	39.8	26.6	100.26	4.40	75
71	1.59	0.072	4.0	43.1	35.3	26.4	100.26	7.07	75
72	1.59	0.119	4.2	43.4	35.6	26.7	100.26	7.07	75
73	1.59	0.177	4.5	43.5	37.0	26.8	100.26	7.07	75
74	1.59	0.240	4.7	43.5	38.3	26.8	100.33	7.07	75
75	1.59	0.307	4.7	43.7	39.4	27.0	100.33	7.07	75
76	2.07	0.072	4.7	42.3	33.3	25.9	100.59	11.20	75
77	2.07	0.119	5.1	42.6	33.5	25.6	100.59	11.20	75
78	2.07	0.177	5.6	42.6	35.0	25.5	100.59	11.20	75
79	2.07	0.240	5.8	42.7	36.7	25.4	100.59	11.20	75
80	2.07	0.307	6.1	43.0	37.7	25.4	100.59	11.20	75
81	2.60	0.072	5.3	42.5	33.1	25.6	100.53	16.27	75
82	2.60	0.119	5.9	42.9	33.3	25.7	100.53	16.27	75
83	2.60	0.177	6.6	42.9	34.3	25.8	100.53	16.27	75
84	2.60	0.240	7.1	42.9	36.0	25.8	100.53	16.27	75
85	2.60	0.307	7.4	43.1	37.1	25.9	100.53	16.27	75

Table C3 Continued – Ethanol/tridecane (smooth surface)

Run no	Air rate [g/s]	Liquid rate [kg/min]	Evap. rate [ml/min]	T_{avg} (T1-T4) [°C]	T5 [°C]	T6 [°C]	Pt [kPa]	P1 [kPa]	mass% ethanol
Ethanol/tridecane (smooth surface)									
1	0.80	0.055	3.4	62.0	40.1	18.6	100.06	2.67	25
2	0.80	0.106	3.6	62.4	43.5	18.7	100.06	2.67	25
3	0.80	0.179	3.8	62.5	48.0	18.7	100.06	2.67	25
4	0.80	0.247	3.9	62.4	49.9	18.7	100.06	2.67	25
5	0.80	0.318	3.9	62.5	53.1	18.6	100.06	2.67	25
6	1.20	0.055	4.7	61.7	42.8	17.9	100.06	4.40	25
7	1.20	0.106	4.6	61.8	43.4	17.9	100.06	4.40	25
8	1.21	0.179	5.2	61.6	48.2	15.1	100.39	4.53	25
9	1.21	0.247	5.1	61.7	49.5	15.1	100.39	4.53	25
10	1.21	0.318	5.5	61.7	51.1	15.2	100.39	4.53	25
11	1.21	0.318	5.5	61.6	51.2	15.2	100.39	4.53	25
12	1.66	0.055	5.3	60.9	38.8	15.3	100.39	7.20	25
13	1.66	0.106	5.4	61.2	41.7	15.3	100.39	7.20	25
14	1.66	0.179	5.9	61.7	45.8	15.4	100.39	7.20	25
15	1.66	0.247	6.7	61.6	48.1	15.4	100.39	7.20	25
16	1.66	0.318	7.0	61.5	50.2	15.4	100.39	7.20	25
17	1.66	0.055	5.4	61.0	38.7	15.4	100.39	7.20	25
18	2.14	0.106	6.6	61.3	39.7	15.5	100.46	11.07	25
19	2.14	0.179	7.3	61.4	44.4	15.5	100.46	11.07	25
20	2.14	0.247	7.7	61.4	46.1	15.5	100.46	11.07	25
21	2.14	0.318	7.7	61.5	48.0	15.6	100.39	11.07	25
22	2.14	0.055	6.8	60.9	41.1	15.6	100.39	11.07	25
23	2.14	0.106	6.8	61.2	40.6	15.7	100.39	11.07	25

Table C3 Continued – Ethanol/tridecane (smooth surface)

Run no	Air rate [g/s]	Liquid rate [kg/min]	Evap. rate [ml/min]	T_{avg} (T1-T4) [°C]	T5 [°C]	T6 [°C]	Pt [kPa]	P1 [kPa]	mass% ethanol
Ethanol/tridecane (smooth surface)									
24	2.14	0.055	5.5	61.1	36.3	15.7	100.39	11.07	25
25	2.68	0.055	6.8	61.1	35.4	15.9	100.39	16.33	25
26	2.68	0.106	7.4	61.5	38.7	15.8	100.33	16.33	25
27	2.68	0.179	8.4	61.5	43.2	15.8	100.33	16.33	25
28	2.68	0.247	9.8	61.8	45.6	15.9	100.33	16.33	25
29	2.68	0.318	10.4	61.7	47.4	15.9	100.33	16.33	25
30	0.81	0.060	4.0	61.3	44.0	16.7	101.26	2.67	50
31	0.81	0.104	3.9	62.1	47.2	16.9	101.26	2.67	50
32	0.81	0.166	3.9	62.4	49.2	17.0	101.26	2.67	50
33	0.81	0.223	3.9	62.3	51.4	17.0	101.26	2.67	50
34	0.81	0.282	4.1	62.3	52.5	17.0	101.26	2.67	50
35	1.22	0.060	4.4	61.1	38.0	16.6	101.26	4.33	50
36	1.22	0.104	4.8	61.7	44.1	16.6	101.26	4.33	50
37	1.22	0.166	4.9	62.0	48.3	16.6	101.26	4.33	50
38	1.22	0.223	5.6	62.0	50.5	16.6	101.26	4.33	50
39	1.22	0.282	5.9	62.0	52.0	16.6	101.33	4.33	50
40	1.66	0.060	5.8	60.8	43.9	16.3	100.99	7.13	50
41	1.66	0.104	6.0	61.3	43.0	16.6	100.99	7.13	50
42	1.66	0.166	6.5	61.5	46.7	16.6	100.99	7.13	50
43	1.66	0.223	6.9	61.7	48.8	16.9	100.99	7.13	50
44	1.66	0.282	7.6	61.7	50.4	17.0	100.99	7.13	50
45	1.66	0.282	7.4	61.7	50.5	17.3	100.99	7.13	50
46	2.14	0.104	8.0	61.5	44.2	17.3	100.93	11.13	50

Table C3 Continued – Ethanol/tridecane (smooth surface)

Run no	Air rate [g/s]	Liquid rate [kg/min]	Evap. rate [ml/min]	T_{avg} (T1-T4) [°C]	T5 [°C]	T6 [°C]	Pt [kPa]	P1 [kPa]	mass% ethanol
Ethanol/tridecane (smooth surface)									
47	2.14	0.166	8.0	61.5	45.6	17.5	100.93	11.13	50
48	2.14	0.223	8.9	61.6	47.8	17.5	100.93	11.13	50
49	2.13	0.282	9.1	61.7	48.8	17.6	100.86	11.13	50
50	2.13	0.060	7.5	60.7	42.6	17.6	100.86	11.13	50
51	2.68	0.060	7.4	60.8	37.3	17.5	100.86	16.47	50
52	2.68	0.104	8.2	61.4	41.0	17.7	100.86	16.47	50
53	2.68	0.166	9.5	61.5	44.4	17.9	100.86	16.47	50
54	2.68	0.223	10.1	61.7	46.5	17.9	100.86	16.47	50
55	2.67	0.282	11.3	61.5	47.9	18.1	100.86	16.47	50
56	2.67	0.282	11.5	61.8	48.1	18.2	100.86	16.47	50
57a	2.67	0.223	11.5	61.8	47.1	18.2	100.86	16.47	50
57b	0.80	0.058	3.7	61.8	44.4	19.0	100.66	2.60	75
58	0.80	0.102	3.8	62.3	47.1	19.0	100.66	2.60	75
59	0.80	0.160	4.0	62.4	50.4	19.1	100.66	2.60	75
60	0.80	0.215	4.2	62.5	52.3	19.1	100.66	2.60	75
61	0.80	0.269	4.3	62.5	53.4	19.1	100.66	2.60	75
62	1.22	0.058	5.0	60.9	43.1	14.8	100.73	4.40	75
63	1.22	0.102	4.9	61.4	44.2	15.1	100.73	4.40	75
64	1.22	0.160	5.3	61.7	48.1	15.3	100.73	4.40	75
65	1.22	0.215	5.7	61.9	50.4	15.6	100.73	4.40	75
66	1.21	0.269	5.9	62.0	51.8	15.8	100.73	4.40	75
67	1.66	0.058	6.0	60.9	42.1	16.3	100.66	7.13	75
68	1.65	0.102	6.1	61.5	43.9	16.5	100.66	7.13	75

Table C3 Continued – Ethanol/tridecane (smooth surface)

Run no	Air rate [g/s]	Liquid rate [kg/min]	Evap. rate [ml/min]	T_{avg} (T1-T4) [°C]	T5 [°C]	T6 [°C]	Pt [kPa]	P1 [kPa]	mass% ethanol
Ethanol/tridecane (smooth surface)									
69	1.65	0.160	6.9	61.6	47.4	16.5	100.66	7.13	75
70	1.65	0.215	7.4	61.8	49.6	16.8	100.66	7.13	75
71	1.65	0.269	7.7	61.8	51.1	16.9	100.66	7.13	75
72	2.12	0.058	6.7	61.2	41.1	18.6	100.59	11.20	75
73	2.12	0.102	7.3	61.5	42.8	18.6	100.59	11.20	75
74	2.12	0.160	8.3	61.7	46.3	18.6	100.59	11.20	75
75	2.12	0.215	9.0	61.8	48.4	18.7	100.59	11.20	75
76	2.12	0.269	9.7	62.1	50.3	18.9	100.59	11.20	75
77	2.12	0.269	10.0	61.9	50.3	19.0	100.59	11.20	75
78	2.66	0.058	7.8	61.2	39.1	19.0	100.59	16.40	75
79	2.66	0.102	8.9	61.6	42.5	18.9	100.59	16.40	75
80	2.66	0.160	9.9	61.7	45.2	19.0	100.59	16.40	75
81	2.66	0.215	11.0	61.8	47.4	19.1	100.59	16.40	75
82	2.66	0.269	11.7	61.8	49.0	19.2	100.59	16.40	75
83	2.66	0.269	12.0	61.8	49.2	19.3	100.59	16.40	75

Table C3 Continued – n-Hexane/tridecane (smooth surface)

Run no	Air rate [g/s]	Liquid rate [kg/min]	Evap. rate [ml/min]	T_{avg} (T1-T4) [°C]	T5 [°C]	T6 [°C]	Pt [kPa]	P1 [kPa]	mass% n-hexane
n-Hexane/tridecane (smooth surface)									
1	0.79	0.059	1.9	38.5	31.9	20.9	100.46	2.87	25
2	0.79	0.100	1.8	38.6	32.7	21.1	100.46	2.87	25
3	0.79	0.154	1.9	38.8	34.1	21.5	100.46	2.87	25
4	0.79	0.200	2.0	38.8	35.1	21.7	100.46	2.87	25
5	0.79	0.248	1.9	38.9	35.7	21.9	100.46	2.87	25
6	1.18	0.059	2.6	38.8	32.8	22.6	100.26	4.40	25
7	1.18	0.100	2.6	39.0	33.0	22.7	100.26	4.40	25
8	1.18	0.154	2.7	39.0	34.6	22.8	100.26	4.40	25
9	1.18	0.200	2.9	39.0	35.3	23.0	100.19	4.40	25
10	1.18	0.248	2.8	39.1	35.5	23.0	100.19	4.40	25
11	1.61	0.059	3.4	38.9	32.3	22.9	100.19	7.20	25
12	1.61	0.100	3.5	38.9	32.9	22.9	100.19	7.20	25
13	1.61	0.154	3.7	39.0	34.3	22.9	100.19	7.20	25
14	1.61	0.200	3.7	39.0	35.2	23.0	100.19	7.20	25
15	1.61	0.248	3.7	39.0	35.7	23.0	100.19	7.20	25
16	2.13	0.059	4.2	38.2	27.7	17.2	100.73	11.07	25
17	2.13	0.100	4.6	38.5	30.0	17.4	100.73	11.07	25
18	2.13	0.154	4.8	38.6	32.0	17.5	100.73	11.07	25
19	2.13	0.200	5.0	38.8	33.4	17.6	100.73	11.07	25
20	2.13	0.248	5.0	38.7	33.9	17.6	100.73	11.07	25
21	2.67	0.059	5.2	38.4	29.0	17.8	100.73	16.33	25
22	2.67	0.100	5.7	38.7	29.9	17.8	100.73	16.33	25
23	2.67	0.154	6.1	38.8	31.4	18.0	100.73	16.33	25

Table C3 Continued – n-Hexane/tridecane (smooth surface)

Run no	Air rate [g/s]	Liquid rate [kg/min]	Evap. rate [ml/min]	T_{avg} (T1-T4) [°C]	T5 [°C]	T6 [°C]	Pt [kPa]	P1 [kPa]	mass% n-hexane
n-Hexane/tridecane (smooth surface)									
24	2.67	0.200	6.2	38.8	33.2	18.1	100.73	16.33	25
25	2.67	0.248	6.3	38.7	33.6	18.2	100.73	16.33	25
26	0.81	0.074	3.2	38.3	30.1	16.4	101.06	2.73	50
27	0.81	0.115	2.9	38.4	30.8	16.6	101.06	2.73	50
28	0.81	0.169	2.9	38.6	32.6	16.7	101.06	2.73	50
29	0.81	0.216	3.0	38.7	33.8	16.8	101.06	2.73	50
30	0.81	0.265	3.6	38.7	34.3	17.0	101.06	2.73	50
31	0.81	0.265	3.1	38.7	34.3	17.0	101.06	2.73	50
32	1.21	0.074	4.4	38.5	29.9	17.0	100.99	4.53	50
33	1.21	0.115	4.3	38.5	30.7	17.0	100.99	4.53	50
34	1.21	0.169	4.2	38.5	32.7	17.0	100.99	4.53	50
35	1.21	0.216	4.5	38.7	33.7	17.2	100.99	4.53	50
36	1.21	0.265	5.3	38.7	34.2	17.3	100.99	4.53	50
37	1.21	0.265	4.6	38.7	34.1	17.4	100.99	4.53	50
38	1.65	0.074	5.5	38.6	28.6	18.1	100.79	7.27	50
39	1.65	0.115	5.5	38.8	30.7	18.2	100.79	7.27	50
40	1.65	0.169	6.1	38.8	32.4	18.2	100.79	7.27	50
41	1.65	0.216	6.3	38.8	33.4	18.2	100.79	7.27	50
42	1.65	0.265	7.1	38.9	33.8	18.2	100.79	7.27	50
43	1.65	0.265	5.2	38.8	33.7	18.3	100.79	7.27	50
44	2.12	0.074	7.4	38.5	28.7	18.2	100.33	10.93	50
45	2.12	0.115	7.9	38.7	29.3	18.4	100.33	10.93	50
46	2.12	0.169	8.4	38.7	30.8	18.5	100.33	10.93	50

Table C3 Continued – n-Hexane/tridecane (smooth surface)

Run no	Air rate [g/s]	Liquid rate [kg/min]	Evap. rate [ml/min]	T_{avg} (T1-T4) [°C]	T5 [°C]	T6 [°C]	Pt [kPa]	P1 [kPa]	mass% n-hexane
n-Hexane/tridecane (smooth surface)									
47	2.12	0.216	8.5	38.8	32.2	18.7	100.33	10.93	50
48	2.11	0.265	8.7	39.0	32.9	18.9	100.26	10.93	50
49	2.65	0.059	9.4	38.7	28.6	19.0	100.26	16.40	50
50	2.65	0.115	10.2	38.8	29.1	19.2	100.26	16.40	50
51	2.65	0.169	10.8	38.9	30.7	19.4	100.26	16.40	50
52	2.64	0.216	11.2	39.0	31.5	19.4	100.19	16.40	50
53	2.64	0.265	11.6	39.2	32.5	19.6	100.19	16.40	50
54	0.80	0.081	3.9	38.5	31.3	17.0	100.39	2.67	75
55	0.80	0.121	3.8	38.7	32.5	17.2	100.39	2.67	75
56	0.80	0.177	3.8	38.8	33.8	17.3	100.39	2.67	75
57	0.80	0.238	4.4	38.9	34.6	17.2	100.39	2.67	75
58	0.80	0.273	3.9	38.9	34.9	17.3	100.39	2.67	75
59	0.80	0.238	3.8	39.0	34.7	17.3	100.39	2.67	75
60	1.20	0.081	5.6	38.5	30.3	15.8	99.86	4.53	75
61	1.20	0.121	5.6	38.5	31.5	15.8	99.86	4.53	75
62	1.20	0.177	5.8	38.6	33.0	16.0	99.86	4.53	75
63	1.20	0.238	5.2	38.8	34.1	16.1	99.86	4.53	75
64	1.20	0.273	5.9	38.8	34.5	16.2	99.86	4.53	75
65	1.20	0.238	5.9	38.9	34.1	16.4	99.86	4.53	75
66	1.64	0.081	6.9	38.6	29.0	16.6	99.86	7.20	75
67	1.64	0.121	7.6	38.7	30.6	16.6	99.86	7.20	75
68	1.64	0.177	8.1	38.9	32.4	16.6	99.86	7.20	75
69	1.64	0.238	9.2	39.0	33.2	16.7	99.86	7.20	75

Table C3 Continued – n-Hexane/tridecane (smooth surface)

Run no	Air rate [g/s]	Liquid rate [kg/min]	Evap. rate [ml/min]	T_{avg} (T1-T4) [°C]	T5 [°C]	T6 [°C]	Pt [kPa]	P1 [kPa]	mass% n-hexane
n-Hexane/tridecane (smooth surface)									
70	1.64	0.273	8.8	39.0	33.8	16.6	99.86	7.20	75
71	1.64	0.238	8.4	39.0	33.4	16.6	99.86	7.20	75
72	2.12	0.081	9.3	38.6	27.3	16.6	99.86	11.13	75
73	2.12	0.121	10.4	38.6	29.2	16.6	99.86	11.13	75
74	2.12	0.177	10.9	38.8	30.8	16.6	99.86	11.13	75
75	2.12	0.238	12.6	38.8	32.2	16.6	99.86	11.13	75
76	2.12	0.273	11.9	38.8	32.7	16.5	99.86	11.13	75
77	2.12	0.238	11.6	39.1	32.5	16.6	99.86	11.13	75
78	2.66	0.081	11.0	38.4	22.9	16.3	99.86	16.40	75
79	2.66	0.121	11.7	38.4	26.6	16.2	99.86	16.40	75
80	2.66	0.177	13.9	38.6	29.4	16.2	99.86	16.40	75
81	2.67	0.238	15.9	38.6	30.9	16.2	99.93	16.40	75
82	2.67	0.273	15.1	38.8	32.0	16.2	99.93	16.40	75
83	2.67	0.238	14.9	38.6	31.4	16.3	99.93	16.40	75

Table C3 Continued – Acetone/methanol (smooth surface)

Run no	Air rate [g/s]	Liquid rate [kg/min]	Evap. rate [ml/min]	T_{avg} (T1-T4) [°C]	T5 [°C]	T6 [°C]	Pt [kPa]	P1 [kPa]	mole% acetone
Acetone/methanol (smooth surface)									
1	1.24	0.094	6.7	37.0	16.0	12.0	101.26	4.27	89.5
2	1.24	0.093	6.0	37.0	21.6	12.4	101.26	4.27	89.5
3	1.23	0.092	6.2	36.9	25.1	12.6	101.19	4.27	89.5
4	1.23	0.139	6.3	37.0	26.9	12.8	101.19	4.27	89.5
5	1.23	0.201	6.2	37.0	28.6	12.9	101.19	4.27	89.5
6	1.23	0.274	6.7	37.1	30.2	13.0	101.19	4.27	89.5
7	1.22	0.340	6.5	37.0	26.5	14.3	100.99	4.27	89.5
8	1.19	0.407	6.8	37.5	30.5	18.7	99.99	4.47	89.5
9	1.63	0.092	7.5	37.1	26.1	19.0	100.06	7.33	89.5
10	1.63	0.138	8.0	37.1	29.4	19.2	100.06	7.33	89.5
11	1.63	0.200	9.2	37.1	31.2	19.4	100.06	7.33	89.5
12	1.63	0.273	9.6	37.4	31.7	19.7	100.06	7.33	89.5
13	1.63	0.273	10.0	37.4	32.1	19.8	100.06	7.33	89.5
14	1.63	0.338	10.4	37.4	32.3	19.5	100.05	7.33	89.5
15	1.63	0.406	10.6	37.5	32.8	19.5	99.99	7.33	89.5
16	2.10	0.091	11.0	37.0	31.4	19.2	99.99	11.07	89.5
17	2.11	0.138	11.0	36.9	31.0	19.1	99.99	11.07	89.5
18	2.11	0.202	11.8	37.2	24.4	19.1	100.06	11.07	89.5
19	2.11	0.275	13.0	37.2	28.6	19.3	100.06	11.07	89.5
20	2.11	0.338	13.2	37.1	30.9	19.1	100.06	11.07	89.5
21	2.11	0.407	14.2	37.1	31.7	19.0	100.06	11.07	89.5
22	2.64	0.092	11.0	36.8	25.3	19.2	100.06	16.27	89.5
23	2.64	0.138	12.5	36.7	29.0	19.3	100.06	16.27	89.5

Table C3 Continued – Acetone/methanol (smooth surface)

Run no	Air rate [g/s]	Liquid rate [kg/min]	Evap. rate [ml/min]	T_{avg} (T1-T4) [°C]	T5 [°C]	T6 [°C]	Pt [kPa]	P1 [kPa]	mole% acetone
Acetone/methanol (smooth surface)									
24	2.64	0.201	14.3	37.0	29.6	19.2	100.06	16.27	89.5
25	2.64	0.274	15.5	37.0	30.0	19.2	100.06	16.27	89.5
26	2.64	0.338	16.5	36.9	30.6	19.1	100.06	16.27	89.5
27	2.64	0.407	17.3	37.2	30.8	19.1	100.06	16.27	89.5

Table C3 Continued – Methanol/ethanol (smooth surface)

Run no	Air rate [g/s]	Liquid rate [kg/min]	Evap. rate [ml/min]	T_{avg} (T1-T4) [°C]	T5 [°C]	T6 [°C]	Pt [kPa]	P1 [kPa]	mole% methanol
Methanol/ethanol (smooth surface)									
1	0.81	0.071	2.9	52.3	26.5	17.1	101.52	2.67	55.61
2	0.81	0.118	2.9	52.5	32.3	17.5	101.52	2.67	55.32
3	0.81	0.181	3.1	52.6	37.0	17.6	101.52	2.67	55.11
4	0.81	0.248	3.6	52.8	40.9	17.7	101.52	2.67	55.16
5	0.81	0.316	3.5	52.8	43.0	17.8	101.52	2.67	55.00
6	0.81	0.381	4.4	53.0	44.8	18.0	101.52	2.67	54.64
7	0.81	0.381	4.1	53.0	45.1	18.0	101.52	2.67	54.42
8	1.22	0.072	3.5	52.2	24.8	16.2	101.52	4.47	53.21
9	1.22	0.118	3.8	52.6	31.1	16.5	101.52	4.53	52.17
10	1.22	0.181	4.2	52.7	36.6	16.8	101.52	4.53	52.71
11	1.22	0.248	4.6	52.8	40.2	16.9	101.52	4.53	52.22
12	1.22	0.317	4.0	52.8	40.4	17.1	101.52	4.53	51.73

Table C3 Continued – Methanol/ethanol (smooth surface)

Run no	Air rate [g/s]	Liquid rate [kg/min]	Evap. rate [ml/min]	T_{avg} (T1-T4) [°C]	T5 [°C]	T6 [°C]	Pt [kPa]	P1 [kPa]	mole% methanol
Methanol/ethanol (smooth surface)									
13	1.22	0.316	4.6	52.9	42.4	17.2	101.52	4.53	51.30
14	1.22	0.381	4.4	52.7	43.8	17.4	101.52	4.53	50.73
15	1.66	0.072	4.0	52.1	22.6	17.2	101.39	7.20	50.73
16	1.66	0.071	4.4	52.3	28.3	17.5	101.39	7.20	50.79
17	1.66	0.118	5.0	52.4	32.1	17.5	101.39	7.20	50.38
18	1.66	0.181	5.4	52.5	36.2	17.6	101.39	7.20	49.96
19	1.66	0.248	5.0	52.7	39.8	17.7	101.39	7.20	50.22
20	1.66	0.248	5.9	52.7	40.2	17.8	101.39	7.20	50.04
21	1.66	0.316	5.8	52.8	42.2	17.9	101.33	7.13	49.85
22	1.66	0.381	6.1	52.8	43.7	18.0	101.33	7.13	49.85
23	2.08	0.071	5.8	52.5	28.6	23.3	100.34	10.80	51.78
24	2.08	0.117	6.1	52.8	35.0	23.6	100.33	10.87	51.78
25	2.08	0.180	6.6	52.9	38.9	23.8	100.33	10.93	48.45
26	2.08	0.248	7.4	52.9	41.5	23.9	100.33	10.93	48.45
27	2.08	0.316	7.5	53.0	42.9	24.2	100.33	10.93	47.95
28	2.07	0.380	7.8	53.2	44.7	24.3	100.26	10.93	47.44
29	2.60	0.071	5.7	52.6	29.5	24.3	100.19	16.40	48.98
30	2.60	0.117	7.0	52.8	34.0	24.4	100.19	16.33	48.00
31	2.60	0.180	8.0	52.7	38.3	24.3	100.19	16.33	47.03
32	2.60	0.248	8.7	52.8	40.3	24.3	100.19	16.33	47.30
33	2.60	0.316	9.4	53.1	42.5	24.4	100.19	16.33	47.58
34	2.60	0.381	9.6	53.0	43.6	24.4	100.19	16.33	47.58

Table C4 Experimental results for binary mixtures – Complex surface

Run no	Air rate [g/s]	Liquid rate [kg/min]	Evap. rate [ml/min]	T_{avg} (T1-T4) [°C]	T5 [°C]	T6 [°C]	Pt [kPa]	P1 [kPa]	mass% methanol
Methanol/ethylene glycol (complex surface)									
1	0.79	0.201	1.5	44.0	38.4	21.2	100.33	2.80	25
2	0.79	0.317	1.5	44.0	39.6	21.4	100.39	2.80	25
3	0.79	0.446	1.5	44.0	40.3	21.5	100.39	2.80	25
4	0.79	0.122	1.6	44.1	37.9	21.5	100.39	2.80	25
5	0.79	0.075	1.2	44.0	35.3	21.5	100.46	2.80	25
6	1.19	0.075	2.2	43.8	34.3	21.4	100.53	4.53	25
7	1.19	0.122	2.1	44.0	35.6	21.2	100.59	4.53	25
8	1.19	0.201	2.1	44.1	36.9	21.0	100.53	4.53	25
9	1.19	0.317	2.2	44.1	38.7	21.0	100.53	4.53	25
10	1.19	0.446	2.3	44.2	39.5	21.0	100.53	4.53	25
11	1.64	0.075	2.3	43.7	34.6	19.4	100.59	7.33	25
12	1.64	0.122	2.7	44.0	35.5	19.7	100.59	7.33	25
13	1.63	0.201	2.7	44.0	36.7	19.8	100.59	7.33	25
14	1.63	0.317	2.7	44.0	38.0	19.9	100.53	7.33	25
15	1.63	0.446	3.0	44.1	39.3	20.2	100.53	7.33	25
16	2.10	0.075	2.6	43.8	34.9	21.2	100.39	11.27	25
17	2.10	0.122	3.0	44.1	35.3	21.2	100.39	11.27	25
18	2.10	0.201	3.1	44.1	36.6	21.2	100.39	11.27	25
19	2.10	0.317	3.2	44.2	37.9	21.3	100.39	11.27	25
20	2.10	0.446	3.3	44.3	39.4	21.3	100.39	11.27	25
21	2.63	0.075	3.1	43.8	33.8	21.4	100.46	16.40	25
22	2.63	0.122	3.2	44.0	34.2	21.4	100.46	16.40	25
23	2.63	0.201	3.6	44.1	35.8	21.6	100.46	16.40	25

Table C4 Continued – Methanol/ethylene glycol (complex surface)

Run no	Air rate [g/s]	Liquid rate [kg/min]	Evap. rate [ml/min]	T_{avg} (T1-T4) [°C]	T5 [°C]	T6 [°C]	Pt [kPa]	P1 [kPa]	mass% methanol
Methanol/ethylene glycol (complex surface)									
24	2.63	0.317	3.8	44.1	37.7	21.3	100.46	16.40	25
25	2.63	0.446	3.8	44.1	38.9	21.3	100.46	16.40	25
26	0.80	0.113	2.2	43.9	36.4	18.0	99.73	2.93	50
27	0.79	0.174	2.1	43.9	36.9	18.3	99.73	2.93	50
28	0.79	0.253	2.3	43.9	38.3	18.3	99.73	2.93	50
29	0.79	0.366	2.3	44.1	39.8	18.6	99.73	2.93	50
30	0.79	0.479	2.3	44.1	40.3	18.6	99.66	2.93	50
31	1.19	0.113	3.3	44.0	35.7	19.0	99.59	4.67	50
32	1.19	0.174	3.4	44.0	36.4	19.1	99.59	4.67	50
33	1.20	0.253	3.6	43.9	38.3	18.9	100.19	4.47	50
34	1.19	0.366	3.6	43.9	39.5	19.0	100.19	4.47	50
35	1.19	0.479	3.8	44.0	40.4	19.2	100.19	4.47	50
36	1.63	0.113	3.9	43.9	35.3	19.4	100.26	7.27	50
37	1.63	0.174	4.0	44.1	35.7	19.7	100.26	7.27	50
38	1.63	0.253	4.1	43.9	37.8	19.6	100.26	7.27	50
39	1.63	0.366	4.5	43.9	38.7	19.8	100.33	7.27	50
40	1.63	0.479	4.7	44.2	39.7	19.8	100.33	7.27	50
41	2.10	0.113	3.8	44.0	34.2	20.6	100.33	11.20	50
42	2.10	0.174	4.3	44.1	35.2	20.6	100.33	11.20	50
43	2.10	0.253	4.6	44.2	36.6	20.7	100.33	11.20	50
44	2.10	0.366	5.0	44.2	39.0	20.6	100.39	11.20	50
45	2.10	0.479	5.5	44.2	39.4	20.7	100.39	11.20	50
46	2.64	0.113	4.8	44.1	33.7	20.8	100.46	16.47	50

Table C4 Continued – Methanol/ethylene glycol (complex surface)

Run no	Air rate [g/s]	Liquid rate [kg/min]	Evap. rate [ml/min]	T_{avg} (T1-T4) [°C]	T5 [°C]	T6 [°C]	Pt [kPa]	P1 [kPa]	mass% methanol
Methanol/ethylene glycol (complex surface)									
47	2.64	0.174	5.2	44.0	34.1	20.7	100.46	16.47	50
48	2.64	0.253	5.7	44.0	36.4	20.7	100.46	16.47	50
49	2.64	0.366	6.3	44.1	37.7	20.8	100.53	16.47	50
50	2.64	0.479	6.9	44.1	38.9	21.0	100.53	16.47	50
51	0.81	0.103	2.6	43.5	34.1	16.7	100.86	2.93	75
52	0.81	0.158	2.5	43.6	35.6	17.1	100.86	2.93	75
53	0.81	0.218	2.9	43.7	37.0	17.2	100.86	2.93	75
54	0.81	0.278	2.8	43.8	37.8	17.4	100.86	2.93	75
55	0.81	0.349	3.5	43.9	38.4	17.4	100.86	2.93	75
56	0.81	0.278	2.9	43.8	38.0	17.5	100.86	2.93	75
57	0.81	0.349	2.9	43.8	38.4	17.6	100.86	2.93	75
58	1.21	0.103	3.7	43.6	34.0	18.0	100.79	4.53	75
59	1.20	0.158	3.5	43.7	34.6	18.3	100.79	4.53	75
60	1.20	0.218	3.9	43.6	36.1	18.4	100.79	4.53	75
61	1.20	0.278	4.6	43.8	37.0	18.6	100.79	4.53	75
62	1.20	0.349	5.6	44.0	37.6	18.6	100.79	4.53	75
63	1.20	0.349	4.9	43.9	37.4	18.6	100.79	4.53	75
64	1.64	0.103	4.1	43.7	33.3	19.0	100.73	7.33	75
65	1.64	0.158	4.1	43.8	33.9	19.2	100.73	7.33	75
66	1.64	0.218	5.0	43.8	35.2	19.3	100.73	7.33	75
67	1.64	0.278	5.3	43.9	36.2	19.3	100.73	7.33	75
68	1.64	0.349	5.8	44.1	37.3	19.5	100.73	7.33	75
69	1.64	0.158	5.2	43.9	34.6	19.4	100.73	7.33	75

Table C4 Continued – Methanol/ethylene glycol (complex surface)

Run no	Air rate [g/s]	Liquid rate [kg/min]	Evap. rate [ml/min]	T_{avg} (T1-T4) [°C]	T5 [°C]	T6 [°C]	Pt [kPa]	P1 [kPa]	mass% methanol
Methanol/ethylene glycol (complex surface)									
70	1.64	0.158	4.8	43.9	34.3	19.6	100.73	7.33	75
71	2.13	0.103	4.6	43.3	32.1	18.1	100.59	11.20	75
72	2.12	0.158	5.1	43.5	33.4	18.4	100.59	11.20	75
73	2.12	0.218	6.0	43.6	34.8	18.7	100.59	11.20	75
74	2.12	0.278	6.1	43.6	35.8	19.1	100.59	11.20	75
75	2.12	0.349	7.3	43.9	36.8	19.5	100.59	11.20	75
76	2.11	0.278	6.6	43.7	36.2	19.9	100.59	11.20	75
77	2.64	0.103	5.3	43.7	32.4	21.2	100.53	16.27	75
78	2.63	0.158	6.0	43.7	33.5	21.4	100.53	16.27	75
79	2.63	0.218	6.9	43.8	34.8	21.7	100.53	16.27	75
80	2.63	0.278	7.3	43.7	35.8	22.0	100.53	16.27	75
81	2.63	0.349	8.8	44.0	36.8	22.2	100.53	16.27	75
82	2.62	0.349	8.6	44.1	36.8	22.6	100.53	16.27	75

Table C4 Continued - n-Hexane/tridecane (complex surface)

Run no	Air rate [g/s]	Liquid rate [kg/min]	Evap. rate [ml/min]	T_{avg} (T1-T4) [°C]	T5 [°C]	T6 [°C]	Pt [kPa]	P1 [kPa]	mass% hexane
n-Hexane/tridecane (complex surface)									
1	0.78	0.100	1.8	37.6	33.3	24.5	100.46	2.80	25
2	0.78	0.154	1.9	37.8	34.2	25.0	100.46	2.80	25
3	0.78	0.213	2.1	37.9	35.2	25.6	100.46	2.80	25
4	0.78	0.274	2.4	37.9	35.6	25.9	100.46	2.80	25
5	0.78	0.332	2.1	38.0	36.2	26.3	100.46	2.80	25
6	0.78	0.274	2.1	38.0	35.9	26.7	100.46	2.80	25
7	1.16	0.100	3.1	38.2	33.8	27.8	100.26	4.47	25
8	1.16	0.154	3.3	38.3	34.4	27.7	100.26	4.47	25
9	1.16	0.213	3.5	38.3	35.2	27.6	100.26	4.47	25
10	1.16	0.274	3.6	38.3	35.4	27.4	100.26	4.47	25
11	1.16	0.332	3.8	38.4	35.9	27.4	100.26	4.47	25
12	1.59	0.100	3.7	38.2	33.4	27.2	100.39	7.27	25
13	1.59	0.154	4.0	38.1	33.7	27.0	100.33	7.27	25
14	1.64	0.213	3.9	37.7	32.6	18.3	100.39	7.27	25
15	1.64	0.274	4.4	37.8	33.3	18.6	100.39	7.27	25
16	1.64	0.332	4.4	37.8	34.1	18.9	100.39	7.27	25
17	1.64	0.213	4.2	37.8	33.3	19.0	100.39	7.27	25
18	2.11	0.100	4.0	37.7	30.8	19.6	100.33	11.20	25
19	2.11	0.154	4.4	37.9	31.8	19.7	100.33	11.20	25
20	2.11	0.213	4.3	37.8	32.2	19.8	100.39	11.20	25
21	2.11	0.274	5.2	38.0	33.4	19.8	100.39	11.20	25
22	2.11	0.332	5.3	37.9	34.3	19.8	100.39	11.20	25
23	2.11	0.213	4.9	37.9	33.1	19.8	100.39	11.20	25

Table C4 Continued – n-Hexane/tridecane (complex surface)

Run no	Air rate [g/s]	Liquid rate [kg/min]	Evap. rate [ml/min]	T_{avg} (T1-T4) [°C]	T5 [°C]	T6 [°C]	Pt [kPa]	P1 [kPa]	mass% hexane
n-Hexane/tridecane (complex surface)									
24	2.65	0.100	5.2	37.7	30.8	19.7	100.39	16.40	25
25	2.65	0.154	5.3	37.9	31.5	19.8	100.39	16.40	25
26	2.65	0.213	5.6	37.9	32.9	19.9	100.39	16.40	25
27	2.64	0.274	6.1	37.9	33.3	20.0	100.39	16.40	25
28	2.65	0.332	6.6	37.9	34.0	19.9	100.39	16.40	25
29	0.81	0.115	3.2	37.1	31.1	17.1	100.86	2.67	50
30	0.81	0.170	3.1	37.2	31.8	17.2	100.86	2.67	50
31	0.81	0.227	3.3	37.5	32.6	17.5	100.86	2.67	50
32	0.81	0.289	4.0	37.5	33.3	17.6	100.86	2.67	50
33	0.81	0.354	3.6	37.7	33.5	17.7	100.86	2.67	50
34	0.81	0.289	3.6	37.7	33.4	17.6	100.93	2.67	50
35	1.21	0.115	5.7	37.3	30.2	17.5	100.93	4.40	50
36	1.21	0.170	5.6	37.4	30.9	17.6	100.93	4.40	50
37	1.21	0.227	6.1	37.5	32.1	17.7	100.93	4.40	50
38	1.21	0.289	7.0	37.6	32.9	17.8	100.93	4.40	50
39	1.21	0.354	6.8	37.7	33.1	17.9	100.93	4.40	50
40	1.21	0.289	6.5	37.7	32.9	18.1	100.93	4.40	50
41	1.65	0.115	6.6	37.6	29.9	18.5	100.93	7.20	50
42	1.65	0.170	6.9	37.6	30.7	18.6	100.93	7.20	50
43	1.65	0.227	7.6	37.8	32.1	18.7	100.93	7.20	50
44	1.65	0.289	8.6	37.8	33.0	18.8	100.93	7.20	50
45	1.65	0.354	8.6	37.8	33.3	18.9	100.93	7.20	50
46	2.13	0.115	8.0	37.7	30.3	19.0	100.93	11.20	50

Table C4 Continued – n-Hexane/tridecane (complex surface)

Run no	Air rate [g/s]	Liquid rate [kg/min]	Evap. rate [ml/min]	T_{avg} (T1-T4) [°C]	T5 [°C]	T6 [°C]	Pt [kPa]	P1 [kPa]	mass% hexane
n-Hexane/tridecane (complex surface)									
47	2.12	0.170	8.0	37.7	30.5	19.3	100.93	11.20	50
48	2.12	0.227	8.9	37.7	31.7	19.4	100.93	11.20	50
49	2.12	0.289	10.3	37.8	32.6	19.4	100.93	11.20	50
50	2.12	0.354	10.5	37.9	33.1	19.6	100.93	11.20	50
51	2.66	0.115	9.4	37.7	28.4	19.8	100.99	16.47	50
52	2.66	0.170	9.7	37.7	30.1	19.7	100.99	16.47	50
53	2.66	0.227	10.9	37.7	31.6	19.8	100.99	16.47	50
54	2.66	0.289	13.1	37.8	32.4	19.9	100.99	16.47	50
55	2.66	0.354	13.0	37.7	32.9	19.7	100.99	16.47	50
56	2.66	0.289	12.3	37.8	32.4	19.7	100.99	16.47	50
57	0.80	0.083	4.2	37.4	31.7	19.9	100.39	2.67	75
58	0.79	0.125	4.4	37.6	32.3	20.3	100.39	2.67	75
59	0.79	0.182	4.5	37.7	33.6	20.6	100.39	2.67	75
60	0.79	0.246	4.6	37.7	34.5	20.8	100.39	2.67	75
61	0.79	0.310	4.9	37.8	35.1	21.1	100.33	2.67	75
62	1.18	0.083	7.4	37.7	31.2	22.6	100.26	4.47	75
63	1.18	0.125	7.9	37.8	31.8	22.7	100.26	4.47	75
64	1.18	0.182	8.3	37.8	32.6	22.7	100.19	4.47	75
65	1.18	0.246	8.8	38.0	34.0	22.7	100.19	4.47	75
66	1.18	0.310	9.7	38.0	34.4	22.8	100.19	4.47	75
67	1.18	0.310	9.7	38.0	34.5	22.9	100.19	4.47	75
68	1.18	0.083	7.9	37.9	31.6	23.0	100.19	4.47	75
69	1.61	0.083	9.4	37.8	30.2	22.9	100.19	7.20	75

Table C4 Continued – n-Hexane/tridecane (complex surface)

Run no	Air rate [g/s]	Liquid rate [kg/min]	Evap. rate [ml/min]	T_{avg} (T1-T4) [°C]	T5 [°C]	T6 [°C]	Pt [kPa]	P1 [kPa]	mass% hexane
n-Hexane/tridecane (complex surface)									
70	1.61	0.125	10.3	37.9	30.5	23.0	100.19	7.20	75
71	1.61	0.182	10.4	37.9	32.1	23.0	100.19	7.20	75
72	1.61	0.246	10.9	37.8	33.4	22.9	100.19	7.20	75
73	1.61	0.310	12.4	38.1	34.1	23.0	100.19	7.20	75
74	1.61	0.310	12.3	38.0	34.0	23.0	100.19	7.20	75
75	2.08	0.083	10.8	37.9	30.2	22.9	100.13	11.27	75
76	2.08	0.125	11.6	37.8	30.5	23.0	100.13	11.27	75
77	2.08	0.182	12.4	37.8	31.4	22.9	100.13	11.27	75
78	2.08	0.246	13.0	37.9	32.7	22.9	100.13	11.27	75
79	2.08	0.310	14.6	38.1	33.3	22.9	100.13	11.27	75
80	2.08	0.310	14.8	38.1	33.5	22.9	100.13	11.27	75
81	2.64	0.083	13.2	37.4	27.3	20.7	100.33	16.47	75
82	2.64	0.125	13.5	37.3	28.3	20.7	100.33	16.47	75
83	2.63	0.182	15.7	37.3	30.0	20.9	100.33	16.47	75
84	2.63	0.246	17.0	37.4	31.4	21.0	100.33	16.47	75
85	2.63	0.310	18.0	37.4	32.3	21.0	100.33	16.47	75
86	2.63	0.083	13.5	37.5	29.2	21.1	100.33	16.47	75
87	2.63	0.125	14.0	37.3	29.0	21.2	100.33	16.47	75
88	2.63	0.310	17.7	37.6	32.3	21.3	100.33	16.47	75

APPENDIX D Experimental distillation data

Table D1 Experimental distillation data

Run no	Conc first comp. [wt%]		Flow rate [kg/h]	Temperatures [°C]					dP	Q_{reb}	Q_{cond}
	Bottoms	Distillate	Reflux	Reboiler	Bottom	Sec1-2	Sec2-3	Top	[mmH$_2$O]	[kW]	[kW]
Acetone/methanol											
1	11.463	82.257	87.1	63.3	62.9	57.3	55.4	55.4	4.5	13.7	16.2
3	17.319	83.115	141.1	62.2	61.5	56.2	54.8	54.8	9	21.7	25.6
5	6.122	81.367	174.8	64.4	63.8	58.3	55.6	55.4	13	29.6	30.2
6	2.773	79.763	197.8	64.9	64.4	60.1	55.8	55.4	16	34.1	33.4
7	4.161	81.079	201.4	64.6	64	59	55.4	55	18	33.4	34.8
8	10.312	82.908	215.0	63.1	62.6	56.9	54.8	54.8	20	35.4	36.4
9	0.647	75.142	238.8	65.5	65.2	63.3	58.7	55.8	22	42.9	41.8
10	0.740	75.619	250.4	65.7	65.3	63.3	58	55.8	25	44.1	44.3
Ethanol/i-propanol (1)											
1	12.214	34.273	292.5	83	82.6	81.7	81.1	80.6	70	60.3	59.9
2	12.045	35.091	289.4	82.9	82.3	81.7	81	80.6	62	59.6	59.3
3	12.113	34.716	282.5	82.8	82.3	81.6	81.3	80.5	57	59.2	56.8
4	12.686	34.492	266.4	83	82.5	81.8	81.1	80.6	50	54.9	54.9
5	12.952	34.372	253.4	83.4	83	82	81.5	81.2	43	52.2	52.4
6	12.822	34.712	230.7	83.4	82.9	82.1	81.5	81.1	35	46.8	48.1
7	12.728	33.854	221.4	83.1	82.7	82	81.4	81.1	28	44.8	46.5
8	12.870	33.666	198.2	83.4	83	82.2	81.8	81.4	21	39.0	42.1
9	14.105	35.157	154.0	83	82.6	81.8	81.4	81	11	30.0	33.3
Ethanol/i-propanoi (2)											
1	51.678	84.593	261.0	81.4	81.1	79.9	79.4	79.3	39	65.1	55.6
2	51.921	85.461	237.8	81.4	81	79.8	79.3	79	31	58.1	51.8
3	52.396	85.013	214.5	80.9	80.7	79.5	79.1	78.8	26	51.0	48.1
4	52.962	83.920	191.2	81	80.7	79.7	79.2	79	22	43.9	44.3

Table D1 Continued – Ethanol/i-propanol (2)

Run No	Conc first comp. [wt%]		Flow rate [kg/h]	Temperatures [°C]					dP	Q_{reb}	Q_{cond}
	Bottoms	Distillate	Reflux	Reboiler	Bottom	Sec1-2	Sec2-3	Top	[mmH$_2$O]	[kW]	[kW]
Ethanol/i-propanol (2)											
5	52.829	84.839	167.7	81	80.6	79.8	79	79	15	38.2	39.3
6	53.542	85.715	142.7	81	80.4	79.6	79	78.9	10	35.6	30.4
Methanol/ethanol											
1	4.731	89.756	157.0	78.5	78.1	75.6	70.7	66	23	47.3	46.8
2	3.257	86.964	144.6	78.8	78.5	76.2	71.7	67.2	19	42.9	43.1
4	2.603	84.412	123.3	78.7	78.3	75.8	70.8	66.6	13	36.2	37.5
5	3.300	87.471	107.7	78.2	77.4	74.2	68.6	65.6	10	33.0	31.8
6	5.668	90.499	99.0	78.4	78	75.3	70.3	66.3	8	28.4	31.1
7	4.319	88.540	83.7	78.3	77.8	74.9	69.6	66	6	23.6	26.6
Methanol/i-propanol											
1	2.309	85.127	149.9	82.9	82.6	80	75.1	67.5	23	44.5	44.3
2	2.714	87.309	135.5	82.9	82.6	79.4	73	66	19	40.0	40.6
3	2.189	84.579	130.2	82.6	82.3	79.7	73.3	66.5	17	38.2	38.7
4	2.572	87.231	124.9	82.9	82.6	79.8	74	67.2	15	36.7	37.5
5	2.472	89.156	116.2	82.6	82.3	79.3	72.8	66.4	13	33.9	35.0
6	2.403	86.551	108.2	82.7	82.3	79.8	74.1	66.8	11	31.8	32.4
7	2.637	86.790	96.4	83	82.5	80.1	74.2	67	9	27.5	29.9
8	2.112	86.666	79.6	82.7	82.2	80	74.7	67	7	22.0	25.0

Table D2 Calculated packed height according to different correlations.

Run no.	Average packed height [m] according to correlation:						
	2.26	2.27	2.33	2.36	2.37	2.44	Crause
Ethanol/i-propanol (1)							
1	3.17	3.84	3.86	2.40	4.01	3.76	2.92
2	3.23	3.90	3.93	2.44	4.07	3.85	3.06
3	3.23	3.88	3.93	2.42	4.05	3.84	3.00
4	3.21	3.84	3.92	2.38	4.01	3.83	2.87
5	3.23	3.83	3.94	2.36	4.00	3.83	2.81
6	3.31	3.90	4.05	2.37	4.07	3.92	2.89
7	3.32	3.88	4.05	2.35	4.05	3.93	2.83
8	3.10	3.60	3.81	2.14	3.77	3.67	2.81
9	3.23	3.66	3.98	2.10	3.83	3.75	2.75
Ethanol/i-propanol (2)							
1	3.76	4.35	4.51	2.74	4.47	4.26	3.46
2	3.97	4.56	4.78	2.84	4.68	4.48	3.62
3	3.90	4.45	4.72	2.72	4.57	4.39	3.52
4	3.69	4.18	4.48	2.50	4.30	4.13	3.30
5	3.99	4.47	4.86	2.63	4.60	4.44	3.52
6	4.22	4.68	5.17	2.67	4.81	4.66	3.67
Methanol/ethanol							
1	4.24	4.49	5.01	2.73	4.34	3.97	3.49
2	4.12	4.35	4.88	2.61	4.23	3.89	3.45
3	4.51	4.71	5.36	2.75	4.58	4.23	3.44
4	4.78	4.93	5.70	2.82	4.79	4.42	3.58
5	4.69	4.78	5.59	2.70	4.62	4.25	3.61
6	4.67	4.73	5.60	2.59	4.59	4.22	3.62

Table D2 Continued – Methanol/i-propanol

Run no.	Average packed height [m] according to correlation:						
	2.26	2.27	2.33	2.36	2.37	2.44	Crause
Methanol/i-propanol							
1	3.78	4.05	4.47	2.46	3.93	3.64	2.80
2	3.99	4.23	4.73	2.53	4.09	3.79	2.90
3	3.84	4.07	4.56	2.42	3.95	3.68	2.83
4	4.02	4.23	4.78	2.50	4.10	3.81	2.95
5	4.09	4.29	4.87	2.51	4.16	3.87	3.17
6	4.07	4.25	4.85	2.45	4.12	3.84	2.97
7	4.21	4.36	5.04	2.47	4.23	3.93	2.96
8	4.20	4.32	5.06	2.36	4.20	3.90	3.14
Acetone/methanol							
1	3.94	4.18	5.17	2.19	4.10	3.65	3.21
2	3.65	3.96	4.70	2.29	3.88	3.45	3.12
3	3.57	3.88	4.52	2.30	3.81	3.41	3.11
4	3.82	4.16	4.79	2.50	4.08	3.66	3.10
5	3.82	4.19	4.82	2.53	4.11	3.67	3.47
6	3.77	4.19	4.77	2.58	4.09	3.64	3.21
7	3.65	3.97	4.50	2.44	3.89	3.50	3.02
8	3.62	3.97	4.47	2.45	3.89	3.48	2.99

APPENDIX E Distillation simulation input and output file examples

Pro II keyword input file for methanol/ethanol run 1

```
TITLE
  DIMENSION SI, TEMP=C, DUTY=WATT, STDTEMP=0, STDPRES=101.325
  SEQUENCE SIMSCI
  CALCULATION RVPBASIS=APIN, TVP=37.778
COMPONENT DATA
  LIBID 1,MEOH/2,ETOH
THERMODYNAMIC DATA
  METHOD SYSTEM=NRTL, SET=NRTL01, DEFAULT
STREAM DATA
  PROPERTY STREAM=S1, PRESSURE=101.55, PHASE=L, RATE(M)=100, &
        COMPOSITION(WT)=1,0.04731/2,0.95269
  PROPERTY STREAM=S2, PRESSURE=101.55, PHASE=L, RATE(M)=100, &
        COMPOSITION(WT)=1,0.04731/2,0.95269
UNIT OPERATIONS
  COLUMN UID=T1
      PARAMETER TRAY=12,IO=150
      FEED S1,11
      PRODUCT  BTMS(M)=S2,100, OVHD(M)=S3,1E-5, SUPERSEDE=ON
      CONDENSER TYPE=BUBB, PRESSURE=101.32, TEST=64
      DUTY 1,1/2,12
      PSPEC PTOP=101.32, DPCOLUMN=0.22563
      PRINT COMPOSITION=WT, PROPTABLE=PART, SUMMARY=WT
      ESTIMATE MODEL=REFINING, RRATIO=1000, CTEMP=64, TTEMP=64, &
                BTEMP=78, RTEMP=78
      TEMPERATURE 2,64/11,78/12,78
      SPEC STREAM=S3, RATE(KGM/H),TOTAL,WET, VALUE=1E-5, RTOLER=0.1
      SPEC REFLUX(WT,KG/H), VALUE=156.95
      VARY DUTY=1,2
      REBOILER TYPE=THERMOSIPHON, BAFFLE=NO, LFRA(M)=0.95
      METHOD SET=NRTL01
END
```

Pro II output file excerpts for methanol/ethanol run 1

COLUMN SUMMARY

TRAY	TEMP DEG C	PRESSURE KPA	NET FLOW RATES LIQUID KG/HR	NET FLOW RATES VAPOR KG/HR	NET FLOW RATES FEED KG/HR	NET FLOW RATES PRODUCT KG/HR	HEATER DUTIES M*WATT
1C	65.2	101.32	157.0			0.0L	-0.0471
2	65.7	101.32	158.9	157.0			
3	66.5	101.35	161.9	158.9			
4	67.7	101.38	166.1	161.9			
5	69.3	101.41	171.4	166.1			
6	71.1	101.44	177.1	171.4			
7	72.9	101.47	182.4	177.1			
8	74.5	101.49	186.9	182.4			
9	75.8	101.52	190.3	186.9			
10	76.7	101.55	192.7	190.3			
11S	77.3	101.55	3896.3	0.1	4513.5L	4513.5L	
12R	77.3	101.55	3703.7	192.6			0.0470

TRAY WEIGHT COMPOSITIONS

COMPONENT	TRAY 1 X	TRAY 1 Y	TRAY 2 X	TRAY 2 Y
1 MEOH	0.91396	0.95013	0.85600	0.91396
2 ETOH	0.08604	0.04987	0.14400	0.08604
RATE, KG/HR	156.967	0.000	158.915	156.968

COMPONENT	TRAY 3 X	TRAY 3 Y	TRAY 4 X	TRAY 4 Y
1 MEOH	0.76993	0.85600	0.65517	0.76993
2 ETOH	0.23007	0.14400	0.34483	0.23007
RATE, KG/HR	161.921	158.915	166.134	161.921

	TRAY 5		TRAY 6	
COMPONENT	X	Y	X	Y
1 MEOH	0.52166	0.65517	0.38788	0.52166
2 ETOH	0.47834	0.34483	0.61212	0.47834
RATE, KG/HR	171.377	166.135	177.063	171.378

	TRAY 7		TRAY 8	
COMPONENT	X	Y	X	Y
1 MEOH	0.27144	0.38788	0.18119	0.27144
2 ETOH	0.72856	0.61212	0.81881	0.72856
RATE, KG/HR	182.431	177.063	186.911	182.432

	TRAY 9		TRAY 10	
COMPONENT	X	Y	X	Y
1 MEOH	0.11695	0.18119	0.07382	0.11695
2 ETOH	0.88305	0.81881	0.92618	0.88305
RATE, KG/HR	190.297	186.912	192.675	190.297

	TRAY 11		TRAY 12	
COMPONENT	X	Y	X	Y
1 MEOH	0.04731	0.07598	0.04593	0.07382
2 ETOH	0.95269	0.92402	0.95407	0.92618
RATE, KG/HR	3896.311	5.060E-02	3703.685	192.625

STREAM ID	B	D	F
NAME			
PHASE	LIQUID	LIQUID	LIQUID
FLUID WEIGHT FRACTIONS			
1 MEOH	0.0473	0.9140	0.0473
2 ETOH	0.9527	0.0860	0.9527
TOTAL RATE, KG/HR	4513.5143	2.9226E-04	4513.5146
TEMPERATURE, C	77.2534	65.2284	77.2533
PRESSURE, KPA	101.5506	101.3250	101.5506
ENTHALPY, M*WATT	0.2523	1.3648E-08	0.2523
MOLECULAR WEIGHT	45.1351	32.9040	45.1351
WEIGHT FRAC VAPOR	0.0000	0.0000	0.0000
WEIGHT FRAC LIQUID	1.0000	1.0000	1.0000

NOMENCLATURE

A	Area	$[m^2]$
a	Packing surface area per volume	$[m^2/m^3]$
a_e	Effective area	$[m^2/m^3]$
a_p	Geometric area	$[m^2/m^3]$
B	Structured packing corrugation channel base	[m]
Bo	Bond number	
C	Concentration	$[mole/m^3]$
Ca	Capillary number	
D	Diameter	[m]
D_{AB}	Diffusion of A in B	$[m^2/s]$
d_h	Hydraulic diameter	[m]
D_l	Liquid phase diffusion coefficient	$[m^2/s]$
F	Enhancement factor	
F	Gas side factor ($=u_g\rho_g^{1/2}$)	$[kg^{1/2}m^{-1/2}s^{-1/2}]$
F_p	Packing factor	
Fr	Froude number	
F_{SE}	Factor for surface enhancement	
g	Gravitational acceleration, 9.81 m/s^2	$[m/s^2]$
G	Vapour flow rate	[mole/s]
h	Height	[m]
h	Packing height	[m]
h_L	Fractional holdup of liquid	
H_T, HTU	Height of a transfer unit	[m]
K	Distribution coefficient	
k	Mass transfer coefficient	[m/s]
L	Liquid flow rate	[mole/s]
m	Slope of equilibrium line	
Ma	Marangoni number	
M_r	Molecular weight	[g/mole]

MTG	Mass transfer group	
n	Molar transfer rate	[mole/s]
n	Number of channels in packing	
N	Molar flux	[mole/(m^2.s)]
N_T	Number of transfer units	
p	Perimeter [m]	
P	Pressure	[Pa]
P_{Bm}	Mean pressure of B	[Pa]
Q	Volumetric flow rate	[m^3/s]
r	Radius	[m]
R	Universal gas constant, 8.314 J/mole.K	[J/(mole.K)]
Re	Reynolds number	
S	Side length of corrugation	[m]
Sc	Schmidt number	
Sh	Sherwood number	
T	Temperature	[K]
u	Velocity	[m/s]
We	Weber number	
x	Liquid mole fraction	
y	Vapour/gas mole fraction	
z	Height	[m]
z	Mole fraction in gas phase	

Greek symbols

θ	Corrugation angle	[°]
υ	Kinematic viscosity	[m^2/s]
Δ	Difference	
α	Angle of packing defined in figure 4.5	[°]
δ	Thickness	[m]
ε	Void fraction	

μ	Viscosity	[Pa.s]
ρ	Density	[kg/m^3]
σ	Surface tension	[N/m]
τ	Interfacial shear force per area	[Pa]

Superscript

*	Property in equilibrium with the bulk of the fluid
liq	Liquid
vap	Vapour

Subscript

avg	average
b	bulk
eff	effective
eq	equivalent
g	gas phase
i	interfacial
l	liquid phase
m	mean
o	overall
r	relative
super	superficial
t	total